Radio-Network Extender Device (RED): Conceptualization, System Design, and Component Prototyping

A Major Qualifying Project Report

Submitted to the Faculty

of the

WORCESTER POLYTECHNIC INSTITUTE

In partial fulfillment of the requirements for the

Degrees of Bachelor of Science in

Computer Science,

Electrical and Computer Engineering,

and Mechanical Engineering

By:

Nisreen Aljumaili Michael Bedard

William Donovan Timothy Feehrer

Michael McCue Matthew Sanford

David Schwartz Matthew Vindigni

Date: March 24th, 2022

Approved By:

Lead Advisor: Prof. K. Notarianni

Co-Advisor: Prof. R. Ludwig

Co-Advisor: Prof. T. Ghoshal

Table of Contents

Abstract

Firefighters regularly experience radio signal loss when operating in locations such as hospitals, warehouses, and high-rises. Signal loss events pose serious risks to both firefighters and civilians by preventing the exchange of information between firefighters, thereby disrupting their coordination and effectiveness, and potentially leading to the loss of lives. To reduce signal losses, the Radio-network Extender Device (RED) will receive a firefighter's incoming radio signal, amplify that signal, and transmit it in conditions where communication would otherwise be impossible. This device was first conceptualized by determining the necessary electrical subsystems, protective enclosure, and communication style with firefighters that would help solve the issue of signal loss. Next, the subsystems for receiving, amplifying, and retransmitting a firefighter's radio signal were designed, developed, built, and tested. An ability to record and display temperature data on a website through direct communication with an onboard microprocessor was shown to be functional. This will provide firefighters with valuable information of how well the device performed following a fire given the temperatures it was exposed to. Heatsinks were designed and manufactured to provide passive cooling to the internal electrical systems so that the device would not overheat itself. An enclosure was designed, manufactured, and tested, in accordance with NFPA standards, to enable a RED to withstand the thermal and physical challenges encountered in the fireground. By insulating the electrical systems, the enclosure is ensuring that the firefighters can maintain communications in high temperature environments.

Acknowledgements

This project would not have been possible without the generosity of firefighters. We appreciate all the time these public servants volunteered to help us. Our work was inspired by Chiefs Matthew Gerhard and Elizabeth Ellis of Newtown Fire Association. Many other firefighters contributed to this project as well, including Mike Golden, FDNY; Cody Stoner, NFA; Brian Gerhard, NFA; Will Heiney, OSFD; and Chris Paige, NFD. In particular, Deputy Chief Ryan Dunn of Meriden Fire Department was instrumental to our work, providing insight and experience to design an optimized device for Meriden.

We recognize our project advisors for supporting this project for nearly two years. Dr. Notarianni, our lead advisor, and Drs. Ludwig and Ghoshal, our co-advisors, patiently shared their wisdom and expertise as we navigated the many diverse challenges we faced.

Our team would also like to thank WPI ECE Professor Noetscher, WPI ECE Professor Guler, and PhD candidate Galahad Wernsing for their expertise and instruction on different types of soldering. We also want to recognize Mitra Anand from the WPI Makerspace, electronic technician Bill Appleyard from the Atwater Kent ECE shop, and Ray Ranellone, Director of the WPI Fire Science Lab. Finally, we thank Kong Soynanhang, the manufacturing manager of NewEdge Signal Solutions who helped us confront RF manufacturing issues.

List of Figures

Executive Summary

Introduction

The first objective of this project was to conceptualize an engineering solution to the problem of firefighters losing radio signals. This resulted in the idea for creating and testing the components for a Radio-Network Extender Device (RED). With this goal in mind, our team's objective became working to design, build, and test components for a RED that would receive a firefighter's incoming radio signal, amplify that signal, and transmit it in conditions where communication would otherwise be impossible.

Firefighters in the northeastern United States regularly lose signal while operating in large buildings of heavy construction such as hospitals and shopping malls. These losses are so common that many firefighters expect them, yet current solutions to this critical safety issue are too expensive for many cities and towns to implement. This issue leads to firefighters being forced to relay communications manually, use other forms of communication such as cell phones during incidents, or just working without proper communications. The RED is meant to be a portable, durable, and affordable device that firefighters can deploy the same RED more than once at different incidents.

Our partner for this project was Meriden Fire Department of Meriden, CT. By designing a RED for one department only, we were able to tailor our approach and the device's specifications to deliver the best possible performance.

The second objective of this project was our research culminating in the development of electrical subsystems which have been built and tested to prove that individual parts of the RED are capable of communicating with each other. An enclosure and heat sinks were also designed and manufactured to house and cool these systems. For firefighters to view the data following an incident, a website was developed that communicates with the onboard microprocessor to display internal temperature data of the RED while in use. This system has

many options going forward such as further development and use for training with Meriden Fire Department as an MQP, or being patented as a new type of affordable signal amplifier to be used by first responders.

High-Level Overview

ECE

In order to create a portable repeater for the Meriden Fire Department, we had to design a system, source parts, and then put those parts together. Our system consisted of a transmit/receive block, a data/control processing block, and another transmit/receive block. Two transmit/receive blocks were needed in order to transmit and receive on two different frequencies. The data/control processing block controls the transmit/receive blocks and passes data between them. A block diagram for the electrical power system can be seen below.

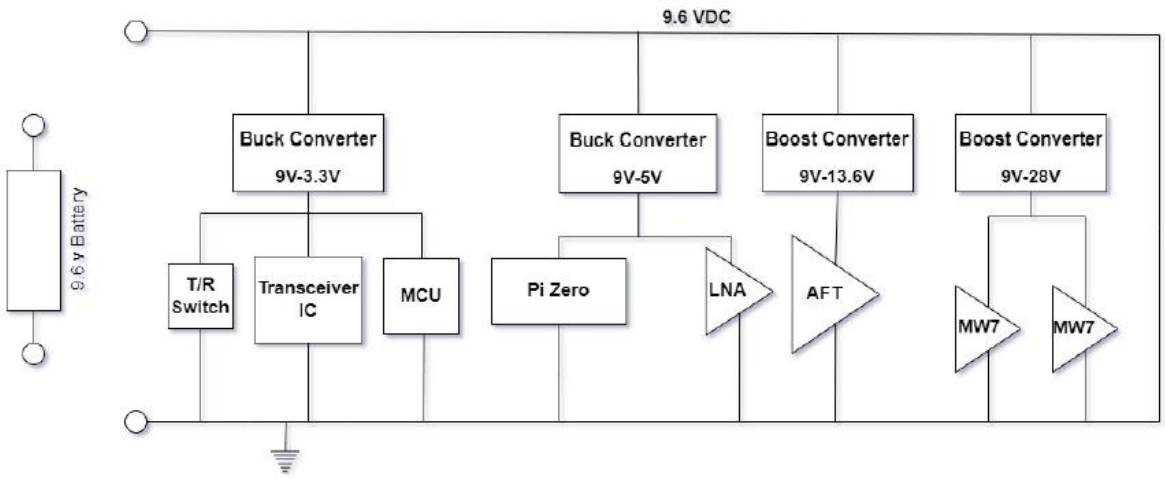

***Figure 1*: Electrical Power System Block Diagram**

Each transmit/receive block consists of an antenna, a low-noise amplifier, a filter, a transceiver integrated circuit, three power amplifiers, and two other antennas. The transceiver integrated circuit is controlled by the data/control block. The intent is to implement a state machine allowing for quick and seamless switching on both frequencies once relevant data is

detected by the control block. Each of these systems was tested individually to make sure it would receive and transmit a sample signal while still being able to amplify that signal.

CS

The MQP team wanted additional features to compliment the signal boosting capabilities of the project. These additional features entail collecting the internal temperature of the signal boosting system, and displaying the data collected as a graph on a website. The collection of this data is useful in determining at what point the device reaches dangerous temperatures. Due to the full system not being able to collect data, sample data was used to test the capabilities of the website communication. However, the website proved to work as intended and help inform first responders of the temperature data coming from the RED. A diagram of the web server and website system can be seen below.

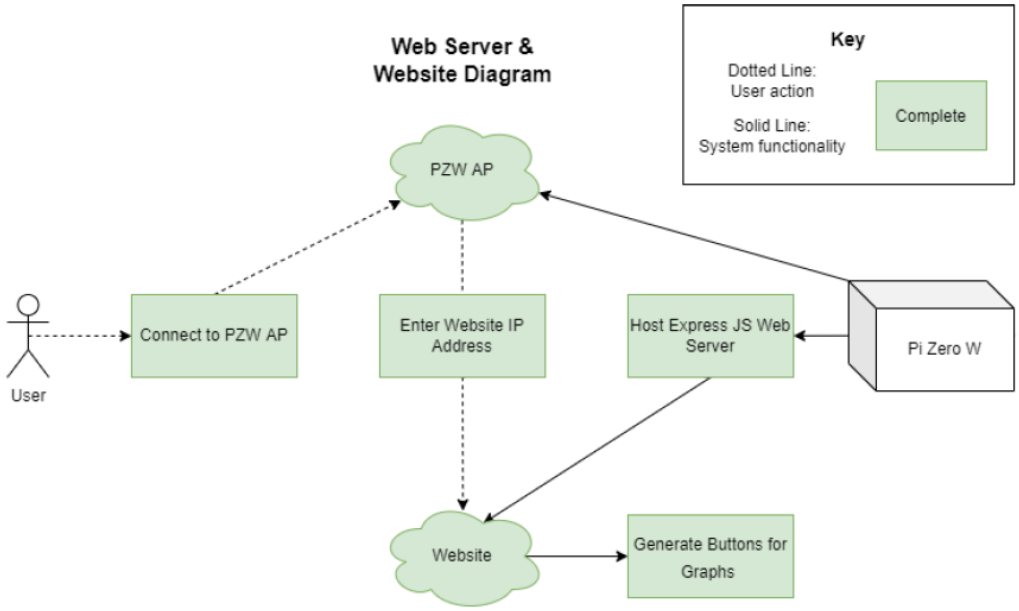

Figure 2: **Web Server / Website System Diagram**

ME

This repeater system faces the challenge of surviving in the harsh environments that firefighters work in daily. This meant that the repeater needed to be housed in an enclosure capable of insulating the electrical system while still being highly functional to the given firefighter. The enclosure was thermally stress tested in accordance with NFPA 1802 and was found to keep the internal temperature well below the maximum operating temperature of the electrical subsystems. The ME team was able to thermally stress test both the low noise amplifier and bandpass filter within the enclosure. Both of the components proved to work properly following this testing. An exploded view of the enclosure can be seen below.

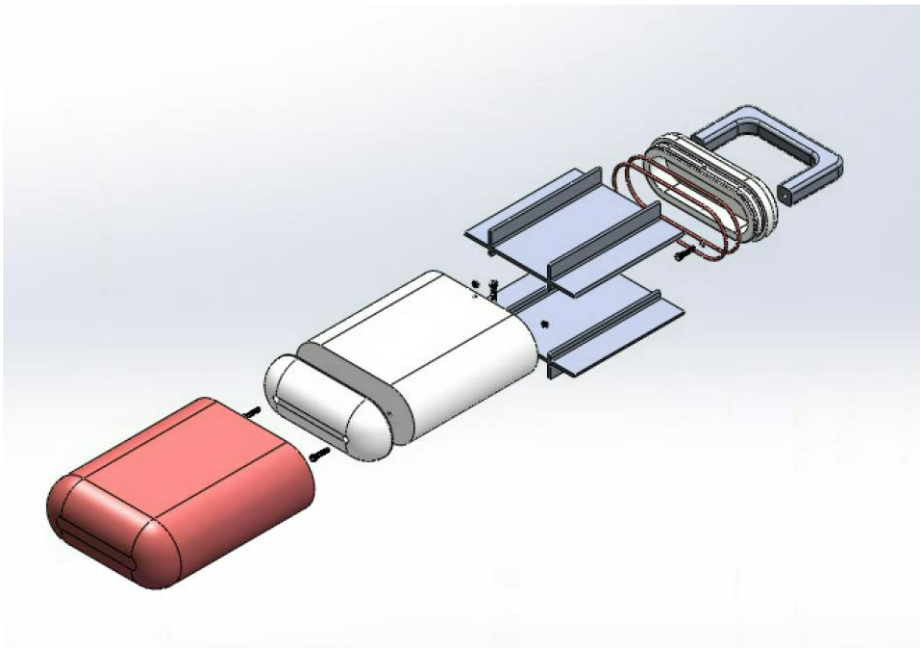

Figure 3: **Isometric View of Exploded RED Mechanical Assembly**

Additionally, the electrical system needed to be properly cooled so that the internal heat generated would not overheat other subsystems. The ME team worked to solve these challenges by creating a layered, insulating enclosure capable of keeping the tested electrical at a working temperature and by creating our own phase change material heat sink that would survive high temperatures while cooling the electrical systems.

Chapter 1: Introduction

Our team began this project with the goal of helping to solve a significant issue within the fire service, either by designing a new product or improving an existing one. One of our team members, Mike Bedard, is a volunteer firefighter and EMT in suburban departments in Massachusetts and Pennsylvania. While talking informally to firefighters and dispatchers in Pennsylvania, Maryland, Delaware, New Jersey, New York, Connecticut, and Massachusetts, Mike noted that each of them had often experienced signal loss on their handheld radios. Radio signal loss was in fact, so expected and so frequent, that no municipality had formally recorded occurrences of signal loss.

To learn more about signal loss, and to identify other potential research topics based on prevalent difficulties in the firefighter community, the team shared a Google Forms survey with six different fire departments in the Northeastern United States. When asked which tools and technologies they wished worked better, one firefighter responded, “radios– they cost a fortune and do not work well in high-rises or below grade” (Appendix A**)**. The team learned that while open-space conditions may allow the effective range of handheld radios to extend for over a mile, catastrophic attenuation often occurs in buildings with thick concrete walls, significant metallic structures, or large underground sections. These so-called “radio-harsh” environments are prevalent in city high-rises, hospitals, factories, and parking garages.

The survey responses demonstrated that signal loss between handheld radios is a common issue, and there is a need for a solution that is affordable for most fire departments. When firefighters lose signal, there is a lack of communication between each firefighter and the command unit. This creates a greatly increased risk of firefighters inside the building who are unable to communicate vital information or call for help. Firefighters are also unable to receive directions from the command unit.

Currently, the most effective solution to the problem of radio signal loss is bi-directional amplifier systems. BDA systems are built into new buildings and support two way communication for emergency responders by receiving radio signals, amplifying them to a repeater antenna outside the building. These systems have multiple disadvantages, firstly they are not portable. Thus, in order to aid communications on the fireground, they would need to be pre-installed in the particular building experiencing a fire incident. BDA systems are not commonly installed in buildings due to their high cost, and when they are the system is often unusable due to signal interference, such was the case during the World Trade Center Attacks. In the absence of BDAs, firefighters respond using a human relay. This strategy can be effective; however, staging a firefighter at the point of signal loss effectively reduces the responding crew size by at least one. A landmark study by NIST demonstrates how crew sizes affect the fire department's ability to save lives properly. For example, four person crews were able to deliver water to a similar sized fire 15% faster than the 2 person crews and 6% faster than 3 person crews. Jason Averill, the study's lead author states, “Fire risk grows exponentially. Each minute of delay is critical to the safety of the occupants and firefighters, and is directly related to property damage” (Swenson, 2020; Averill, 2010).

Therefore, our team directed our effort towards developing an effective low-cost, portable and reusable device that would improve radio signal strength for firefighters working in environments where radio communication would otherwise be difficult or impossible. Our first step was to conduct comprehensive background research.

Chapter 2: Background

The team identified the US national codes and standards for fire department radios, as well as previous university and corporate research on radio signal amplification. We researched databases such as “IEEE Xplore” and other George C. Gordon WPI library databases for articles about the issue but found very few sources. The sources we did find were not always current or specific to handheld radios. We then reached out to experts and leaders in the national fire service, who provided meaningful insight on the problem of signal loss. Upon recommendation from these interviews, we set out to establish a working partnership with a fire department for baseline testing and an infrastructure to work with.

2.1 US National Standards

Our team identified the current national standards that fire service radios and other devices employed on the fire ground are designed to meet. The US National Fire Protection Association (NFPA) develops and publishes such standards based on the consensus of a committee made up of manufacturers, researchers, firefighters, and other industry leaders. For each code, the committee determines what is required for these devices based on their knowledge of fireground conditions, as well as what is feasible from a manufacturing perspective. The standards development process also incorporates input from a public review/comment period. Our team identified two NFPA standards relevant to our proposed system, those being: Standard on Two-Way, Portable RF Voice Communications Devices for Use by Emergency Services Personnel in the Hazard Zone (NFPA 1802) and Standard on Thermal Imagers for the Fire Service (NFPA 1801).

2.1.1 NFPA 1802

NFPA 1802: “Standard on Two-Way, Portable RF Voice Communications Devices for Use by Emergency Services Personnel in the Hazard Zone” was first published in January 2021. This document specifies operating parameters, as well as performance and design requirements for two-way radios and microphones used in hazardous environments. This standard references known standardized tests for speech quality, water leakage, impact acceleration, power source performance, high temperature performance, product label durability display surface abrasion resistance, corrosion resistance tumble vibration, cable pullout strength, and electronic temperature stress. It is important to note that there are currently no two-way radios on the market that meet all specifications listed in the document. Tests specified in 1802 relating to resistance to electric temperature stress and high temperature performance will inform the development of specifications used in the RED design.

2.1.1.1 Pass Device

We also researched PASS devices at the suggestion of Ray Ranellone, fire protection lab director at WPI, as well as Bob Athanas, a former FDNY Chief officer and chair of the NFPA 1802 committee. These devices are used to alert fire incident command and nearby firefighters on a lack of movement, indicating a firefighter is immobile and could need assistance. If a firefighter stands still for 30 seconds, the PASS device will begin to beep loudly, alerting nearby firefighters of their location. Firefighters can also activate PASS alarms manually if required. Since PASS devices are carried by firefighter, they must be able to withstand the harsh conditions on the fire ground, thus our research on these devices focused mainly on the materials used in their composition, as well as how they are assembled to guide the design of the REDs protective enclosure.

2.1.2 NFPA 1801

NFPA 1801: “Standard on Thermal Imagers for the Fire Service” provides standards for Thermal Imaging Cameras (TICs), such as maximum operating temperatures and resistance to vibration. First published in 2018, this standard has been used to guide the design processes for different TICs used in firegrounds such as the FLIR K1 Situational Awareness Camera. TICs are designed to work under the harsh environmental conditions of the fireground such as sustained high temperatures, significant water and gas exposure, and extreme force in cases of structure collapse. We found that the enclosures for TICs are generally made from different kinds of polymers, one example being a polyphenyl sulfone (PPSU) called Radel R, produced by Solvay Advanced Polymers (FLIR K1). This material is used in the FLIR K1. We used this standard, as well as the TICs that fulfill its requirements, to direct our research when considering enclosure designs and their constituent materials.

2.2 Existing Technology and Previous Research

In addition to NFPA standards, the team researched existing signal improvement systems, both commercially available products, and those in various states of research or development, to ascertain the current state of the technology. Specific projects that our team took inspiration from include WPI’s Precision Personnel Location Device (PPL) and the Department of Homeland Security’s GLANSER/WISPER systems. We considered existing portable radios repeaters, as well as stationary repeaters meant to be integrated directly into buildings.

2.2.1 Bi-Directional Amplifier (BDA) System

Bi-Directional Amplifier (BDA) systems are signal amplification devices that are installed into large buildings to receive and transmit radio signals for firefighter radios and

other public safety systems. These systems work by relaying the signal from firefighters' two-way radios through an antenna that connects to a radio repeater outside the building, usually a carrier's radio tower, and heavily boosts its signal (AFA, n.d.). This radio repeater then sends the signal to receivers on the fire trucks outside the building to be relayed to the incident commander. This process is similar to the idea of a Wi-Fi repeater that does the same process, but for connecting devices to the internet. BDAs on the other hand are specifically designed to interface with public safety radios and the associated operating frequencies. BDAs are typically found in buildings such as hospitals or airports where fire radios are more likely to lose coverage due to thick walls made of concrete, metal, and other materials or construction that can cause significant attenuation.

These systems satisfy the purpose of reducing signal loss, but generally cost too much and can get very expensive in large buildings like high-rises where the systems are typically used (SignalBooster.com). With a new system being needed for every building, expenses for the city or business can rise quickly, and without the pre-existing infrastructure, the firefighters will still lose signal in a harsh environment. A system such as the RED would serve as a much more affordable alternative to the BDA system that could be used in smaller cities and buildings without the established infrastructure.

2.2.2 WPI Precision Personnel Locator (PPL) System

The PPL system, developed by WPI professors James Duckworth, David Cyganski, Sergey Makarov, and others, is an RF-based precision locator that aims to conduct real-time tracking of firefighters in dangerous environments. This system is stand-alone, meaning that it requires no existing infrastructure in order to function in harsh RF environments. Instead, firefighters would bring a transmitter into the building with them that would connect and relay with another transmitter in the emergency vehicles outside. Information on the firefighters is then relayed, either through GPS or electronic floor plans that are laid out

beforehand, both tracking firefighter movements and paths through the building (Amendolare, 2008).

The WPI PPL system served as the general inspiration for our project, as we originally wanted to improve on this system by continuing the research that had already been done. We were able to have a meeting with one of the main contributors to the PPL project, Professor Makarov. After some discussion, Professor Makarov recommended that we do not pursue this project, but instead use it as a guide for amplifying radio signals since the geolocation aspect of the PPL system was far too complicated and required a significant setup time before being effective. We took Professor Makarov's advice in this issue and focused our efforts on radio signal amplification by a portable system, as this is a task that is not only much more manageable in our time frame but is also a need described by several of the fire departments that we had sent a survey to including FDNY and Newtown Fire Association.

2.2.3 DHS GLANSER System

Similar to the PPL system, the DHS GLANSER system uses a mix of GPS, internal measurements, and a 900 MHz transmission frequency to locate firefighters, aiming for a 1-meter accuracy (Where there's smoke, 2021). GLANSER is an acronym for Geospatial Location Accountability and Navigation System for Emergency Responders and operates using small devices that relay this mix of signals to a base station outside the burning building. This system is used in conjunction with the PHASER, or Physiological Health Assessment System for Emergency Responders system, that can detect the vital signs of firefighters and alert personnel on the outside of the testing environment when a firefighter's life is in danger. When firefighters are in danger, the combination of these two systems aids rescue efforts.

The PPL and GLANSER systems never made it out of testing, only being tested in controlled environments. As such, a lack of continued funding caused discontinuation of research. According to the Department of Homeland Security, it was hoped that private industries would support further research and development after a proof of concept was provided back in 2011. The devices however were too expensive, and for the volume needed would not make a large profit. The devices were also not accurate enough to be relied upon.

2.2.4 WISPER System

Developed by Oceanit and DHS, the WISPER team is looking for private sector funding to further develop their location systems. WISPER uses disposable hardware that relays the geolocation signal of firefighters within buildings in what they call a “Hansel and Gretel" design where a user would drop small blocks capable of relaying radio signals as they traversed deeper into the fireground. This system is not a standalone product, however. It must work in conjunction with other existing technology besides the radios that firefighters are already bringing with them to the firegrounds. Originally, the WISPER system was designed to work with the GLANSER and PHASER systems, however seeing as the GLANSER systems never made it out of testing, the DHS is looking for a private company to pick up the research and create a more viable product.

2.3 Expert Interviews

After familiarizing ourselves with the background literature, our team felt comfortable discussing further details with industry experts. To gather further information and to form a partnership, we interviewed firefighters and two NFPA members.

2.3.1 Firefighter Interviews

First, the team reached out to several fire departments to interview end users and understand their personal experiences with signal loss. Initially, Worcester Fire Department and Boston Fire Department were contacted, however both of these cities had already begun building Bi-Directional Amplifier (BDA) systems into their infrastructure and there was much less of a need for our research. Next, the New York City Fire Department (FDNY) was contacted as a possible partner. The team spoke extensively with FDNY firefighters, in particular Mike Golden, regarding the lack of research conducted regarding radio signal loss within buildings. Although the team was not able to continue a formal partnership with FDNY, the firefighters provided excellent insight into the current state of radio signal improvement research done by FDNY, expressing a need for radio signal amplification that does not rely on existing infrastructure. Mr. Golden suggested that we look at how firefighter two-way radios and PASS devices are designed in order to inform the enclosure design of our research. Additionally, the firefighters provided the team with contacts within Motorola, L3Harris, and JVCKenwood, although these contacts were unable to be interviewed by the team.

2.3.2 NFPA Interview

Our team met with the NFPA 1802 Technical Chair, Bob Athanas, and the NFPA committee liaison, Chris Farrell. During the meeting, Mr. Athanas told us that there is a need for a radio-repeating device. He recommended that we focus on a single fire department for the first iteration, rather than our original plan of accommodating as many departments as possible. This was because different fire departments do not necessarily share the same communications systems and needs. This single-department approach narrows the scope of this project which would allow our team to test fewer variables and build a stronger

relationship with firefighters and their system. Once a working model has been developed, we can expand the scope of the project to involve more departments.

2.4 Forming a Partnership with the Fire Service

After months of discussion with a variety of departments, we were grateful to form a partnership with the Meriden Fire Department (MFD) and Deputy Chief Ryan Dunn. Meriden is a city of about 60,000 inhabitants with a variety of challenging RF environments. These environments cause the fire department to experience regular signal losses while using their portable two-way radios transmitting at 6W operating on both Very High Frequency (VHF) and Ultra High Frequency (UHF) ranges. These losses are significant enough that Deputy Chief Ryan Dunn explained firefighters are sometimes stationed inside buildings to relay radio communications. That is, firefighters must be diverted from regular fire operations to stand in places with strong radio signals in order to relay messages to and from teams in places throughout the building experiencing poor radio signal.

Chapter 3: Objective

This project had two objectives: to conceptualize and provide a layout for a device to serve as an engineering solution to the signal loss problem, and to design, build, and test the component parts of this device. The proposed engineering solution, the Radio-network Extender Device (RED), would be low cost, portable, and reusable. It would receive a firefighter's incoming radio signal, amplify that signal, and successfully transmit it in conditions where communication would otherwise be impossible.

The research in this report first establishes the need for such a RED and then provides background on national codes and standards that govern the requirements for fire service radios and other devices as well as previous research in this area. Next, the methodology that was used in the design is described and the resulting conceptual design is presented in full. Finally, the process of designing and testing each component part of the RED system is presented. A future vision of the integrated system prototype and the work required to achieve this system is included.

Chapter 4: Methodology

In an effort to better understand the capabilities and limitations of current radios used by the Meriden Fire Department (MFD), the conceptualization process began with field testing of the existing radio systems used by MFD. Structured field testing allowed for observations of where and how radio signals degraded. This data was used to create a "baseline" profile of current MFD radios.

After developing a system-level concept for deployment and operation of the repeater, the electrical and mechanical modules necessary to realize this concept were identified. Important aspects of the design of each component related to how each component would effectively communicate with other components in the system. Then, technical specifications were derived for each electrical and mechanical system module. Many electrical specifications were adopted from the performance capabilities of the radios already used by Meriden, while many mechanical and thermal specifications were adopted from NFPA standards.

These RED components were then manufactured and tested using WPI or industry-standard professional resources. In general, each component was first tested for basic functionality, and once their function was proved, they were tested at elevated temperature and/or in conjunction with other system components.

Chapter 5: System Design Conceptualization

Chapter 5 represents the team's first deliverable, the conception and layout of a device that would serve as an engineering solution to the problem of signal loss on the fireground. Our process is presented in sections 5.1-5.3 and our conceptualized design is presented in section 5.4. After baseline testing was done to characterize the issue of radio signal loss, the team worked to develop a concept and the components for a device that would solve this problem that the firefighters face. The components developed were based on specifications that the team found would be necessary to successfully amplify a firefighters' radio signal in a harsh environment. This section outlines the processes the team took to develop these components and the device concept.

5.1 Results of Baseline Testing in Meriden

Communications tests were conducted in a shopping mall, hospital, school, and hiking trail in Meriden County. The procedure involved two teams–one stationed outside of the building (or at the trailhead), while the other walked throughout the building (or along the hiking path). This represented the status of MFD used on their own during an incident response, without a firefighter stationed as a relay. The quality of communication was tracked in relation to horizontal distance, vertical distance, amount of material obstruction, and type of material obstruction, between the two groups, each using one radio. Approximately every 50 ft, the interior firefighters attempted to hail the exterior firefighter with their radios. Structural features of the environment were considered, such as turning a corner or walking up or down stairs. If communication was lost or otherwise indiscernible, the interior group back-tracked to the last known location where signal was positive, and progressed along their route in roughly 10 ft increments. In each increment, the interior and exterior teams attempted communication, and noted how the audio output progressively

degraded along the path. This involved four qualitative descriptions: either the audio was “discernible”, “noisy”, “very noisy”, or “completely lost” (the qualification “noisy” meant that spoken language was identifiable, but difficult to understand as a result of the worsening signal-to-noise ratio of the radio system). A signal-quality map was made to illustrate the results of baseline testing, and eventually be used as a “before-after” comparison to determine the efficacy of a finalized prototype, as described in section 7.2.3 Baseline Testing Revisited.

The observations made during baseline testing were used to conceptualize how a repeater or range-extending system would need to deploy and operate. For instance, if signal was lost only when moving behind a building, then a single repeater located behind the building would suffice. On the other hand, if signal was lost in multiple locations within a building, then either multiple low-power repeaters, or one high-power repeater, would need to be deployed within the building. Baseline testing will also be used to established how a repeater would integrate into the existing radio communication systems. Crucially, it would function within the “push-to-talk” procedure used by handheld radios, where a radio is by default in receive (“listening”) mode, and a firefighter manually switches into transmit mode when they want to communicate. Lastly, direct feedback from Meriden Firefighters informed us how a new device would be carried and used.

Baseline testing in Meriden confirmed that catastrophic attenuation and signal-loss occurs within buildings containing thick walls, metal, and large material obstructions. It was often found the signal quality could abruptly transition from somewhat “discernable” to “completely lost” over a relatively short distance. On the other hand, signal range with even handheld portable radios extended for several miles in open-space environments.

When conducting radio tests along the hiking trail at the Bradley Hubbard Reservoir, no signal degradation was encountered traveling nearly two miles away from the stationary

team at the trailhead, at which point an incident fire call diverted the attention of our firefighters. While the trail contained somewhat dense woodland around the reservoir, compared to the interior of a mall or hospital, it is still considered an “open-space” area.

Signal attenuation was only observed once communications tests were brought to the Meriden mall, hospital, and high school. Shown in Figure 4 is a heat-map for radio testing in the Meriden Mall using the radio channel “Fireground 2” (153.89 MHz, type A, 94.8). The stationary exterior team was located at the main entrance by TJ Maxx. On the first floor, as the interior team moved down the hall and out of the line-of-site of the exterior radio, audio became “noisy” by the Old Navy store, and abruptly transitioned to a “completely lost” outside the Verizon store and Gamestop. As seen in the map, this location had the greatest material-blockage between the interior and exterior radios team on the first floor. Moving into Bosco’s, line-of-sight with the exterior team was re-established through the glass-doorways leading to the parking lot, and signal quality moved back to nominal.

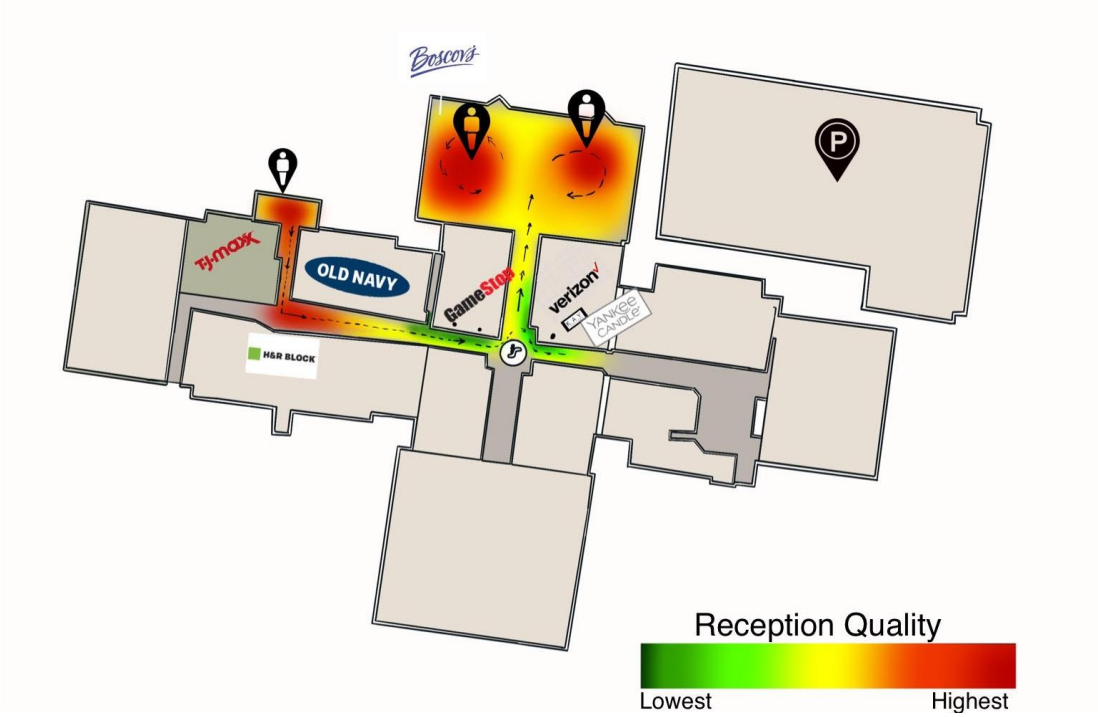

***Figure 4*: Meriden Mall Heatmap**

5.2 Operational Overview

In the original design, the firefighter would wear a device that would auto-deploy a repeater when it detected signal loss. The repeaters would act as “breadcrumbs' ' extending the range as the firefighters progressed into a building. This is similar to the process used by WISPER (described in 2.2.4 WISPER System). However, our team had moved away from this concept for several reasons.

First, according to our on-location baseline tests with MFD, signal loss is not gradual. Rather, it occurs abruptly when moving to different locations in a building. This means that an automated “signal integrity” routine would not reliably determine the appropriate time and location for deployment. Second, feedback and echo between different repeating devices deployed within range of each-other would be a major issue. Third, since a repeater works by receiving a signal on one frequency (input) then re-transmitting the information on a different frequency (output), a frequency shift would be required every time a firefighter places a “breadcrumb.” Since every “crumb” would require two different frequencies to operate, the system would become unmanageable after even a few deployed units. Finally, the breadcrumb approach would require the firefighters to wear additional gear on top of everything else they carry.

The approach ultimately pursued avoids the problems described above. Instead of small “breadcrumbs,” there is a single high-power repeater or “lunchbox.” The device would be carried in by a firefighter or safety officer. As soon as they lose radio signal, the user would then step or crawl backwards about five feet, place the device on the ground, and return to fireground operations. In this way, the device would extend signal coverage without causing significant burden to the user. To avoid feedback and interference, the device

communicates over two frequency channels. Once the device is placed, the firefighters do not need to carry anything else.

If the repeater were to transmit on the same frequency it received, then real-time relaying of the signal would result in uncontrolled feedback and cross-talk between the transmit and receive branches onboard the device. Therefore, to relay radio communications in real time, the repeater needs to receive on one frequency group (radio channel), and transmit on another. The repeater also needs to be integrable within the existing communication channels licensed by MFD. The MFD licenses four primary channels: the first two are in the VHF range at 154MHz and 159MHz, and the second two are in the UHF range at 460MHz and 465MHz.

As shown in Figure 5A, when idle, the repeater is in a receiving mode for both channels. When a firefighter communicates on one channel, say VHF, the repeater needs to detect that it is receiving on the VHF channel, and switch its output stage to re-transmit on the UHF channel. Once the firefighter is done talking, the system needs to detect that communication has stopped, and transition back to "listening" mode on both channels, most likely until the other firefighter on the receiving end responds with his or her own transmission. In this case the process repeats, only with the repeater set to receiving on the UHF channel, and retransmitting on the VHF channel.

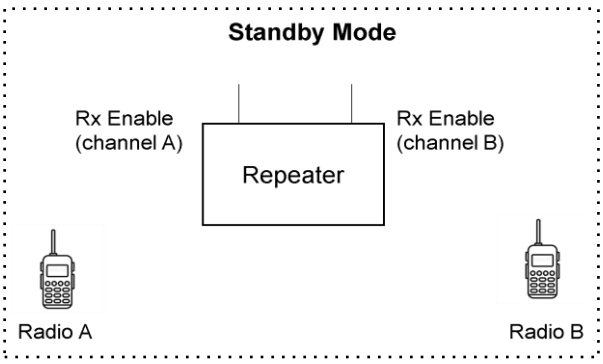

***Figure 5A*: System in "standby" mode is monitoring both channels, waiting to detect transmission**.

Figure 5A shows the system in “standby” mode, or its default state, which monitors the VHF and UHF channels for transmissions. This mode is the most used mode and consumes the least power.

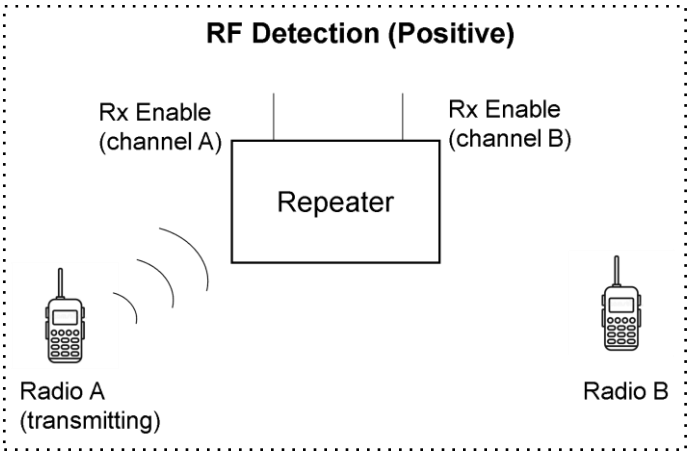

Figure 5B. **Upon RF detection on channel A, the stage corresponding to channel B is enabled to Tx mode.**

Figure 5B shows the system in “detection” mode. In this case, the system detected a signal on channel A, so to repeat the signal, the system must first enable transmission (Tx mode) on channel B.

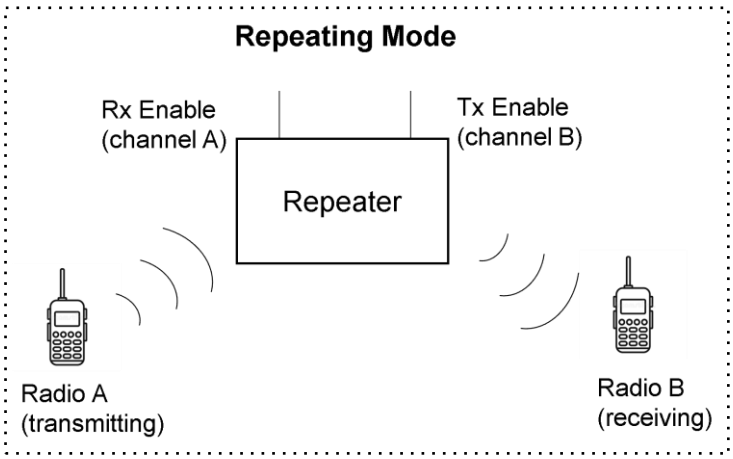

Figure 5C. **The system is continuously receiving on channel A and re-transmitting on channel B at the same time.**

Figure 5C shows the system repeating the firefighter’s radio signal. Here, the transmission from channel A is received continuously and is then re-transmitted at higher power on channel B. This mode uses the most power.

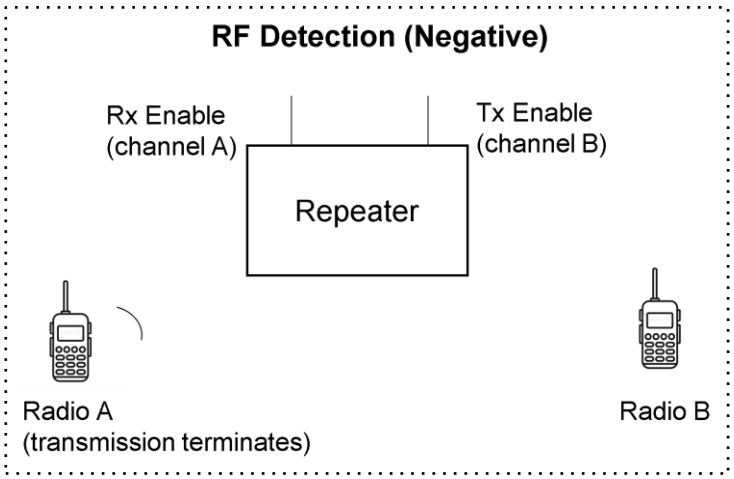

Figure 5D. **The system detects transmission on channel A has ceased and switches the branch corresponding to channel B back to Rx mode.**

Figure 5D shows the system stop repeating the firefighter's radio signal. With no transmission from channel A to re-transmit, the repeater returns to its default monitoring state shown in Figure 5A.

5.3 Device Specifications

Given our partnership with Meriden Fire Department, the radio repeater was designed for targeted compatibility with the specifications and protocols used by Meriden's current communication system. More specifically, the MFD RED minimum specifications were designed to meet the same specifications as MFD's current portable radios. In this way, the RED would function as a replacement for firefighters stationed as relays described previously. If this RED were to be built for a department other than Meriden, the design of certain electrical components would change, which is explained further in this section. The following section illustrates the specifications required that would be required to be met to solve the signal loss problem the team found with Meriden Fire Department radios.

Electrically, the RED must receive a signal of at least -80 dBm across either 150-160 MHz (VHF) or 460-465 MHz (UHF). These specifications are sourced from MFD's current portables for the reasons described above. REDs must then process the received signal and

convert from either VHF to UHF or UHF to VHF. Once the signal is converted, the RED must transmit at a minimum of 37.8 dBm across, for example, VHF without interfering with the UHF channel.

Mechanically, the RED enclosure must be able to protect the electronic components from an environment with ambient temperature of 350 degrees Fahrenheit for 15 minutes. It must also be water resistant, corrosion resistant, and high strength. It should be able to withstand impact loading from dropping from a height of 3 meters and cannot block or significantly attenuate the radio signals. Additionally, cooling systems must be present to prevent the electrical systems from overheating.

The RED software should record internal temperature every 30 seconds via a temperature sensor connected to the MSP430 and transmit the recorded data to the Raspberry Pi Zero W for processing and visualization. The data must be processed into graphs that accurately display the temperature values over time. Finally, the generated graphs should be viewable on the RED website hosted by the Raspberry Pi Zero W.

5.4 System Design and Layout

This section details our first deliverable: the design conceptualization and layout of an engineering solution to alleviate Meriden's signal loss problems. The system was designed to meet specifications discussed in 5.3 Device Specifications.

5.4.1 Electrical Design and Layout

To realize the operational procedure described in 5.2 Operational Overview, the system will contain two "RF-branches"—one dedicated to the VHF channel at 151-159

MHz, and the other dedicated to the UHF channel at 460-465 MHz. Each branch will have a corresponding receive and transmit stage, but these will be isolated from one another by SPDT RF switches controlling access to the antennae.

The primary handheld used by the Meriden Fire Department is the L3Harris XL200P Land Mobile Radio. The 200P uses P.25 C4FM modulation (a type of 2-bit FSK). For the licensed VHF and UHF channels, L3Harris specifies a receive sensitivity of less than -121dBm and a transmit power of 5-6W. To be comparable with the 200P, the objective for the repeater is to have a receive sensitivity of at least -80dBm and transmit power of at least 6W (37.8dBm). The compromise in sensitivity was made due to the relative difficulty in designing an RF front-end.

The block diagram in Figure 6 shows the architecture for the electrical and computer system. The receive stages of each RF branch consist of a low-noise amplifier (LNA), a bandpass filter, and a transceiver IC. The transmit stages of each RF branch consist of the same transceiver IC, a power amplifier (PA), and a bandpass filter. Two antennae, one tuned for 154 MHz, and the other for 460 MHz, begin/terminate their corresponding RF branches. Interfacing the two RF branches is a Micro-Controller Unit (MCU) serving as the state-machine for the operational procedure illustrated in Figure 6. The MCU also serves as the digital signal processing center, providing the interconnection from the VHF receive stage to the UHF transmit stage, and the UHF receive stage to the VHF transmit stage.

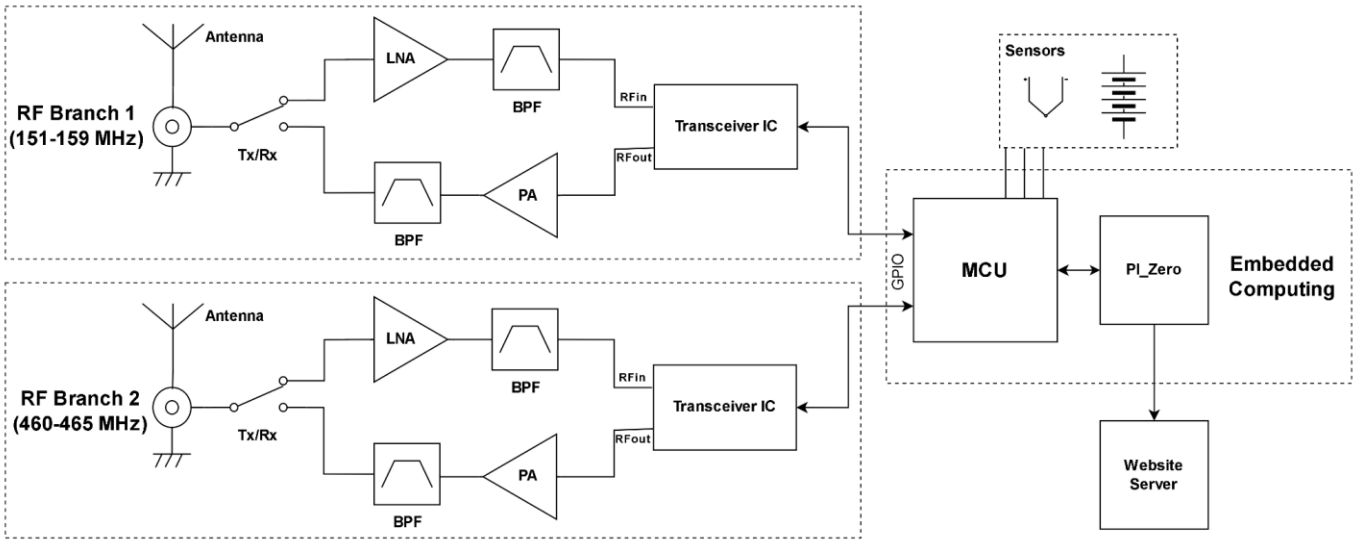

Figure 6: **Electrical and Computer Block Diagram**

The purpose of an antenna is to act as a transducer between the voltages and currents in a circuit to unbounded electromagnetic waves propagating in space. A single antenna may be considered a one-port network at the terminal of an electrical system. A typical qualification of good matching is less than -10dB of return loss (>90% power transfer) over the desired bandwidth. For the RED, -10dB bandwidth of 150-160MHz (6.5%) for the VHF antenna, and 455-470MHz (3%) for the UHF antenna, is more than sufficient. While for more general radios, a wider-band, tunable antenna would be required, the narrowband construction in favor of the Meriden Fire Department's frequency allocations allows for a greater degree of sensitivity and miniaturization. The antennae must also have a compatible radiation pattern and polarization relative to the other radios participating in the communications link. Since the L3Harris radios use a monopole or dipole antennas, typically oriented perpendicular or roughly perpendicular to the ground, the antennae on the repeater must be able to receive and transmit E-field polarization perpendicular to the ground, with directivity in the plane roughly parallel to the ground. Patterns with symmetry in this plane are an added benefit in that they afford a degree of "omnidirectionality", which means the

orientation of the repeater would be a non-factor. The design of the VHF and UHF antenna would change if the RED was adapted for another department.

Access to the antenna by the receive and transmit stages of a given RF branch needs to be regulated by a SPDT switch controlled by the RF detection subroutine running on the MCU. For instance, when transmitting at 6W (7.8dB), it is desired for the PA to be loaded by only the antenna impedance, not the input impedance of the LNA on the receive stage. Given a maximum rating of -8dB input power to the LNA, and a 7.8dB output power from the PA stage, 15.8dB of isolation is the absolute minimum required for the RF switch. Beyond isolation, to provide acceptable efficiency between the PA stage and transmitting antenna, the insertion loss across the switch should be less than 0.5dB (10% power loss). It should be noted that when a given branch is in transmit mode, the transceiver IC, which has its own internal RF switch, will be in "transmit enable" mode as well. Furthermore, the power MOSFET regulating current supply to the LNA rails should be turned off by the MCU. Thus, the RF switch at the antenna port is not the only isolator preventing positive feedback when the repeater is in transmit mode, and its purpose is primarily to isolate the input impedance of the LNA.

The low-noise amplifier (LNA) will be the first active stage of the receiving end of the system. Its purpose is to amplify the received signal above the noise-floor required for the transceiver, and its noise-gain performance affects the overall noise figure of the receiver. Therefore, the third-order intercept and noise figure were primary considerations when selecting an off-the-shelf component. A gain of at least 20dB or greater was desired to meet the sensitivity requirement of the RF-front end.

For a given RF branch, the RED VHF and UHF filters isolate and reduce interference on the desired frequency band by cutting-off the signals that are outside the selected band

and passing those that are within the selected band. By designing custom filters, one is able to optimize and troubleshoot more effectively than buying off-the-shelf designs. However, commercial designs do not require separate prototyping and development, so the team balanced these two considerations when deciding on both custom and commercial filters. Filter selection and design would change if the RED was adapted for another department.

The transceiver IC is the core of the RF system. For the receive stage, the transceiver IC provides the heterodyne frequency selectivity, power level sensitivity, 4FSK demodulation, and analog to digital conversion. Given one LNA of at least 20dB gain, the minimum sensitivity of the transceiver must be at least -60dBm to meet the -80dB sensitivity specification. The digital output can be sent to the MCU board using a serial dataline. For the transmit stage, the transceiver provides 4FSK modulation, frequency stability with low harmonic distortion, and moderate gain. The programmable RF out in Tx mode allows automatic gain control before the power amplifier stage. To adapt the RED for another department, the code governing the transceiver IC would have to change, but the hardware would remain.

To transmit signals at high voltage and current, the power amplifiers (PAs) provide efficient amplification of the modulated signal from the transceiver IC, and drive the antenna transducer. To achieve high gain with acceptable linearity and efficiency, the PA stage consists of two amplifiers. The first is designed for small-signal operation with high linearity, and the second for large signal input with great power-added efficiency and P1 compression point. Given a nominal transmit power of 7.8dB, the RF output compression point of the second amplifier needs to be well above this value.

5.4.2 Cascade Analysis

An approximation of signal characteristics at each stage of the system was required in order to achieve the required signal gain, noise figure, and input/output compression points. This "cascade analysis" was conducted using Excel spreadsheets. The team performed a variety of cascade analyses to test multiple input signal levels across different gain stages. The example shown in Figure 7 shows the signal path for a -90 dBm input signal across the amplifiers the team selected.

User Input:		
RF Input Power, dBm	-90	
Temperature, °C	25	Spec:

Comments	Component Number	Component	Gain (dB)	Noise Figure(dB)	Gain Temperature Coefficient, (dB/°C)	NF Temperature Coefficient, (dB/°C)	Gain @ Temperature (dB)	Noise Figure at Temperature (dB)	TOI Temperature Coefficient (dB/°C)	Small Signal Gain (dB)	Running Noise Figure (dB)	Power At Input (dBm)	Power At Output (dBm)	Input Compression Point (dBm)	Output Compression Point (dBm)	Output Third Order Intercept (dBm)	Input Third Order Intercept (dBm)	Input Third Order Intercept (dBm)	Compression State Limiting Component	L -
														Insert One Only!!						
Antenna to System	1	SMA Transition	-0.1	0.1			-0.1	0.1		-0.1	0.1	-90.0	-90.1			99.0		99.1	Linear	
TQP3M9036	2	LNA	22.00	0.65			22.0	0.7		21.9	0.75	-90.10	-68.10		20.0			8.0	Linear	
MBUF001	3	Filter	-3.00	3.00			-3.0	3.0		18.9	0.77	-68.10	-71.10	50.0				60.0	Linear	
ADF7021-N	4	RX IC	30.00	1.00	0.008		30.0	1.0		48.9	0.79	-71.10	-41.10		-15.0			-35.0	Linear	
MBLF001	5	Filter	-3.00	3.00			-3.0	3.0		45.9	0.79	-41.10	-44.10	50.0				60.0	Linear	
ADF7021-N	6	TX IC	17.00	1.00	0.008		17.0	1.0		62.9	0.79	-44.10	-27.10		13.0			6.0	Linear	
MW7IC008NT1	7	TX PA	23.50	1.80	0.024		23.5	1.8		86.4	0.79	-27.10	-3.60		40.4			26.9	Linear	
MW7IC008NT1	8	TX PA	23.50	1.80	0.024		23.5	1.8		109.9	0.79	-3.60	19.90		40.4			26.9	Linear	
AFT05MS031NR1	9	TX PA	23.20	3.00			23.2	3.0		133.1	0.8	19.9	43.1		44.9			31.7	Near	-L
MBUF001	10	Filter	-3.00	3.00			-3.0	3.0		130.1	0.8	43.1	40.1	50.0				60.0	Linear	
System to Antenna	11	SMA Transition	-0.1	0.1			-0.1	0.1		130.0	0.8	40.1	40.0			99.0		99.1	Linear	

***Figure 7*: RED Cascade Analysis Stages**

Small Signal Gain	130.00 dB
Noise Figure	0.79 dB
Gain	130.00 dB
Output Power	40.00 dBm
Intercept Points	
Input Coherent	-79.43 dBm
Output Coherent	50.57 dBm
Compression Points	
Input	-89.43 dBm
Output	40.57 dBm

***Figure 8*: RED Cascade Analysis Results**

The summation of the RED cascade analysis is shown in Figure 8, with 130 dB gain, 40 dBm output power (10W), and a noise figure of 0.79 dB. This analysis demonstrates that if each of these system blocks performs correctly, the RED will perform to the desired specifications described previously.

Figure 9 shows the intended RF signal pathway at the minimum receive sensitivity and transmit power. Insertion loss of the T/R switch and filters are included, although it assumes perfect match between ports. In going from the digital signal to RF-out within the second transceiver IC, the programmable power output involves automatic gain control that allows a consistent RF-out, even as the input at the receive end varies. To provide 46dB of gain, the PA stage is most effectively implemented by cascading two amplifier ICs.

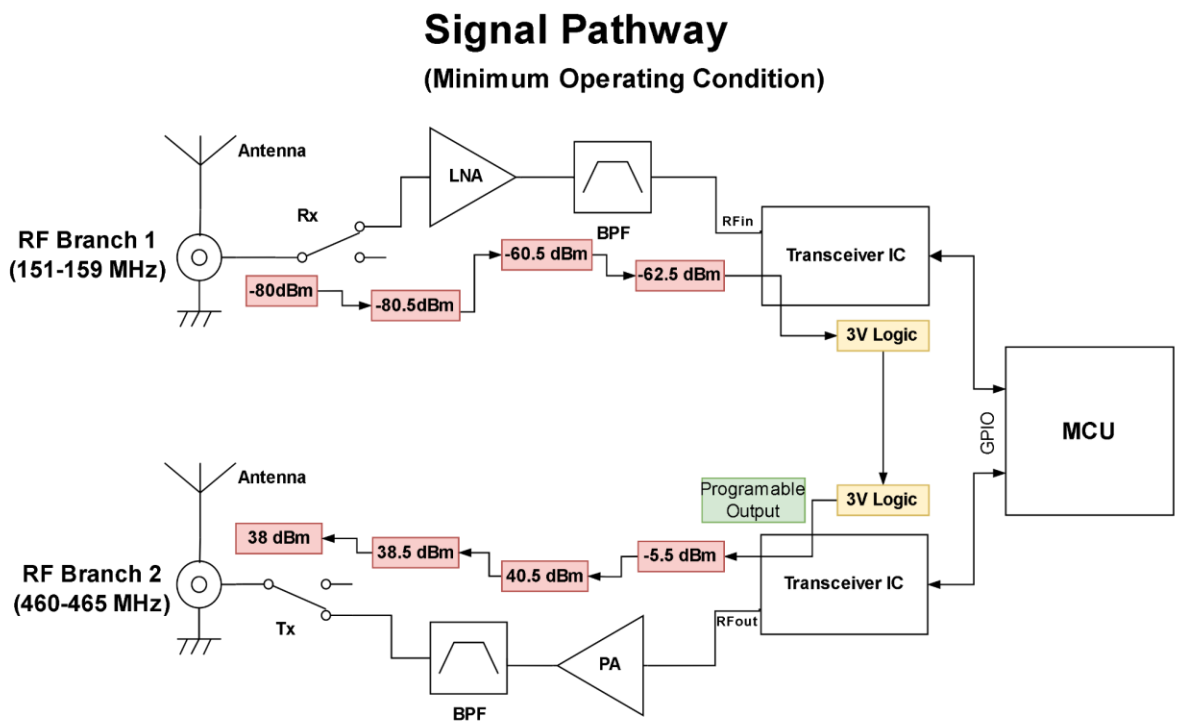

***Figure 9*: RED Signals Pathway (VHF to UHF)**

While Figure 9 presents the case of receiving at the VHF channel and transmitting at the UHF channel, similar analysis is carried out when relaying from VHF to UHF. The same filters, LNAs, and PA chips can be used at either frequency range with similar performance,

provided they have the appropriate peripheral components and matching networks for the desired frequency range.

5.4.3 Mechanical Design and Layout

The RED enclosure requires materials that can withstand high levels of heat from the fire ground, given that the device will be in operation while firefighters are actively handling the fire. Specifically, this device would be able to adhere to NFPA 1802 standards for systems in fire grounds to withstand 350 F^o for 15 minutes while still maintaining performance. Additionally, the material for the RED needs to be waterproof, high strength, corrosion resistant and cannot block RF signals. The RED also needs to be able to handle hard impacts from being dropped or bumped into by the firefighters. As a result, the structural body of the device was made from NylonG High-Temperature composite. This 3D printable filament is composed mainly of nylon and is filled with approximately 20% glass fiber to increase the thermal resistance, impact strength, and tensile strength of the enclosure. Of the components making up the enclosure, the handle, bottom cap, top cap, shell, and internal inserts are all made of NylonG.

To thermally insulate the inside of the RED further and to make it more resilient to bumps and drops, a silicone wrap was designed to fit around the outside of the device. This is a high-temperature silicone sheath that goes around the 3D printed body. This silicone is known as Mold Max 60 High-Temperature silicone. The silicone was poured around a 3D printed surrogate model of the main body, and then slid over the actual device. Outside these two primary materials, the RED also has a few different screws, nuts, and threaded inserts throughout the enclosure to attach the different parts securely. These fasteners are all size M4 and either coated or stainless steel, with the screws varying in length depending on the location within the device.

To handle cooling of the electrical components, phase-change material heat sinks were constructed. These heat sinks are 4in long 0.5in x 0.5 in square 6061 aluminum tubes that are filled with paraffin wax and sealed at both ends. These heat sinks passively cool the electrical systems by storing the heat that they create.

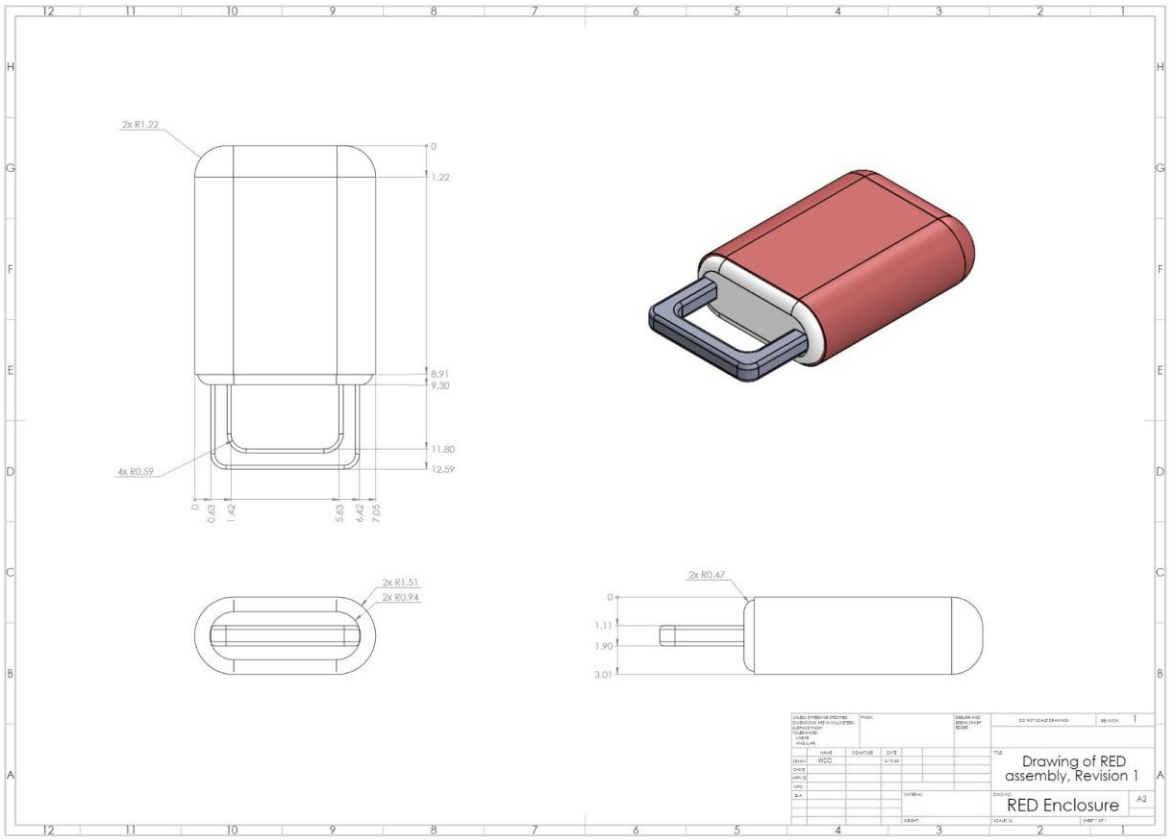

***Figure 10*: Drawing of RED Assembly**

5.4.4 Software Features

The RED software has two separate states, data collection mode and data visualization mode. The data collection state utilizes the connection between the Raspberry Pi Zero W (PZW) and a MSP430 (MSP) to collect data points while it's in use. After the RED has been run, the user can switch the RED into the data visualization state where it graphs the data points and displays the generated graphs on a website hosted by the PZW. The website is accessible in the data visualization state by connecting to the PZW network and typing 192.168.4.1:8081 into the address bar of a web browser.

In the RED's data collection state, the PZW and the MSP communicate using general purpose input/output (GPIO). The MSP acts as an interface with the RED hardware, collecting data from the temperature sensor and the PZW listens for the MSP to send the data over.

In the RED's data visualization state, the data collected from the data collection state passes through a python script using the Pandas and Matplotlib libraries to create graphs. The graphs generated allow the user to see the internal temperature of the device at specific times. The graphs are loaded onto a website hosted by the PZW, where the user can select a date when the RED was used, and view the data associated.

Chapter 6: Component Design, Prototype Building, and Testing

Chapter 6 presents the team's second deliverable: the design, build, and test of each component of the device conceptualized in Chapter 5. Assembled together as a full RED, these components would provide a solution to fireground signal losses. In general, the design concept of each component is presented first, followed by the selection and/or design process. Then, test results are explained, including the troubleshooting steps the team took when taking measurements. Finally, the current status of each component is discussed as well as component-specific future improvements.

6.1 Electrical Subsystems

6.1.1 Planar Inverted F-Antenna (PIFA) Antennae for VHF/UHF Communications

6.1.1.1 Motivation

The L3Harris radios used by the Meriden Fire Department employ a flexible, rubber-enclosed helical monopole antenna. The same product can be purchased from Waveband Communications for $100. While able to provide 360° omni directionality in the azimuthal plane, monopole designs usually require the antenna body to stick-out from the device, and achieving resonance typically requires their physical lengths comparable to the radiation wavelength. For instance, the wavelength of Meriden fireground 1 is nearly 2m, while fireground 3 is around 65cm, and the department radios use a 21cm helical antenna. This is longer than the main body of the handheld radio itself. With mobile cell phones, use of monopoles has long-since been abandoned in favor of PCB-fabricated antennas and chip-

antennas. This was aided by the fact that the wavelengths used in cellular communication are much smaller than those used by most portable radios.

We therefore sought to develop an antenna system that could be fabricated using PCB technology and have adequate performance at VHF or UHF frequencies. Its physical size should be miniaturized, allowing it to be contained within the radio chassis, and the polarization of the outgoing waves must be compatible with other radios using monopole antennas. To these ends, the Planar Inverted F-Antenna (PIFA) structure was adopted.

6.1.1.2 PIFA Background

PIFAs have received much attention in the area of mobile communications over the past 20 years. The development of planar antenna designs has been driven by demand for low-profile radiating structures and the proliferation of printed circuit board (PCB) technology. The basic PIFA structure seen in Figure 12 is an adaptation of the micropatch antenna. The micropatch consists of a “top” layer of copper and a “ground plane” separated by a dielectric substrate. For rectangular geometries, this structure is resonant when the electromagnetic wavelength (in the dielectric medium) is twice that of the patch length. The PIFA miniaturized the micropatch approximately in half by adding a “shorting sheet” at the edge of the PIFA that connects the top copper layer to the ground plane. This in principle makes the PIFA an equivalent “half-section” of the corresponding micropatch, hence resonance occurs at approximately quarter-wavelength (when the shorting sheet is the same length as the width of the patch). The PIFA is fed via coaxial cable, and the position of the feed can be changed to adjust the radiation impedance.

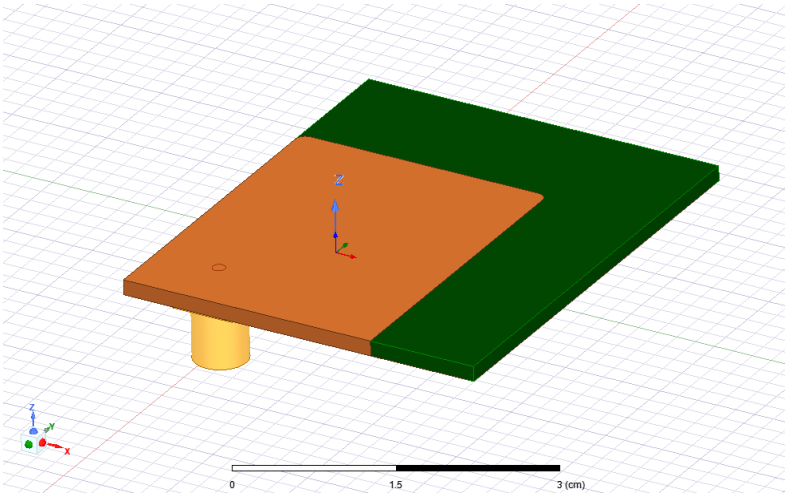

Figure 12: **Standard PIFA Structure with Coaxial Feed**

6.1.1.3 Shorting Sheet/Pin

The λ/4 design of the PIFA applies when the shorting sheet is connected along the entire edge of the top patch, as it is in Figure 12. However, the length of the shorting sheet may be reduced to increase the electrical length of the antenna, as shown in Figure 13.

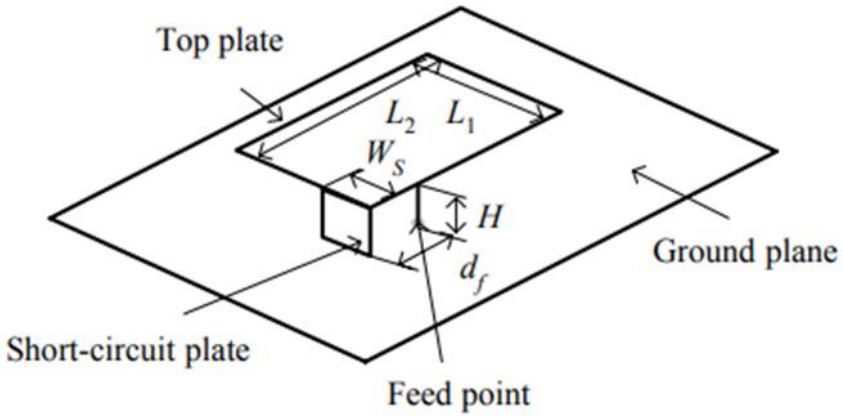

Figure 13: **Structure of PIFA with Variable Shorting Sheet.**

The top patch is shorted to the ground plane by a plate of width W-$_s$, and the impedance can be tuned by controlling the displacement of the feed-point with respect to the shorting sheet. Can also be thought of as a folded monopole that is broadened into a sheet (Jianwei He, 2006)

The resonant frequency depends not only on the dimensions of the radiating patch, but those of the shorting sheet as well. Assuming an infinite ground plane, the resonant frequency can be approximated the following (*Jianwei He, 2006)*:

Equation 1

$$f_r = \frac{v_p}{4 * (L_1 + L_2 + H - W_s)} \left[1 + \left(\frac{W_s}{L_1}\right)\frac{L_1 - W_s}{L_2 + H}\right]$$

L_1 is the length of the top patch parallel to the shorting sheet (x-direction)
L_2 is the length of the top patch perpendicular to the shorting sheet (y-direction)
W_s is the length of the shorting sheet
H is the height of the shorting sheet
V_p is the phase velocity in the medium

For now, the displacement from the feed-point to the shorting sheet is not taken into account. The two extreme cases are where the length of the shorting sheet is the same as patch dimension ($W_s=L_1$), or when the shorting sheet is replaced with a "pin" and is practically zero ($W_s=0$). Both see the second term in *equation 1* vanish. Note that second condition minimizes the resonant frequency to:

Equation 2

$$f_r = \frac{v_p}{4 * (L_1 + L_2 + H)}$$

For this reason, the shorting pin is commonly used in PIFA designs, albeit at the expense of radiation bandwidth. In practice, this shorting pin was implemented using a plated through-hole via and placed at the corner of the top patch.

6.1.1.4 Location of the Feed

The location of the feed provides the primary adjustment for the radiation impedance of the antenna. Bringing the feed point closer to the shorting pin decreases the maxima of the radiation resistance and reactance curves. This can be controlled to achieve good matching to

a 50Ω transmission line. Since the resonant frequency will be lightly affected by the displacement between the feed and the shorting pin, a corresponding adjustment in the antenna dimensions may compensate.

6.1.1.5 Tuning Slots and Meandering Trace

To finalize the miniaturization of the antenna, slots can be etched into the top copper patch to give the rectangular surface a slightly meandering path. This increases its effective electric size by lengthening the average flow path of current along with the patch, as seen in Figure 11. The tradeoff of the meandering patch is a loss in the bandwidth of the system, as resonant current flow occurs for only a narrow frequency band.

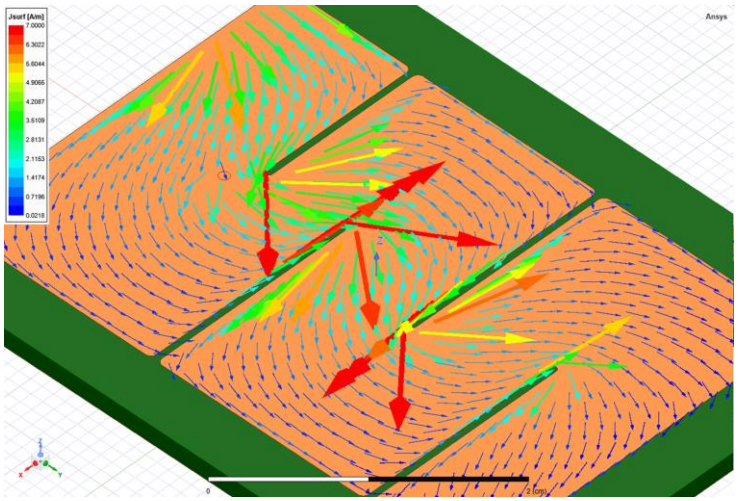

Figure 14: **Surface Current Along the PIFA Top Patch with Meandering Trace**

The slots provide an on-bench tuning option for the antenna. By removing copper to lengthen the slot, the effective electrical length may be increased, while by adding copper tape over the end of a slot, the effective electrical length may be decreased. This means that if the antenna is designed to resonate at a slightly lower than intended frequency, the resonant curve can be easily shifted upward with trial and error to exactly target the desired frequency.

6.1.1.6 UHF PIFA (460MHz)

The shorting-sheet PIFA with the addition of a meandering trace is suitable for Fireground 2 at a 65cm wavelength (460 MHz). Using an FR4 substrate with a standard 60 mil thickness, Eq 2 was used as a starting point for selecting a width and length for the top patch, and adjustments were made using Ansys HFSS. Due to the simplicity of the design, the WPI Makerspace was capable of fabricating the UHF antenna. The shorting sheet was realized with a strip of copper tape connecting the top and bottom layers of the PCB. This required the edge-cut of the board to be at the edge of the top copper layer. The feed pin was realized with a plated through-hole and copper wire that was soldered on either side of the through the hole.

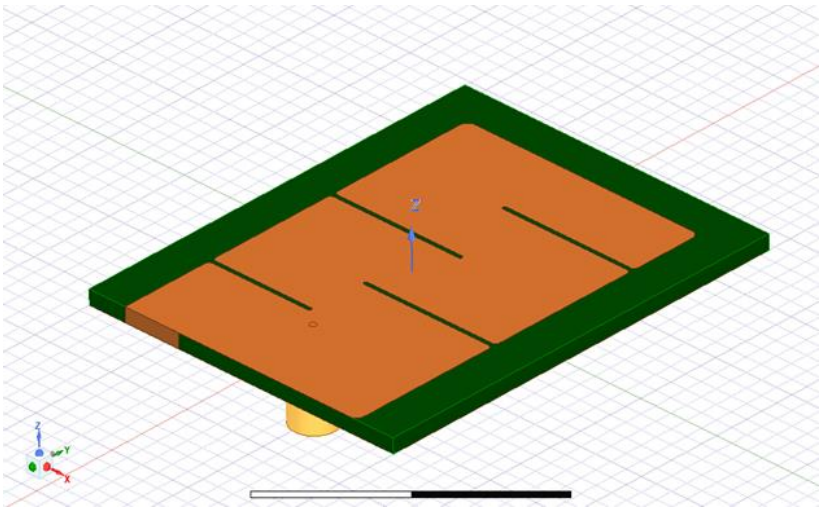

***Figure 15*: UHF PIFA HFSS 3D-Model**

The dimensions of the top patch are 31mmx45.5mm, (which we classify as a λ/7 design, since the longest dimension is 1/7 of a wavelength at 460 MHz in media). Seen in Figure 16, the return loss computed through HFSS simulation has a -10dB bandwidth of 13.3 MHz (2.9%). The value at Fireground 2 (460.1625MHz) is -16.13dB.

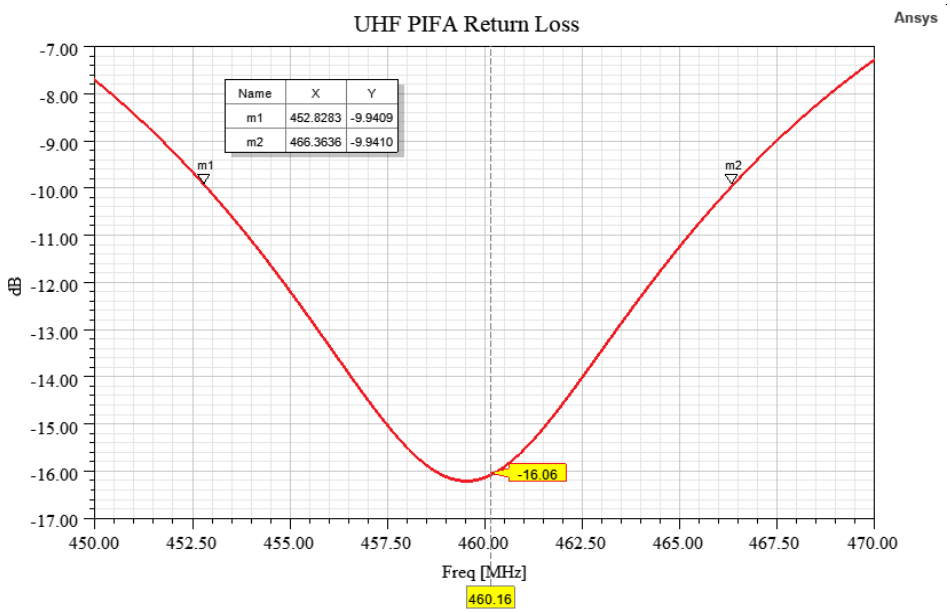

Figure 16: **HFSS: Return Loss of UHF PIFA**

6.1.1.7 Far Field Pattern

The simulated far-field radiation pattern seen in Figure 17 has two main lobes oriented opposite one-another. Each lobe has peak directivity of 1.15 and beamwidth angle of 53° at 90% power.

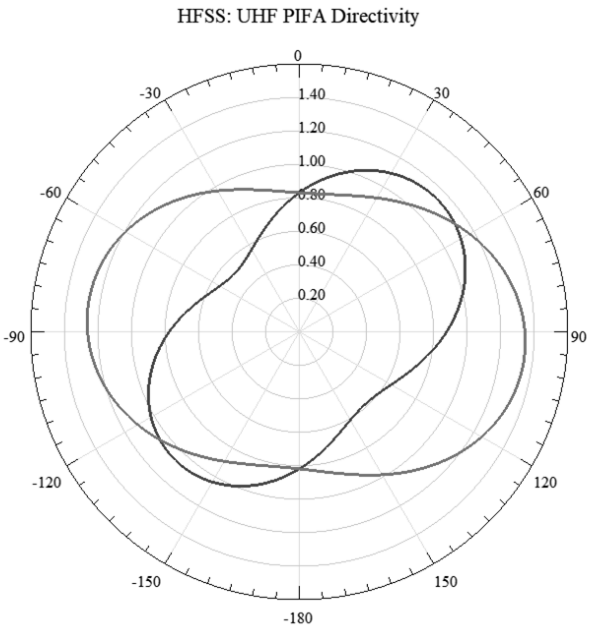

Figure 17: **E Plane (gray) and H Plane (black) Directivity of UHF PIFA**

6.1.1.8 Simulation Inside Enclosure

To predict the effects of placing the antenna inside an enclosure, a 5mm thick nylon box (PA6 30% glass fiber) was placed around the antenna in the 3D model, as shown in Figure 18.

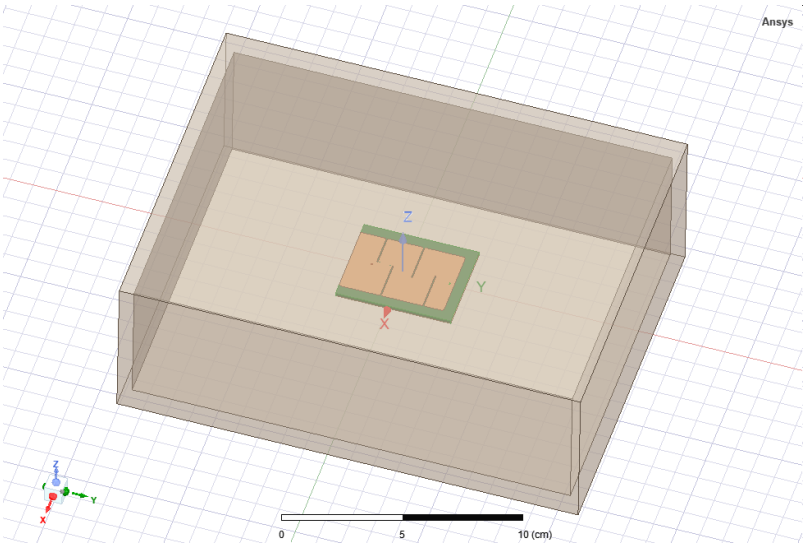

Figure 18: **PIFA Within 1cm Nylon Box**

The HFSS simulation found the enclosure had negligible impact on the antenna impedance. However, as seen in Figure 19, the radiation pattern has greater directivity and inferior omni-directionality. The peak directivity is now 1.3 with a 90% power-density angle of 45^{o}. The minimum of the directivity curve dropped from 0.5 to 0.4.

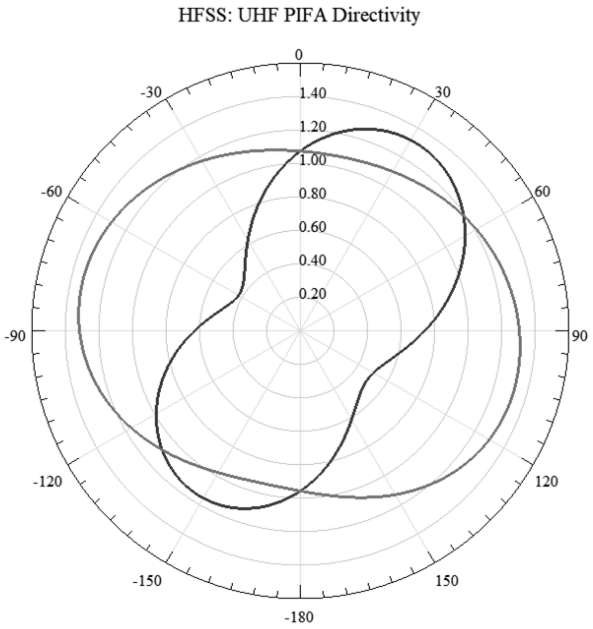

Figure 19: **UHF PIFA E-plane (gray) and H-plane (black)**

Directivity within 1cm Nylon Box

6.1.1.9 Fabrication and Measurements Results

The UHF antenna went through design review and fabrication at the WPI Makerspace. After fabrication at the Makerspace, the SMA connector was soldered to the antenna. Since the Makerspace was not able to include plated through holes, a solid copper wire was used as a substitute. The wire was forced through the non-plated through-hole and soldered to the top patch as well as the inner conductor of the SMA connector. To add the shorting sheet, a copper sheet was taped with Kapton in the appropriate location. Shown in Figure 20, the antenna was connected to the RF analyzer. Additional strips of copper were added as part of the convenient tuning option discussed in 6.1.1.5 Tuning Slots and Meandering Trace.

Figure 20: **UHF PIFA with Implemented Tuning Strips**

Seen in Figure 21, the tuning option of covering the slots with copper tape was successfully able to raise the resonant frequency such that the minimum return loss was in the range of 460-465MHz. The measured impedance at 460MHz is approximately 72-j14Ω.

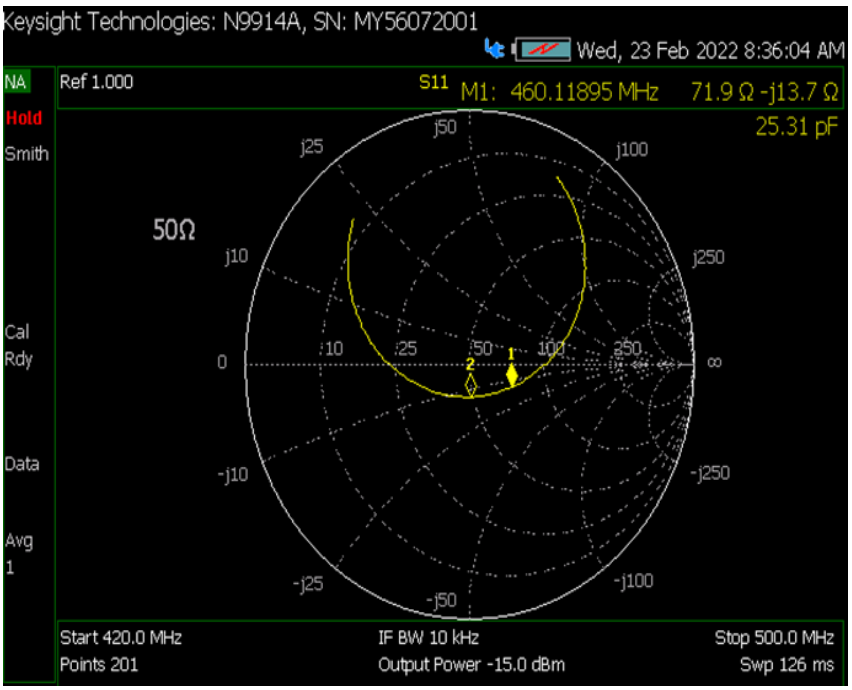

Figure 21: **UHF PIFA with Implemented Tuning Strips on Network Analyzer Smith Chart**

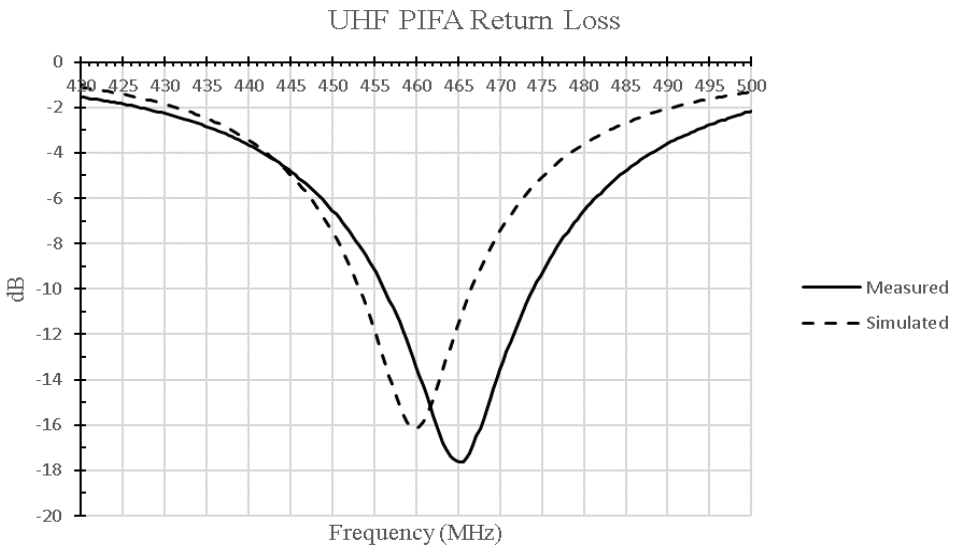

Figure 22: UHF PIFA Return Loss Comparison

Seen in Figure 22: the antenna impedance measured with the RF analyzer follows the characteristic PIFA impedance curves observed in literature as well as the HFSS simulations. However, seen in Figure 23, the measured values differ from those that were computed in HFSS. For instance, the maximum antenna resistance was measured to be 120Ω, while in the simulation this was expected to be 70Ω.

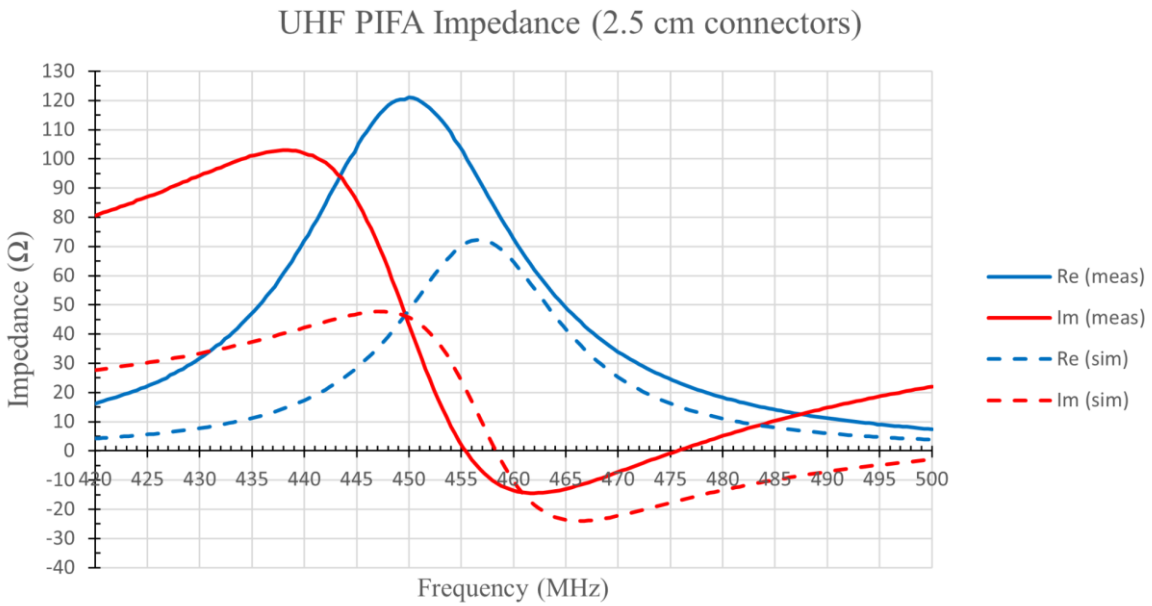

Figure 23: **UHF PIFA Impedance with 2.5cm Connectors**

When taking these measurements, the RF analyzer was not calibrated to the BNC-SMA connector, which were not modeled in the simulation. Transforming the impedance back across the 2.5cm of 50Ω Teflon-insulated (lossless) transmission line gives the curve shown in Figure 24, which very closely resembles the results of the HFSS simulation. For instance, the maximum antenna resistance is now 75Ω at 459MHz, compared to the simulated 70Ω at 457MHz. It is important to note that the addition of the TL hardly changed the magnitude of the reflection coefficient–it primarily changed the phase only– and this leads to the significant difference in input impedance at the input of the line.

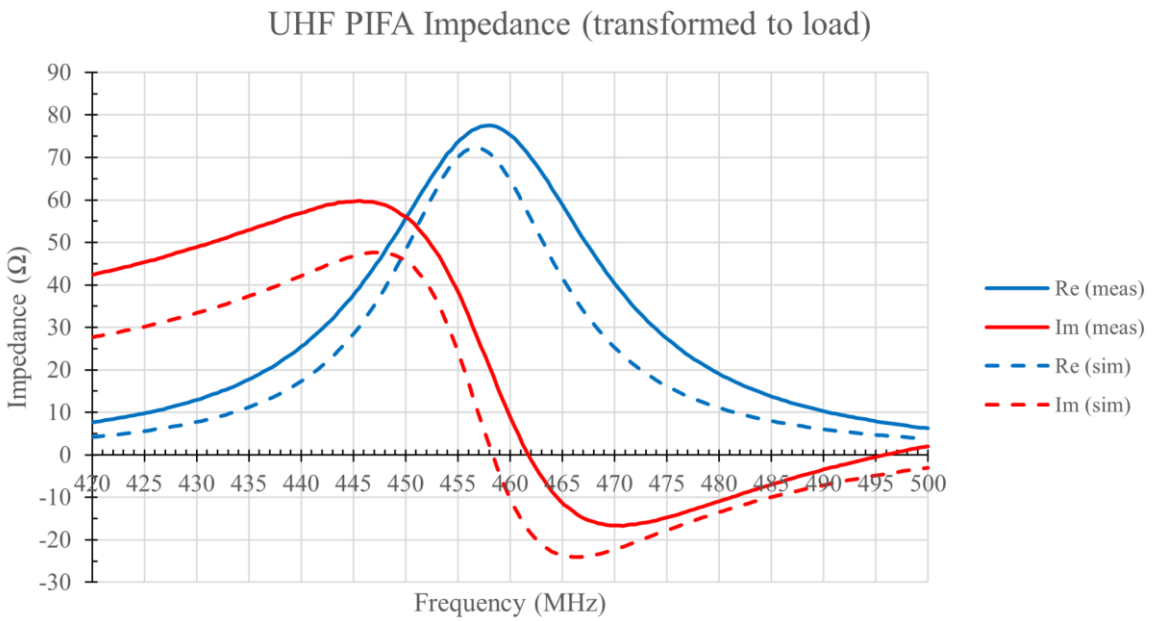

Figure 24: **Measured UHF PIFA Impedance with 2.5cm, 50Ω, 0.69 Velocity Factor TL**

With the assistance of Professor Makarov (as part of ECE 5105), we will be able to use anechoic chamber to measure the radiation pattern of each antenna.

6.1.1.10 VHF PIFA

The shorting pin and meandering path, however, are not alone sufficient to miniaturize the design for Fireground 1 or 3, whose wavelengths are nearly 2m (150 MHz). Following *equation 1*, a PIFA with a shorting pin (W_s=0) would be called for. However,

given the thickness of FR4 boards is typically less than 1cm, and supposing a square patch, the length would need to be around 12cm (since the wavelength in medium is 95cm, this would be described as a (λ/8) design). With a goal of the largest dimension being less than 8cm, this analysis demonstrates that the PIFA structure is not alone sufficient to miniaturize the antenna for our purposes. Furthermore, we assumed an infinite ground plane, which is not realizable with a PCB. To increase the electrical size of the antenna, we employed the use of a capacitive load and capacitive feed as described in the following sections.

6.1.1.11 Capacitive Load

The capacitive load increases the electrical length of the antenna by effectively adding another stretch of transmission line to the terminal of the antenna. In principle, a lumped capacitive termination is equivalent to a stretch of open-circuit line with the length.

Equation 3

$$l = \frac{\lambda}{2\pi}\tan^{-1}\left(\frac{1}{\omega Z_0 C}\right)[m]$$

In practice, however, a discrete capacitor is not used; the load is realized by the addition of a layer of copper between the top patch and ground plane. Either side-plating or blind vias are needed to connect this inner layer to the top patch or ground plane. Modeling this element as a lumped capacitance is not very precise–it is more accurately described as an additional length of transmission line with a characteristic impedance determined by the dimensions of the copper patch and the thickness and material properties of the prepreg layer. Nevertheless, the principle of the capacitive load suffices in its prediction of increasing the electrical length. Using ANSYS HFSS, we were able to design a capacitive load which provided another doubling of the electrical length, corresponding to a λ/16 physical design.

The capacitive load is not without its drawbacks. While resonance occurs at a lower frequency, this frequency is more specific, and the electrical properties of the antenna are more sensitive to a change in operational frequency. Hence, the impedance bandwidth of the antenna is drastically reduced. Additionally, the requirement for blind vias introduces costs to PCB fabrication.

6.1.1.12 Capacitive Feed

The canonical radiation resistance and reactance curves for the PIFA are shown in Figure 24. Resonance occurs when the imaginary component (reactance) is zero, which coincides with a maxima of the real component (resistance). A drawback to the PIFA's reactance curve is that it crosses zero where its slope is greatest, meaning the device is sensitive to any deviations in the operational frequency, manufacturing tolerance, and simulation accuracy. The capacitive feed can in part compensate for this in that adding a lumped capacitor at the input adds a discrete negative reactance to the radiation impedance of the antenna, shifting the reactance curve down, and allowing the resonant frequency to be more precisely controlled. In the same manner as the capacitive load, a discrete component is not used—rather, an inner layer of copper is added to the antenna. While this copper layer is most accurately described as a distributed element line rather than a discrete capacitance, HFSS simulation supports the principle of the capacitive feed. Seen in Figure 25 the capacitive feed adds a negative reactance to the reactance curve of the PIFA, moving it down and thereby shifting the resonant point.

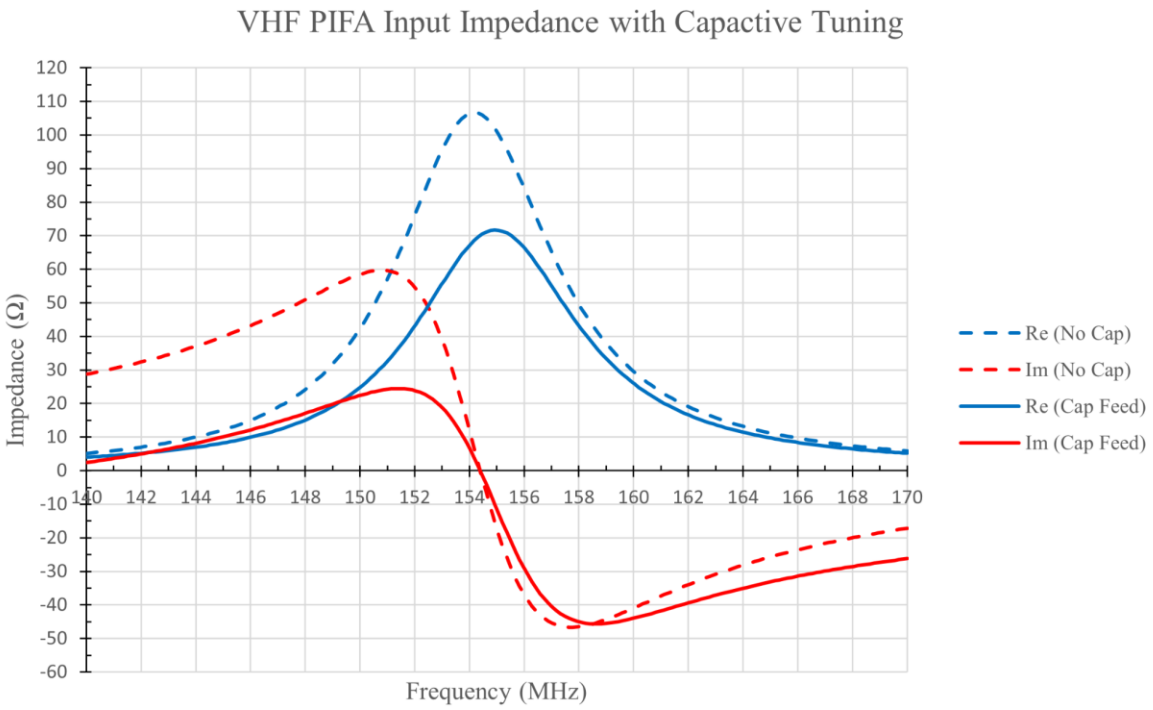

Figure 25: **Impedance Curves of the PIFA With and Without Capacitive Feeding**.

A capacitor adds a negative reactance, shifting the reactance curve (red) downwards. This enables selective tuning of the resonant frequency of a miniaturized antenna.

In practice, the feed is realized with a surface mount coaxial connector. The outer coaxial conductor is connected to the ground plane, and the inner conductor leads to a via. With no capacitive feed, the via is a through hole, going to the top patch. With a capacitive feed added onto the second layer, the via is blind and connects to the patch on the underside of the prepreg.

Eq. 2 was used as a starting point for selecting a width and length for the top patch. Thickness and material properties for the core and prepreg were chosen for compatibility with the PCB manufacturer. Table 1 shows the parameters used to design the PIFA for fabrication by PCBway. The core material is FR4 150g, with 2116 prepreg. The dimensions of the top patch are 40mmx55.4mm, (which we classify as a λ/17 design, since the longest dimension is 1/17 of a wavelength at 153.835 MHz in media).

Table 1. VHF PIFA Parameters for PCBway

Parameter	Value
Design Frequency	153.89MHz
Top Patch Dimensions (L1 x L2)	40mm x 55.4mm
Bottom Plane Dimensions	60mm x 80mm
Capacitive Load Dimensions	40mm x 4.155mm
Capacitive Feed Dimensions	12mm x 13.85mm
Copper Layers	35µm (1oz/ft2),
Core Material	(FR4 140g)
Core Thickness	1.6mm
PrePreg Material	2116 (Resin)
PrePreg Thickness	0.11mm
Via Diameter	0.5mm
Connector Material	Gold plated, , Teflon insulator

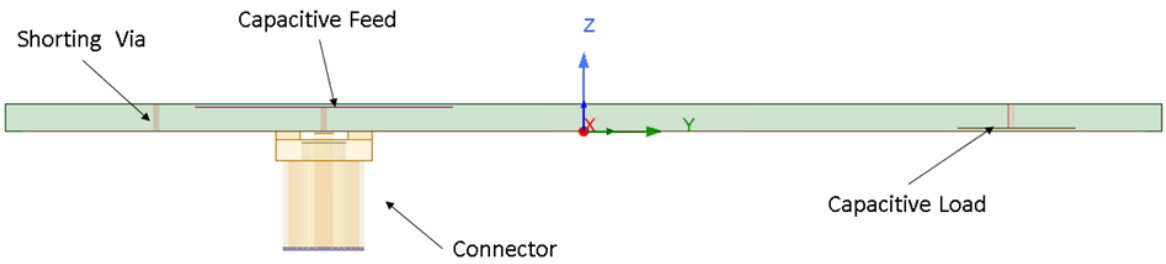

Figure 26: **3D Model of the PIFA from the Side-View**. A model of an SMA connector was used as the reference for the wave-port to conduct modal analysis in HFSS.

6.1.1.13 Return Loss and Bandwidth

Figure 27 shows the simulation result for return loss of the VHF PIFA. Referenced to 50 ohms and choosing -10dB (90% power transfer), the impedance bandwidth of the antenna is 3.4%. The minimum return loss of -16dB coincides with 153.89MHz (input impedance of 59.4+j1.95 Ω).

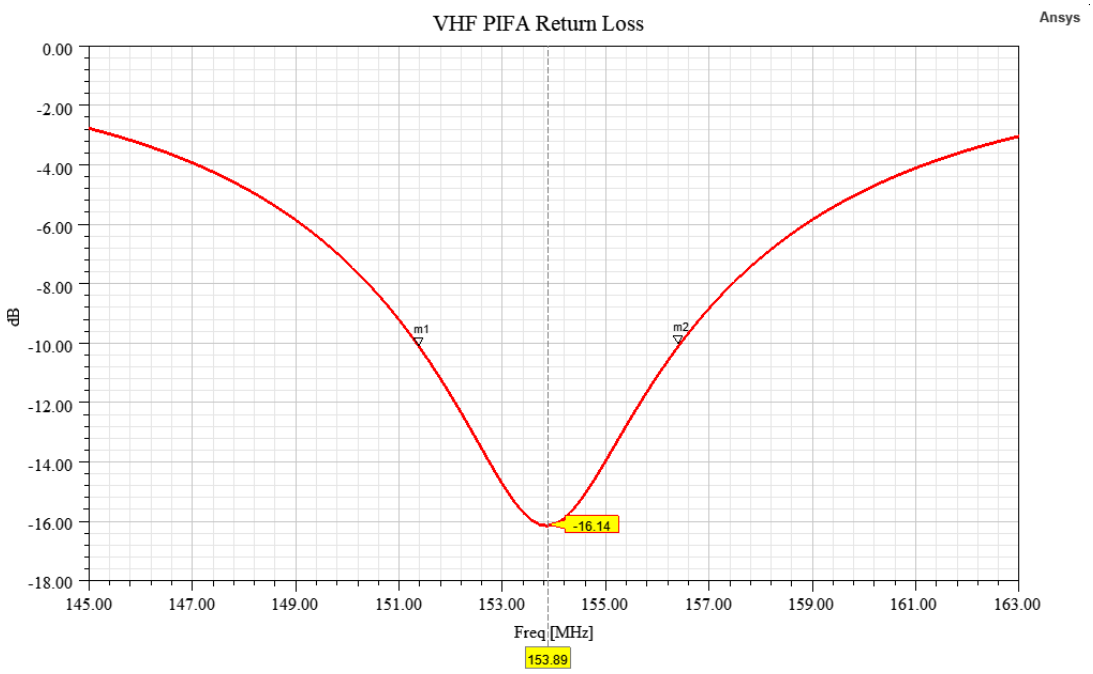

Figure 27: **HFSS: VHF PIFA Return Loss**

6.1.1.14 Far-Field Radiation Pattern

The simulated PIFA far-field pattern seen in Figure 28 resembles a torus shape whose axis is rotated 90° along the polar and -60° along the azimuth. This is consistent with the shorting via being located in the back-right corner (3rd quadrant) at an angle of -53.7. This is disadvantageous compared to the monopole due to the orientation of the PIFA in the radio. It will be placed flush the substrate, meaning the pattern will not spread out omnidirectionally in the plane of the antenna profile.

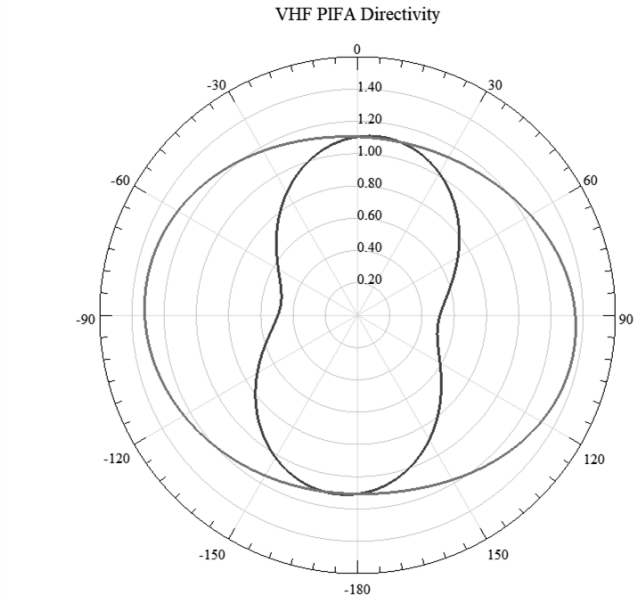

Figure 28: **VHF PIFA E-plane (gray) and H-plane (black) Directivity**

With the VHF antenna, gerber and drill files were placed in an order to PCBway. Initially, we attempted to work with a PCB manufacturer with facilities in New England, however their customer support was not attentive enough to make us feel comfortable with sending them an atypical PCB design. Given the time constraints, we chose the overseas manufacturer in PCBway who provided an expedient response to our requests. Unfortunately, the arrival date was March 7th, a few days after the submission of this report.

6.1.1.15 Current Status of Antennae

The UHF antenna was successfully verified using the network analyzer. Measurement of the gain profile and radiation pattern could be conducted in an anechoic chamber, and compared to simulated results. A possible design improvement to the UHF antenna is to use a shorting pin rather than a shorting sheet, as well as a Rogers material rather than FR4. A Rogers material would be more expensive but would reduce antenna losses. For the VHF antenna, to complete assembly, an SMA connector needs to be soldered onto the feed. The

performance of the VHF antenna in terms of S parameters can be tested using the network analyzer, and the gain and pattern can be measured in the same way as the UHF antenna.

6.1.2 Transmit/Receive Switch (T/R Switch)

When the RED is using a given antenna as a transmitter, the connection between that antenna and its corresponding LNA on the receive-branch needs to be attenuated. Otherwise, the input impedance of the LNA would be in parallel with the antenna, diverting power away from the antenna and possibly damaging the input of the LNA. In turn, when the antenna is used as a receiver, the connection to the LNA needs to be re-established, while the connection from the antenna to the power amplifier on the output branch needs to be attenuated. Towards this end, a single-pole double-throw RF switch was designed using PIN diodes. PIN diodes are useful for RF applications because their off-characteristic has low junction capacitance, allowing them to attenuate high frequency signals. They are also excellent for medium-power applications because their on-characteristic has high parallel capacitance, so even if the signal amplitude exceeds the DC bias voltage, the PIN diode will not go into its reverse-bias region.

Seen in Figure 29, a simple configuration was constructed in ADS using two PIN diodes (MACOM-4P7104). Each diode connects the antenna (port 1) to either the Rx (port 2) or Tx (port 3) stages. The Tx_CTRL and Rx_CTRL lines supply the DC bias voltages for each diode, and should be at opposite logic-levels. 4.7uH RF-chokes and 1uF DC blocks are used to control the RF and DC signal paths.

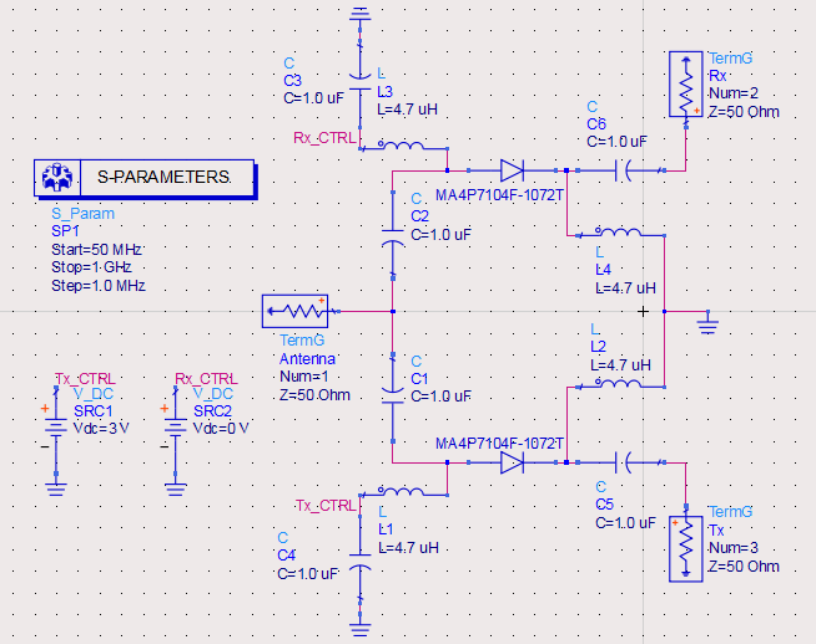

Figure 29: **PIN Diode SPDT Switch Schematic**

Figure 30 shows an S-parameter simulation looking at the RF signal pathway from the transmitter (port 3) to the antenna (port 1) and receiver (port 2) when Tx is enabled. Since S31 sees only one PIN diode, the insertion loss is minimal, with -0.05dB at 154MHz and -0.1dB at 460MHz. The greater loss at high-frequencies is largely due to the parasitic inductance of the diode package. Since S32 sees only one diode in reverse bias, the isolation is far from ideal, with -30dB at 154MHz and -20dB at 460MHz. The inferior isolation at the higher frequencies is largely due to the junction capacitance.

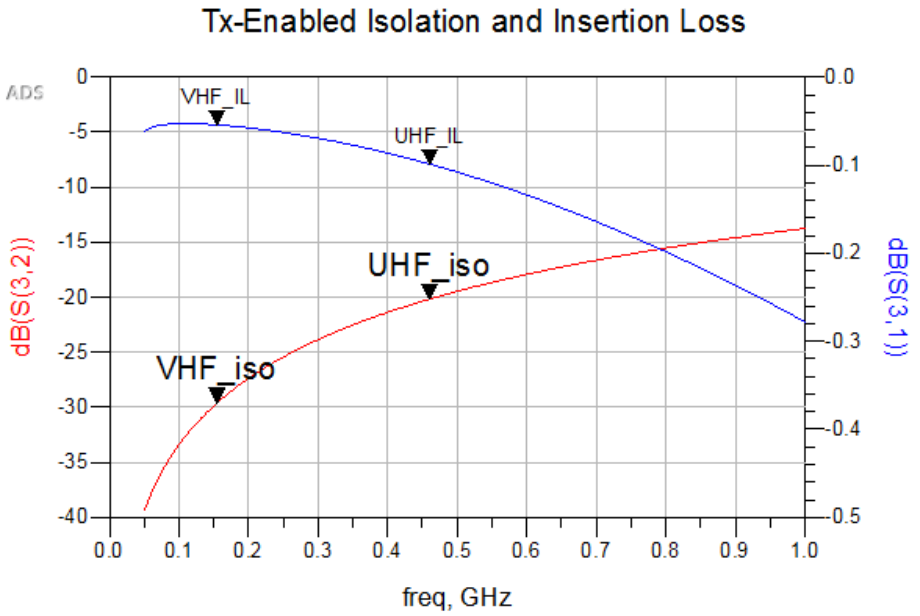

Figure 30: **Isolation and Insertion Loss in Tx mode**

Since the maximum rated RF input power of the LNA (TQP3M9036) is +22dBm, and the nominal transmit power from the PA-stage is 37.8dBm, -20dB of isolation satisfies the absolute minimum requirement to not damage the LNA. Still, improved isolation can be achieved by adding additional PIN diodes at the expense of insertion loss. This method is frequently used in off-the-shelf ICs, which expand upon the basic two-diode SPDT circuit. A suitable off-the-shelf component for the RED is the Skyworks 13278-313LF RF switch. The device is rated to 0.4dB insertion loss and -32dB isolation at 460MHz. The switch can be powered by the same 3.3V supply as the MCU, and its logic can similarly be controlled by an MCU GPO. Its 0.1dB compression point at 900MHz is at an RF input of 40dBm, enough above the 37.8dBm specification of the RED to avoid issues with linearity.

6.1.2.1 Current Status of T/R Switch

Since no T/R switch was manufactured, no testing with the network analyzer was completed. Going forward, the T/R switch can be used to integrate the antenna into the front end of the RF system. If one were to use the current LNA and PA modules, a separate evaluation board with the T/R switch would be needed. It would have three RF ports, one for

the LNA, PA, and antenna each. It would also have a 3-5V header for the buck converter, and two control headers for the microcontroller. A pre-made eval board can also be bought directly from Mouser. Alternatively, a fully integrated front-end would have the T/R switch placed onto the same board as the LNA and PA, in which case the antenna could be mounted nearby on the PCB, rather than at the end of a long coax cable.

6.1.3 Low-Noise Amplifier (LNA)

This section covers the design concept of the RED Low-Noise Amplifier (LNA), LNA selection and testing, and current status. The LNA purchased worked as intended before and after integration with the bandpass filter and thermal testing, so this system block was completely successful.

6.1.3.1 LNA Design Concept

REDs must receive an incoming signal and amplify it to reduce instances of radio signal loss for firefighters. Low Noise Amplifiers (LNAs) are commonly used for such repeaters because “Low Noise” refers to a weak input signal received by a system. This means that LNAs are a contributor to a given system’s “sensitivity;” that is, the minimum receivable signal that the system can process.

At a minimum, each RED was intended to replicate the specifications of the L3Harris XL-200P, the handheld radios used by MFD. The XL-200P is rated for -122 dBm, and the team found this design goal very challenging because the output power of each RED must be a minimum of 6 W (~37.8 dBm). This would have required 159.8 dB of gain.

While possible, the team does not have enough experience with high power applications and gain stability management. Therefore, REDs were designed for a minimum of -80 dBm, reducing the gain required to ~117.8 dB. -80 dBm was also more realistic because REDs can be placed in a given location before firefighter radio signals are weaker than -80 dBm. For

example, if a fire crew walks far enough into a building that the chief outside cannot reach the crew, a RED could be placed at a point in between these two MFD handhelds such that neither signal drops lower than -80 dBm.

6.1.3.2 LNA Selection and Testing

With these signal amplification needs in mind, the team selected the TQP3M9036 LNA manufactured by Qorvo. This LNA exhibits excellent noise and stable gain characteristics across the RED operational frequencies at the cost of 5V and no more than 1A.

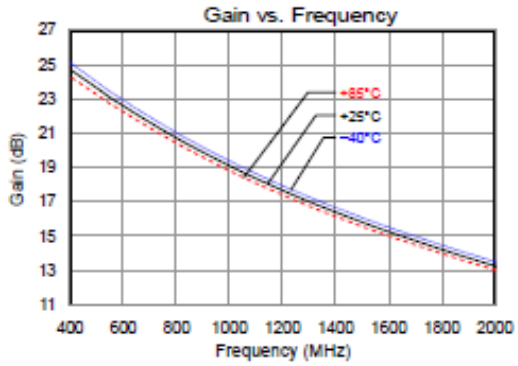

***Figure 31*: RED LNA Gain vs. Frequency**

As shown above, the TQPM9036 provides a typical 23.5 dB gain across RED operational frequencies and temperatures. The TQP is also rated for a noise figure of no more than 0.45 dB:

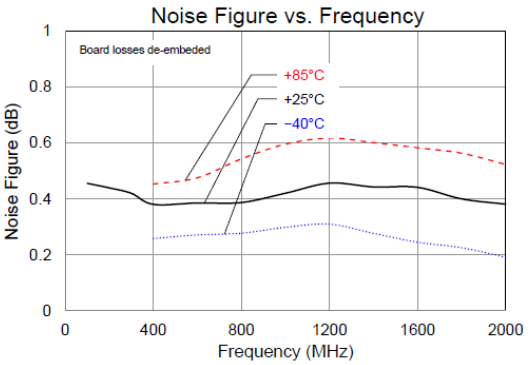

***Figure 32*: RED LNA Noise Figure vs. Frequency**

In this case, noise figure measures how much TQP degrades the signal-to-noise ratio. This is a ratio to compare the strength of a given signal to the background noise of the

system, and the TQP does not degrade the signal strength more than what is typical of the amplifiers researched for the RED.

Furthermore, the input power limit is specified as +22 dBm, and the output power limit is +20 dBm. Given the previously described RED approach and the TQP's purpose in the RED system, this LNA will not need to receive signals of more than about +10 dBm, nor will this LNA need to amplify signals beyond +20 dBm. Additionally, due to power limits on available lab equipment, the TQP's output compression cannot be examined in detail without risking damage.

Once the LNA arrived, the team verified the serial number, visually inspected the PCB for soldering issues, and connected the device to a lab power supply per the datasheet. 5V was supplied via alligator clips, and the current limit was set to double the anticipated current requirement. To avoid destroying the FieldFox network analyzer by exceeding the input power limit, the team set the analyzer output power to -25dBm and connected a 20dB attenuator to the output side of the LNA as below. To avoid causing RF interference in Atwater Kent, the team attached the VHF bandpass filter to the LNA eval board. The team then the team powered up the LNA and found that it performed according to specifications:

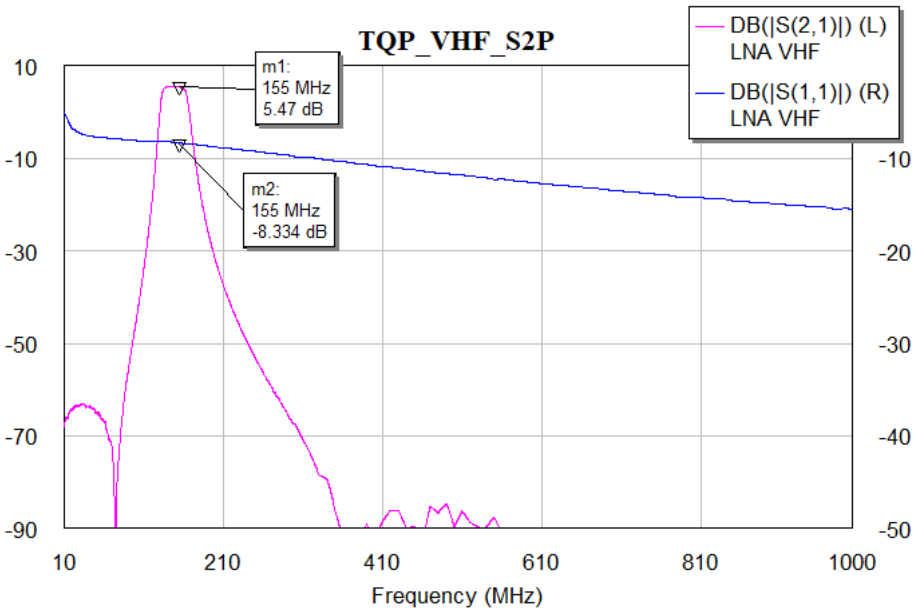

Figure 33: **TQP3M9036 Measured Gain**

The team expected a gain of at least 25dB. Starting at a -25dBm signal, amplifying, attenuating with -20 dB, and then attenuating with the filter's -2dB insertion loss before reaching 3.44 dB on the analyzer, the amplifier therefore provides approximately 25.44 dB gain over the filter's 140-160MHz bandwidth. Thus, the LNA worked as intended. Furthermore, the VHF filter works in conjunction with the TQP as shown in Figure 33, so this means the two system blocks were successfully integrated.

After validating the LNA, the mechanical team tested the eval board inside their RED enclosure at temperatures up to 71.5 degrees Celsius without operating the LNA. This is well within the maximum storage (non-operational) temperature of 150 degrees Celsius. The LNA performance following the test is shown in Figure 34:

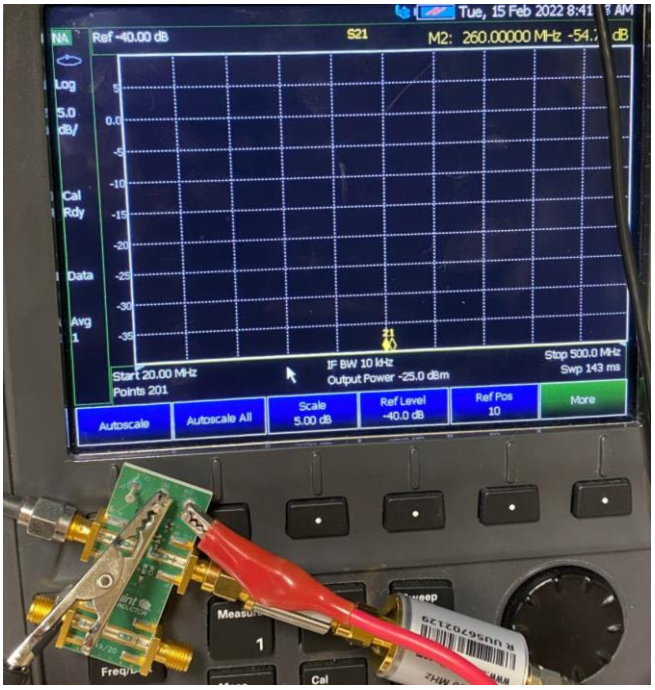

Figure 34: **TQP3M9036 Failure Following Temperature Test**

As shown in Figure 34, some part of the test damaged some part of the LNA such that no signal appears on the network analyzer. The network analyzer and power supply have the same settings as in the first test. The team found that part of this issue was caused by the RF connector shown below. The cable terminator did not screw into the board connector fully, so no contact to the board RF line was made:

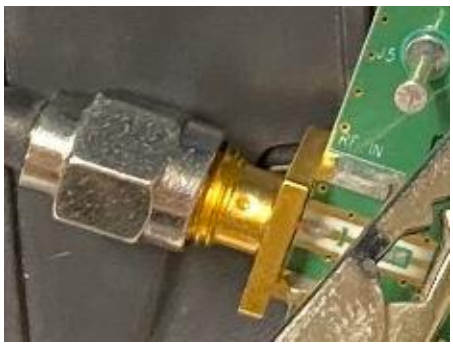

Figure 35**: RF Connector Tightness**

Upon closer inspection, the team found that the board connector was damaged, preventing tightening:

***Figure 36*: RF Connector Damage**

Therefore, the team replaced the damaged connector to determine if the cause of the failure was the connector, or if the cause was thermal damage to the TQP. Again, the TQP is rated for more than twice the temperature it was exposed to in the thermal testing. So, upon replacing the connector, the TQP resumed proper operation as expected:

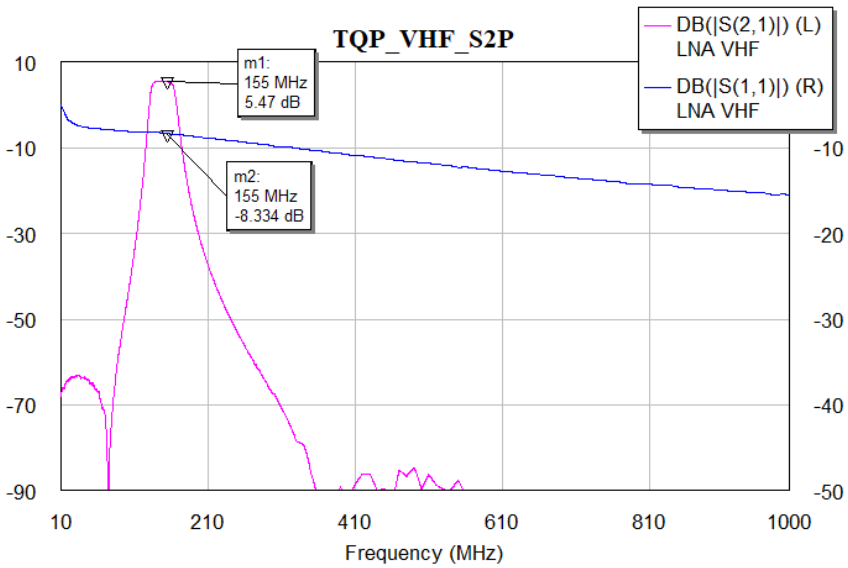

***Figure 37*: TQP Repaired**

As shown in Figure 37, replacing the broken connector enabled expected amplification of at least 25dB. Thus, the mechanical enclosure enables the TQP withstanding the preliminary temperature tests specified in NFPA 1802.

While the team was focused on a VHF receive chain, the TQP's UHF functionality was also examined:

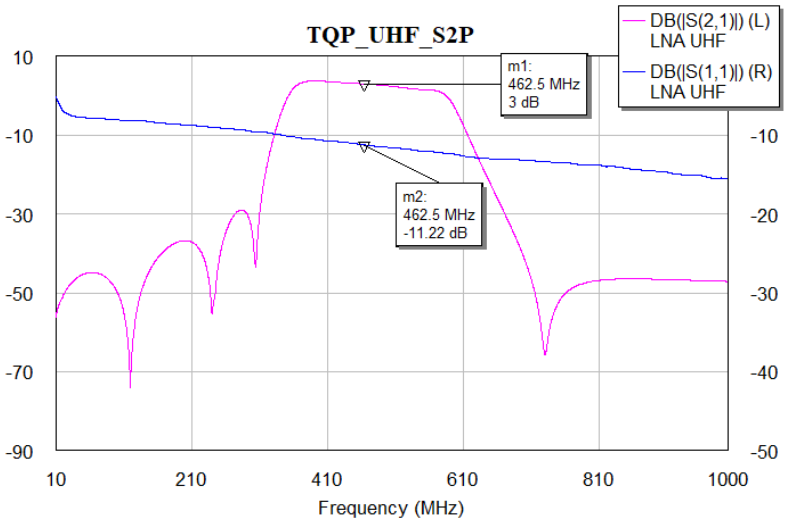

Figure 38: **TQP UHF Performance**

Figure 38 shows the gain expected given the TQP's datasheet specifications, UHF filter loss, and 20 dB attenuator used to protect the Fieldfox.

Before testing with the spectrum analyzer, the TQP integrated circuit was destroyed during testing of the maximum DC input voltage. Despite a datasheet specification of 7 V DC maximum, the TQP chip began smoking when the input was set to 5.5 V. The team determined that it was unlikely that the chip itself failed, but rather that a short occured between the input voltage connection, ground connection, and input capacitors. The lab alligator clips on the input and ground were likely loose enough to contact in such a way that the current limit of the lab power supply was reached, so the power on the TQP exceeded maximum ratings. Thus, the team learned to improve the power supply setup, and recognized that the LNA functioned according to manufacturer specifications; however, the team was unable to purchase a new TQP due to budget and shipping constraints.

6.1.3.3 Current Status of LNA

As demonstrated, the LNA worked as intended before and after integration with the bandpass filter and thermal testing. The LNA could be integrated further into the RED using RF cables on its SMA ports to connect to the antenna.

Given that this LNA is an off-the-shelf integrated circuit, the team is only able to improve the matching network by replacing the as-built components. However, the amount of time, modeling, and testing required to increase the gain or decrease the noise by selecting new matching network components would be very significant. A more realistic improvement could be based on further testing of the SMA connector that was damaged, specifically its thermal rating and susceptibility to mechanical stress. A new connector may be required for full system integration and full system stress testing.

6.1.4 Bandpass Filters (BPF)

This section covers the design concept of RED Bandpass Filters (BPF), BPF selection and testing, and current status. The filters purchased worked as intended before and after integration with the LNA and thermal testing, so this system block was completely successful.

6.1.4.1 BPF Design Concept

As previously described, filters reduce signal interference. The filters in the RED focus only on the radio frequency channels used by Meriden Fire Department. The VHF channels are located between 150 and 160 MHz, and UHF channels are located between 460 and 465 MHz. While multiple MFD radio channels exist across these MFD-specific VHF and UHF ranges, the RED filters will not need to select between each channel. Instead, REDs receive a signal at either VHF or UHF, and then transmit at either UHF or VHF.

For example, if a firefighter uses the RED system inside a building and has their handheld radio set to a UHF channel, the chief outside the building will receive that firefighter's transmission by tuning their chief's radio to VHF.

In this way, RED signal processing and channel selection is simplified. RED bandpass filters prevent transmissions at VHF from interfering with those at UHF and vice versa. RED filters also prevent the transmission of firefighter signals at "harmonics," which act as re-transmissions that occur at multiples of a given center frequency. This capability, called "rejection," reduces the chance that a RED will interfere with other devices in the area using the radio frequency spectrum. Thus, the RED signal processing approach is enhanced by the use of filters.

Originally, the team attempted to design custom filters to provide the best possible performance for our system. Custom filters also enable a simplified improvement process given that the team would be able to adjust the component values and performance. Off-the-shelf filters are sealed, making such improvements impossible.

However, manufacturing challenges prevented the team from constructing custom filters. Given that no team member had surface mount soldering experience, and that the manufacturers the team worked with had no RF surface mount soldering capability, the team ultimately had to order off-the-shelf filters from Mini-Circuits.

6.1.4.2 BPF Selection and Testing

The team selected the ZABP-450-S+ for the RED UHF filter, and the SBP-150-S+ for the RED VHF filter. Across the frequencies of interest, both filters exhibited no more than -2dB of insertion loss, no less than -10dB of return loss, acceptable rejection, and a noise floor of no more than -50dB. Both filter ports are SMA connectors.

Rejection on the SBP-150-S+ is specified to be at least -10dB at +/- 30 MHz (20%) from the center frequency. This filter's specified band is 140-160 MHz, or a 20 MHz

bandwidth. At UHF frequencies, the VHF filter noise floor is specified at about -90 dB, satisfying the purpose of the RED VHF filter.

The ZABP-450-S+ filter is specified for at least -10dB at about +/- 150 MHz (30%) from the center frequency. This filter's specified band is 400-510 MHz, or a 110 MHz bandwidth. At VHF frequencies, the UHF filter noise floor is specified at 45dB. While other filters with higher rejection and narrower bandwidth are on the market, this filter promised much lower loss.

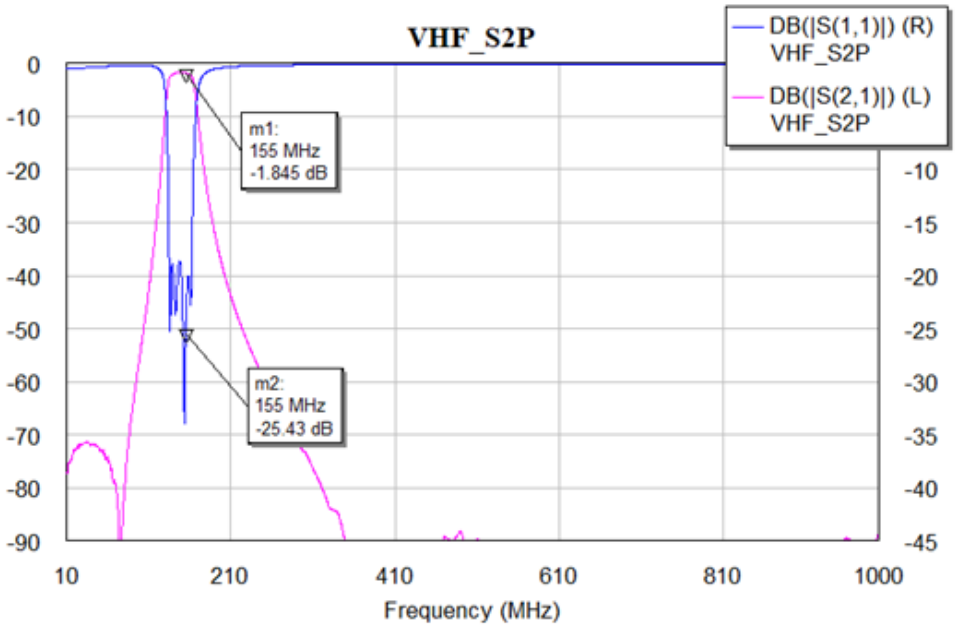

Figure 39: **SBP-150-S+ Measured**

Seen in Figure 39, the SBP-150-S+ exhibits no more than -2dB of insertion loss at Meriden's UHF frequencies. Across the band, return loss is no more than approx. -10dB. The filter bandwidth is only slightly larger than necessary, and the filter provides at least -45dB rejection out of band. In other words, our goal with this filter was largely to prevent interference at UHF, and the SBP-150-S+ performs as expected according to the datasheet.

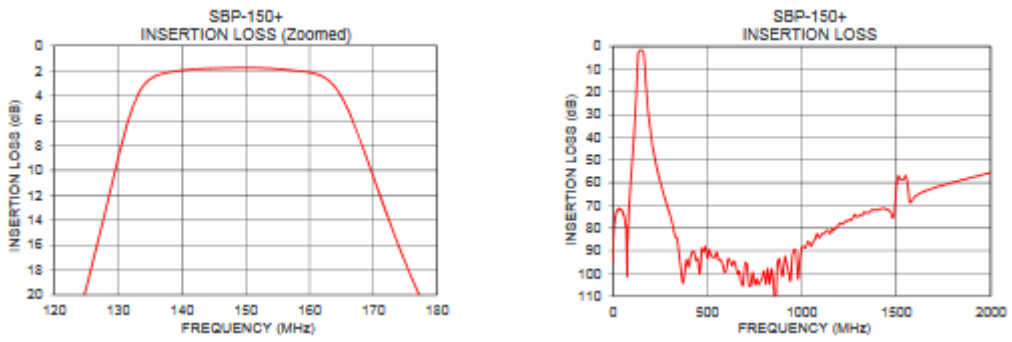

Figure 40: **SBP-150-S+ Datasheet Specification**

Next, the team tested the UHF BPF:

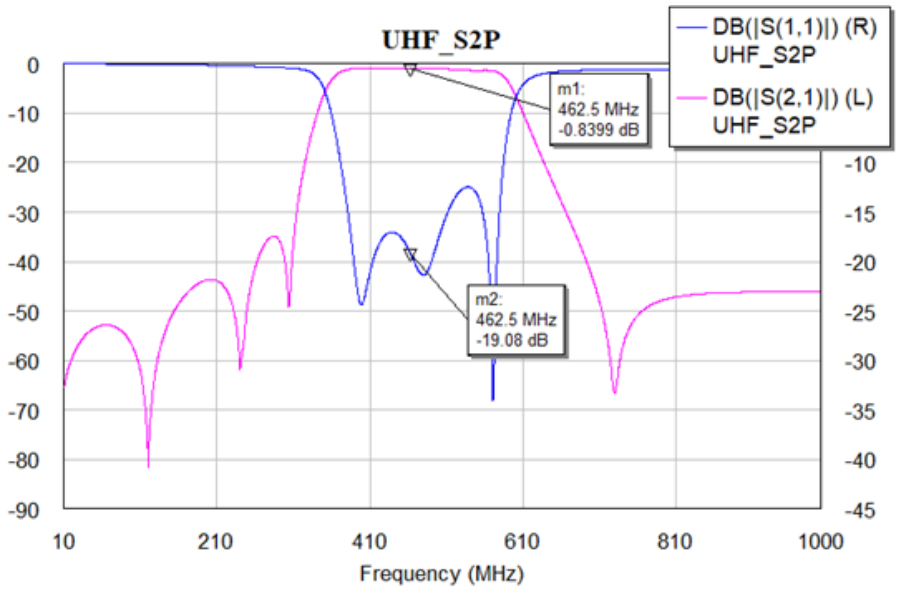

Figure 41: **ZABP-450-S+ Measured**

As shown in Figure 41, the ZABP-450-S+ exhibits no more than -0.82dB of insertion loss at Meriden's UHF frequencies. Across the band, return loss is no more than -10.32dB. While the filter bandwidth is larger than necessary, the filter provides at least -45dB rejection out of band. In other words, the team's goal with this filter was largely to prevent interference at VHF, and the ZABP-450-S+ does just that. The team found that this filter performs as specified according to its datasheet, so this block is a success.

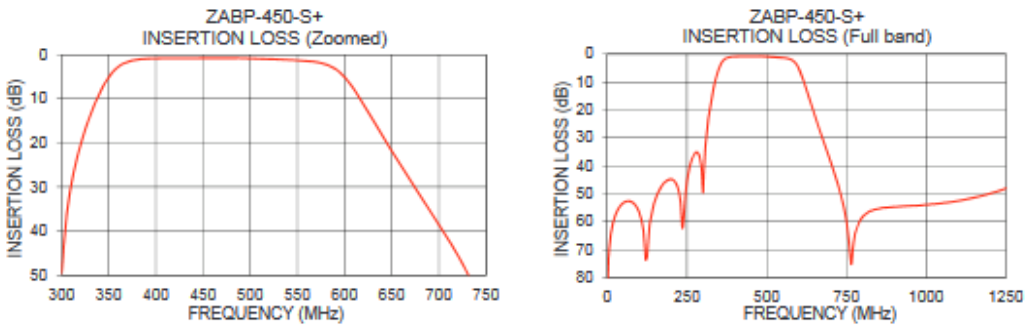

Figure 42: **ZABP-450-S+ Datasheet Specification**

6.1.4.3 Current Status of BPF

As shown, the filters worked as intended before and after integration with the LNA and thermal testing. The BPF could be integrated further into the RED using RF cables to and from its SMA ports to connect to the ADF.

Given that these filters are off-the-shelf products, the team is unable to improve filter performance and characteristics. By purchasing a new set of filters, or by successfully manufacturing our original filter design, future improvements could include lower insertion loss, higher return loss, and increased rejection.

6.1.5 Power Amplifiers (PAs)

This section covers the design concept of the RED Power Amplifiers (PAs), PA selection and testing, and current status. The PAs purchased and designed were functional, but did not entirely meet desired specifications during testing.

6.1.5.1 PA Design Concept

Once the team decided the input and output signal levels required for a RED to at least replicate the minimum specifications of Meriden's XL-200P, the team was able to begin searching for power amplifier integrated circuits.

Power amplifiers, when provided a RF signal at their input pins, amplify the signal to a specified level. The change between the input and output signals is commonly described in

decibels, dB. To describe the power level of the signal, the unit dBm (dB referenced to one milliwatt) is used. As described in 5.3.3 Low-Noise Amplifier (LNA), each RED must receive a signal of at least -80 dBm and amplify that signal to at least 37.8 dBm (6 W, nonlinear conversion). Other important PA considerations include the interference, or "noise," generated by the PA, operational temperatures, and supply voltages. For the RED, the primary concern is input and output power limits. These limits are also called "compression points:"

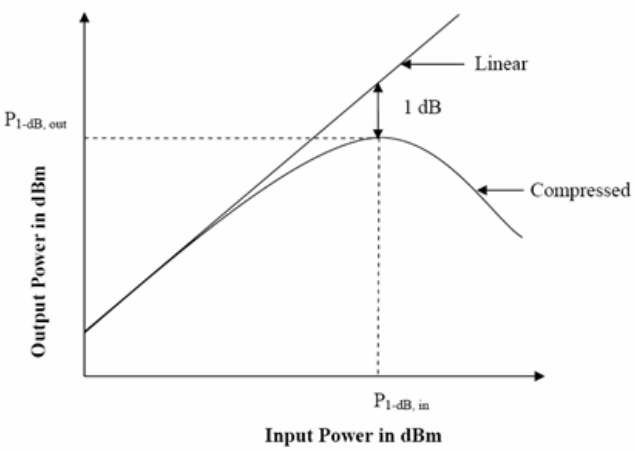

Figure 43: **Compression Point Plot**

As shown in Figure 43, the relationship between these points is not necessarily linear. The team took great care to ensure that any parts selected worked in tandem to maintain linear amplification, as nonlinearities would introduce unpredictable behavior that may damage other system blocks.

6.1.5.2 PA Selection

User Input:	
RF Input Power, dBm	-90
Temperature, °C	25

Spec:

Insert One Only!!

Comments	Component Number	Component	Gain (dB)	Noise Figure (dB)	Gain Temperature Coefficient, (dB/°C)	NF Temperature Coefficient, (dB/°C)	Gain @ Temperature (dB)	Noise Figure at Temperature (dB)	TOI Temperature Coefficient (dB/°C)	Small Signal Gain (dB)	Running Noise Figure (dB)	Power At Input (dBm)	Power At Output (dBm)	Input Compression Point (dBm)	Output Compression Point (dBm)	Output Third Order Intercept (dBm)	Input Third Order Intercept (dBm)	Input Third Order Intercept (dBm)	Compression Stats Limiting Component	L.
Antenna to System	1	SMA Transition	-0.1	0.1			-0.1	0.1		-0.1	0.1	-90.0	-90.1			99.0		99.1	Linear	
TQP3M9036	2	LNA	22.00	0.65			22.0	0.7		21.9	0.75	-90.10	-68.10		20.0			8.0	Linear	
MBUF001	3	Filter	-3.00	3.00			-3.0	3.0		18.9	0.77	-68.10	-71.10	50.0				60.0	Linear	
ADF7021-N	4	RX IC	30.00	1.00	0.008		30.0	1.0		48.9	0.79	-71.10	-41.10		-15.0			-35.0	Linear	
MBLF001	5	Filter	-3.00	3.00			-3.0	3.0		45.9	0.79	-41.10	-44.10	50.0				60.0	Linear	
ADF7021-N	6	TX IC	17.00	1.00	0.008		17.0	1.0		62.9	0.79	-44.10	-27.10		13.0			6.0	Linear	
MW7IC008NT1	7	TX PA	23.50	1.80	0.024		23.5	1.8		86.4	0.79	-27.10	-3.60		40.4			26.9	Linear	
MW7IC008NT1	8	TX PA	23.50	1.80	0.024		23.5	1.8		109.9	0.79	-3.60	19.90		40.4			26.9	Linear	
AFT05MS031NR1	9	TX PA	23.20	3.00			23.2	3.0		133.1	0.8	19.9	43.1		44.9			31.7	Near -L	
MBUF001	10	Filter	-3.00	3.00			-3.0	3.0		130.1	0.8	43.1	40.1	50.0				60.0	Linear	
System to Antenna	11	SMA Transition	-0.1	0.1			-0.1	0.1		130.0	0.8	40.1	40.0			99.0		99.1	Linear	

Figure 44: **Cascade Analysis Example**

After extensive team discussion, the MW7IC008NT1 and AFT05MS031NR1 were selected. These were selected with help from "cascade analysis," which examines the effects of adding power amplifiers to a system, or "cascaded" together. The team then ran many different cascade analyses as part of this PA search process, and one such example is shown in Figure 44.

Thus, the team's intent was to use the LNA, the ADFs, two MW7s, and one AFT to provide the gain and output power required for the RED. Each MW7 provides 23.5 dB of gain, with output compression points of 40.4 dBm. This limit meant that the AFT, with a gain of 23.2 dB gain and an output power limit of 44.9 dBm, was best used as the final gain stage. The team found that the following system characteristics could be expected:

Small Signal Gain	130.00 dB
Noise Figure	0.79 dB
Gain	130.00 dB
Output Power	40.00 dBm
Intercept Points	
Input Coherent	-79.43 dBm
Output Coherent	50.57 dBm
Compression Points	
Input	-89.43 dBm
Output	40.57 dBm

Figure 45: **Cascade Analysis Results**

Given that the input signal for this analysis was -90 dBm (lower than the -80 dBm needed), and the output was 40 dBm (10W, 3.5W higher than needed), the team considered the two MW7s and one AFT to be a strong approach. It follows that a higher input signal enables higher output power as long as the input and output compression points of the PAs are not exceeded.

Furthermore, the noise figure (as defined in 6.1.3 Low Noise Amplifier (LNA)) remained under 1 dB during simulation as shown in Figure 45. Given the high output power shown in Figure 44, this noise figure was considered acceptable.

6.1.5.3 PA Manufacturing and Testing

Once the PAs were selected, the team began designing the required printed circuit boards to provide the best possible performance at UHF. While the MW7 and AFT provide the required gain across the VHF and UHF bands used by the RED, the team did not have the budget or the number of students required to build up separate PCBs for both bands. So, the team focused on building circuits for optimal MW7 and AFT performance across the UHF band, 460-465 MHz.

To this end, the team based their board designs on the manufacturer evaluation boards used to generate the PA datasheets. While these evaluation boards were not necessarily optimized for 460-465 MHz alone, these boards provided a high degree of confidence because this approach eliminated spending time choosing the peripheral circuits and board

layouts that would not necessarily work at all, let alone provide a marginal performance improvement. Additionally, these PCBs were "laid out" in KiCad using manufacturer-supplied component footprints and top-layer copper .dxf files wherever possible. These KiCad PCB documents are shown in Appendix G: Power Amplifier PCBs. RED PA PCBs were also manufactured with a professional board manufacturer, JLCPCB. In this way, the only real limitation was soldering ability and equipment. Thus, at the beginning of testing, the team had the high confidence in the board design and the boards themselves, and the main uncertainty was in the team's ability to manufacture the PAs.

MW7:

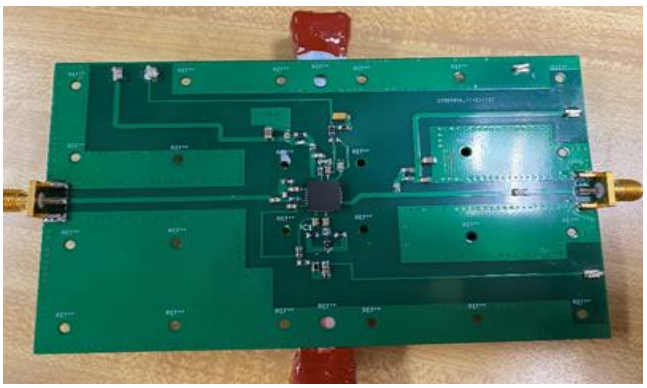

Figure 46: **MW7 with PCM**

In Figure 46, the MW7 is pictured with a PCM heatsink attached underneath the PA chip in the center of the board. As the PA chip generates heat during operation, the PCM was placed directly underneath using a thermal glue. After the heatsink was attached, the team began electrical testing.

First, DC power supplies were set to the manufacturer's specified gate and drain values. Both drain inputs were set to 28V, both gate inputs were set to 3.5V, and all input current limits were set to 2A. Before enabling the output of the lab power supply, input RF test cables were connected to either the network or spectrum analyzer (depending on the test), and output RF test cables were connected to a 20 dB attenuator (protecting the

analyzers), the UHF filter, and either the network or spectrum analyzer (depending on the test). As the spectrum analyzer used had a higher input power limit than the network analyzer, to be as safe as possible, the team decided to characterize PA output with the spectrum analyzer before the network analyzer. To take output measurements with the spectrum analyzer, the Fieldfox was used to generate the 0 dBm CW input signal centered at 462 MHz. Next, the DC power supply output was enabled to observe the following results:

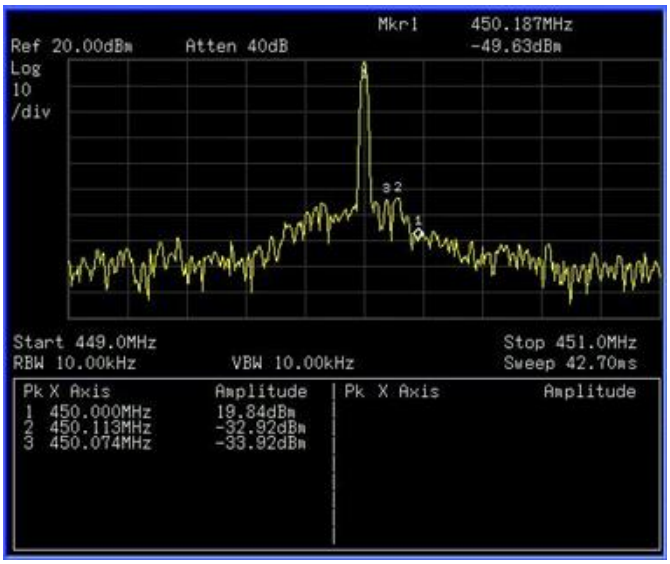

Figure 47: **MW7 Result on Spectrum Analyzer**

Figure 47 shows that the MW7 output is approximately 12 MHz and 3.66 dBm lower than expected. These differences are caused in part by manufacturing limitations; specifically, the cumulative differences in capacitance and inductance introduced by soldering, vias, and the differences in mounting between the two RF connectors. The signal spectral regrowth, or "shoulders," are shown at approximately -32.92 dBm. The team also searched for harmonics across the RED bands of interest by setting the spectrum analyzer span from 10 MHz to 1 GHz but found no spurious peaks higher than the -30 dBm trigger level. To further characterize the MW7, the team next used the network analyzer:

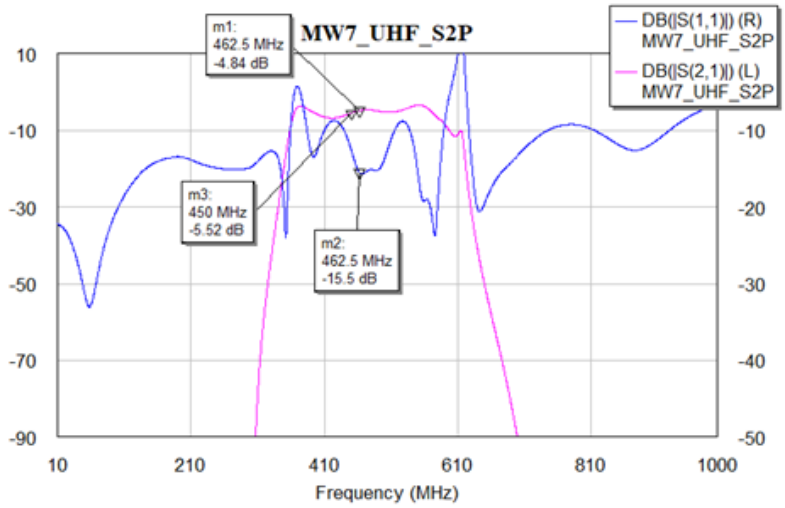

Figure 48: **MW7 Result on Network Analyzer**

Figure 48 shows that the MW7 output is 0.36 dB lower than expected. This additional loss is caused in part by manufacturing limitations and cable losses. Additionally, as is clear in Figure 48, the return loss is significantly higher than expected at, for example, about 610 MHz. Again, this is likely caused by manufacturing limitations, particularly the differences in RF connector mounting on either side. However, it is important to note that between 460-465 MHz, return loss is approximately a desirable -16 dB. The team expected to meet the specifications from the MW7 datasheet:

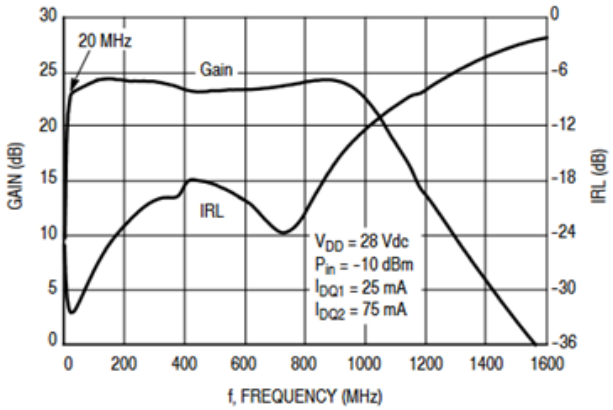

Figure 49: **MW7 Gain and Return Loss vs Frequency**

Thus, the MW7 built by the team nearly achieved the specified 23 dB of gain and -18 dB return loss. Also, the power added efficiency was approximately 28%, 13% lower than

the specified 41%. This difference is most likely due to aforementioned manufacturing limitations.

AFT:

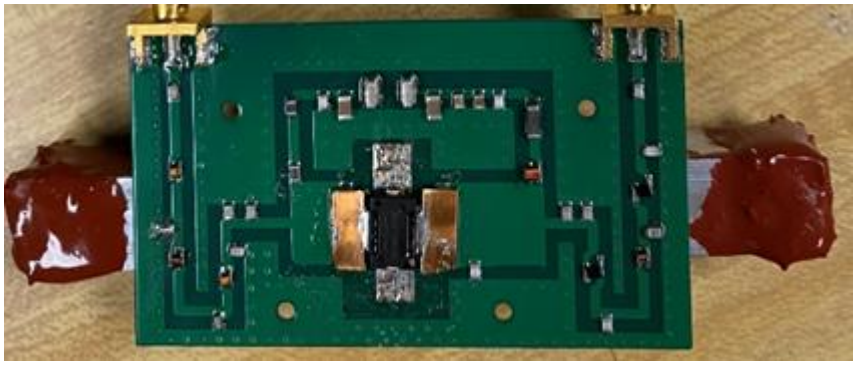

Figure 50: **First AFT Iteration**

In Figure 50, the first AFT iteration is pictured with a PCM heatsink attached underneath the PA chip through the middle of the board to address the thermal concerns described for the MW7. It is also important to note that the PA chip was connected to the rest of the board with copper cutouts. This was necessary because no AFT KiCad model existed, and the team had low confidence in the model created from the AFT datasheet. In fact, the online services from Mouser and KiCad that create any chip model for free within 48 hours refused to create an AFT model. The team had issues with the AFT datasheet, too, so the team cut copper pieces to fit, carefully scratched out the PCBS's soldermask below, and soldered using WPI's toaster oven. After "ohm-ing out" the connections, the RF pin fixed was verified at DC. The team then began electrical testing.

Following the same procedure used for the MW7, DC power supplies were set to the manufacturer's specified gate and drain values. The drain input was set to 13.6V, and the gate input were set to 2V, and all input current limits were set to 2A. The RF cables were connected as previously described to the analyzers, attenuator, and UHF filter. Again, to take output measurements with the spectrum analyzer, the Fieldfox was used to generate the

0dBm CW input signal centered at 462 MHz. Next, the DC power supply output was enabled to observe test results.

Unfortunately, the first iteration of the AFT exploded during testing when the team increased the PA gate-source voltage from 2V to 4V. With the drain-source voltage set to 13.6 V as specified, increasing the gate-source voltage explored the relationship outlined in the AFT datasheet here:

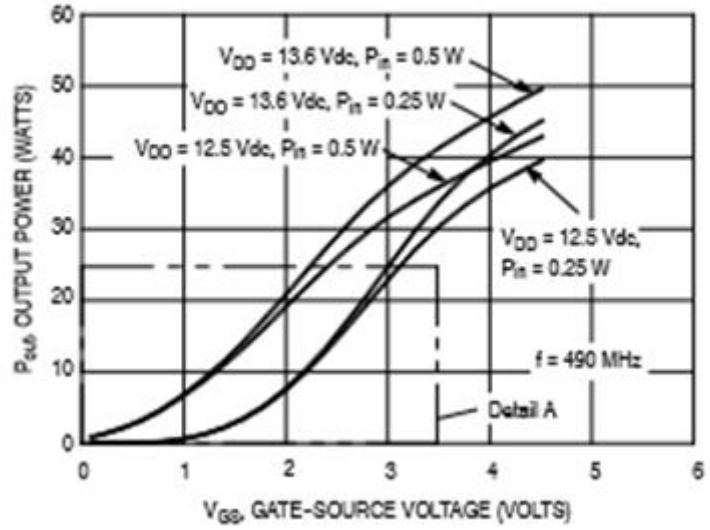

Figure 51: **AFT Output Power vs Gate-Source Voltage**

As shown in Figure 51, increasing the gate-source voltage should have only increased the output power. The output power did increase by 10 dBm for a few seconds, but the AFT then exploded with a distinct popping noise and smoke. The team powered down the AFT and began investigating the cause of the failure.

The AFT and its heatsink were painfully hot to the touch, and while this would normally indicate a heatsink failure causing the AFT chip itself to overheat and explode, the team had high confidence in the heatsink because it was specifically designed for our application. The team felt that it was more likely the board was hot enough to melt enough of the solder surrounding the copper cutouts used for the chip. This may have caused a brief short circuit, or a loss of grounding. Alternatively, the copper cutouts may have been too

large and too thick such that they conducted too much heat next to the chip. A final possibility is that the power rating for one of the other components was exceeded, which is possible because the lab power supplies used do not provide tolerance ratings and can vary by up to 0.2V. So, when the DC supply display showed 4V, 4.2V may have been delivered to the AFT.

Therefore, the team's second AFT iteration included smaller, thinner, and more precisely placed copper cutouts, a better ground connection, and a test procedure that included gate voltages set 0.2V below specified. This was made possible by building this AFT second board with new parts equipment at NewEdge Signal Solutions. The second AFT iteration is shown here:

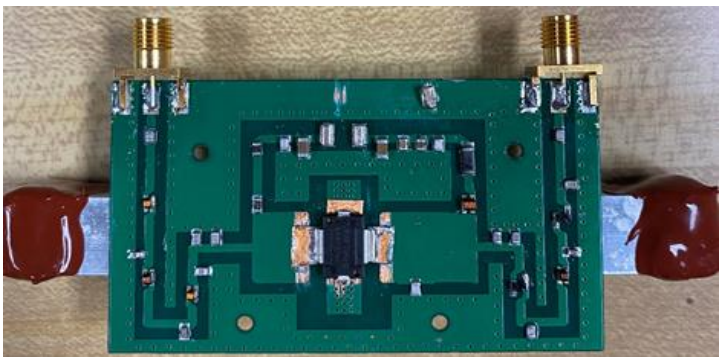

Figure 52: **AFT Iteration Two**

Except for setting the gate voltage to 3.8V instead of 4V, the team followed the same test procedure described previously. This proved successful as shown below:

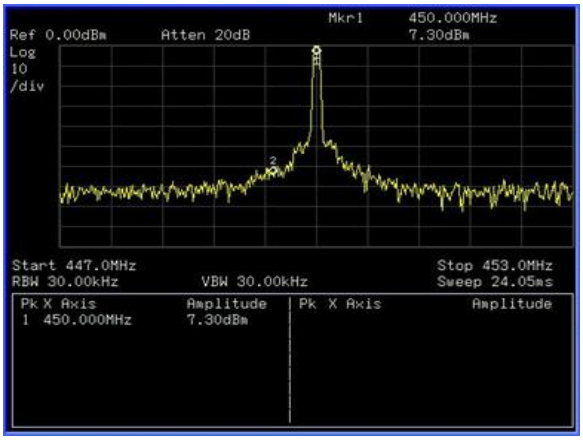

Figure 53: **AFT Result on Spectrum Analyzer**

Figure 53 shows that the AFT output is approximately 12 MHz and 10.4 dBm lower than expected. Much like the MW7, these differences are caused in part by manufacturing limitations; in this case, the cumulative differences in capacitance and inductance introduced by the different copper cutouts on either side of the PA chip. The signal spectral regrowth, or "shoulders," are shown at approximately -50.0 dBm. The team also searched for harmonics across the RED bands of interest by setting the spectrum analyzer span from 10 MHz to 1 GHz but found no spurious peaks higher than the -30 dBm trigger level. To further characterize the AFT, the team next used the network analyzer:

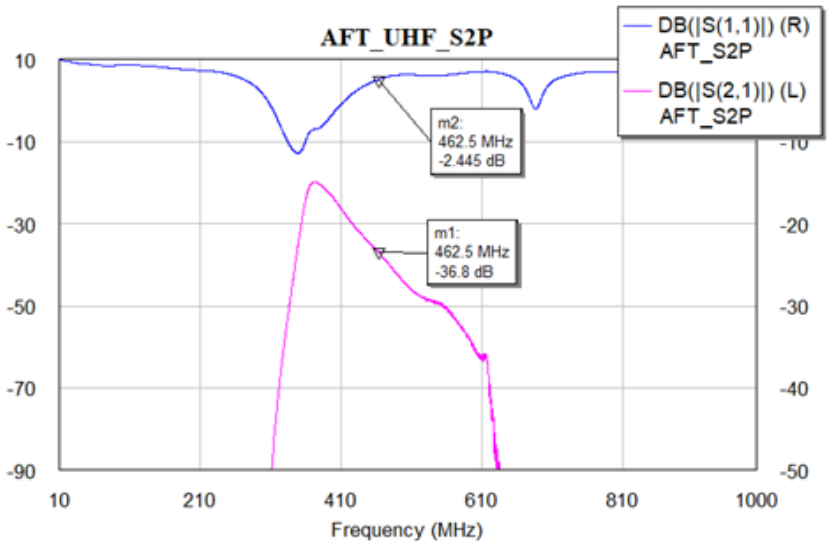

Figure 54: **AFT Result on Network Analyzer**

Figure 54 shows that the AFT output is about 7.3 dB lower than expected. This additional loss is caused in part by manufacturing limitations and cable losses but is most likely caused by the copper cutout mismatch as previously described. Additionally, the return loss is higher than is desirable. While return loss is not specified in the AFT datasheet, -2.45 dB is not ideal.

Thus, the AFT built by the team worked, but did not achieve the 17.7 dB of gain specified. Also, the power added efficiency was approximately 24%, 38% lower than the specified 62%. This difference is most likely due to aforementioned manufacturing limitations.

6.1.5.4 Current Status of PAs

As described above, the PAs are functional, but not fully meeting the expected specifications. The AFT initially failed, and needed a re-build, whereas the MW7 worked from the start of testing.

Future improvements must include higher quality manufacturing. The failures documented may have been prevented entirely with better access to professional assembly. Once characteristics of the current designs are thoroughly tested with better builds, improvements could include optimization of matching network component values to increase output power and reduce noise at the frequencies of interest.

6.1.6 ADF7021 Transceiver

In order to retransmit firefighter radio signals according to the approach discussed, simple signal processing techniques were implemented on the RED. By using a MSP430 (a microcontroller, or MCU) in conjunction with a Raspberry Pi (a single-board computer, or control board), the team was able to carry out basic signal processing to convert a signal from VHF to UHF or vice versa. The MSP430 also acts as the main interface with the hardware, controlling and monitoring the system then passing relevant data to the Raspberry Pi. This setup is advantageous for two reasons. The first is it allows us to use dual processing, allowing the MSP430 to monitor and update in response to signals continuously without needing to pause for long periods of time to process data. The second is it is far easier to

integrate the MSP430 with our required hardware than if we were solely using a Raspberry Pi because the MSP430 has an integrated analog to digital converter; the Raspberry Pi lacks such capabilities.

To display data on websites, the Raspberry Pi hosted data transmission via WiFi. The RED website was intended to display system status and system characteristics such as temperature readings for the benefit of development team members and firefighters alike. This would provide a unique status report functionality and simplify the test process.

The MSP430 and Raspberry Pi use a serial interface to communicate with each other. The MSP430 uses the same serial protocol to communicate with the ADF7021. The interface requires four pins: a chip enable, a latch, a clock, and a data I/O. The chip enable is active low and it tells the device to start listening. The latch pin is active high and it tells the device that the data transmission is over. The clock controls the speed of the transmission, and the device latches data on the rising edge of the clock. The data I/O is self-explanatory. We wrote code to handle the whole process. We also wrote code that handled the setting registers for the ADF7021 making configuration easier.

Several registers control the ADF7021's settings and operation. In order to transmit, we have to be able to change and set these registers. This requires the MSP430 to have a serial connection to connect to the ADF. The code that allows the MSP430 to communicate with the ADF consists of three libraries. One library, serialiolib, contains functions allowing for the use of the serial interface. The other library, registerset, contains functions for generating registers to send to the ADF. The third adf7021 contains the transmit functions which utilizes the other two libraries to set the ADF to transmit and configure it.

To test the communication protocol, we had the MSP430 read the identification number from the ADF7021. To do this, we wrote to the ADF instructions to readback its id number. The test was a success. We were able to read the id number.

We also tested the functions for RF transmission. These functions contain multiple writes to the ADF and require setting the chip up with specific settings. The ADF did not end up transmitting data. This could be due to two possible errors. The first is it was transmitting, but the spectrum analyzer does not update fast enough to see the transmitted data. We can fix this by using a software defined radio system to make a waterfall plot. The second is we are misconfiguring the registers. This is harder to fix, and it would require changing the register settings.

6.1.7 Battery and DC to DC Power Converters

For field-testing of the RED, an integrated power system is required to provide power to each active device in the system. This includes the LNA, PAs, MCU, T/R switch, transceiver IC, and Raspberry Pi. While the MCU, T/R switch, and transceiver IC can work off a 3.3V supply, and the LNA and Raspberry Pi require a 5V supply, the AFT PA requires a nominal 13.6V, and the MW7 PA typically requires 28V. Using a NiMH 9.6V battery, two buck converters, one stepping 9.6V to 3.3V, and the other 9.6V to 5V, will be a simple and effective approach to meeting the power demands of the LNA and digital hardware. Such buck converters are commonly used and in high supply. For the power amplifiers, boost converters will be required. Implementation of the 9.6V to 28V boost converter for the MW7 will likely be most challenging because it will require an extreme duty cycle on the switching converter. An alternative would be to put the two 9V batteries in series for 18V, but this would make it more difficult to find appropriate buck converters. If these cannot be found, less efficient linear voltage regulators would be required. In choosing power converters with the desired specifications, it is also important to determine the maximum current draw from the battery, as well as the effects on the power system when the battery voltage drops due to discharge.

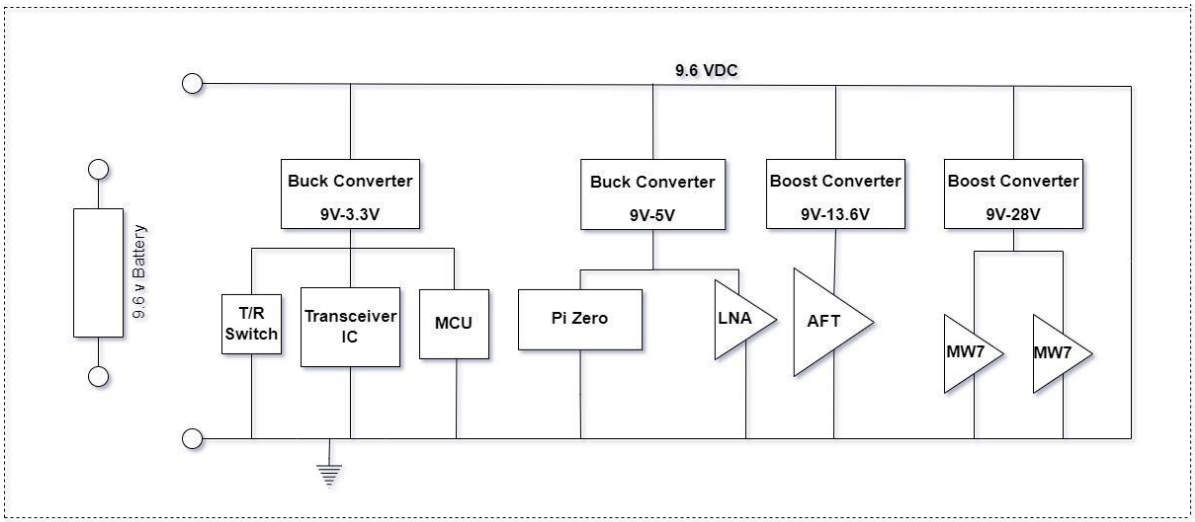

***Figure 55*: Electrical Power System Block Diagram**

The two buck (step-down) converters are a simple and effective approach to meeting the power demands of the LNA and digital hardware. Such buck converters are commonly used and in high supply. For the power amplifiers, boost converters will be required. The MCU, T/R switch, and transceiver IC can be supplied by 3.3V, and the LNA and Raspberry PI require 5V. For our buck converters, we selected the TEC 2-0910 for the Microcontroller (MCU), the transceiver (ADF), and the T/R switches to step down the voltage down to 3.3V. The team is also using the TEC 2-0911 buck converter to bring the voltage down to 5V for the LNA and Raspberry Pi zero. The operating temperature of the two converters ranges from -40°C to +95°C with the reduction of thermal loss. The boost converter is used to step up the battery voltage to the higher level required by the load. The AFT PA requires a nominal 13.6V and the MW7 PA typically requires 28V. For the MW7 PA, the 65W Boost Converter (ABXS002A3X41-SRZ) was selected as it is rated to convert up to 65W of output power. Due to its high range of the output voltage we were able to adjust the Vout by adding an external resistor.

The module can operate over a wide range of input voltage from 8Vdc-16Vdc and provide an adjustable 16 to 34Vdc output. The output voltage is programmable via an

external resistor and includes over-temperature protection. The analog output voltage programming of each output of the module can be programmed for our purposes. We need to have a Vout of 28Vdc by connecting a resistor between the Trims and GND pins of the module.

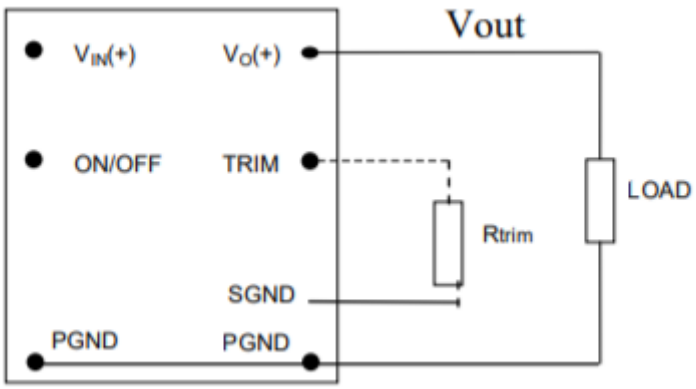

***Figure 56*: Circuit Configuration Programming for Output Voltage Using an External Resistor**

$$Rtrim = \left[\frac{1.2}{(Vo - 1.2)}\right] x200.5k\Omega$$

The external resistor Rtrim calculated using the equation above in [kΩ] for the desired Vout.To get the 28 volt we need a 8.978kΩ ≈ 8.97kΩ. The second boost converter that we selected was The THR3-2413WI dc-dc converter for our AFT to get an output voltage of 13.6v with a high efficiency up to 85% allowing a safe operation from –40°C to +92°C.

The team will measure the performance of these DC-to-DC power converters to get the efficiency curve, or the ratio of the output power compared to the input power. The team will also measure how much power is being dissipated through the system. Each separate DC-DC converter circuit, as well as all circuits at full load, will be tested. Once the testing period is complete, the next step will be assembling the whole power system complete with its case. The two Buck converters tested individually by connecting each of them to a (2

KOhm) resistor and to a 9.6Vdc power supply. The ripple voltage of the output voltage (peak-to-peak) was measured using the oscilloscope channel.

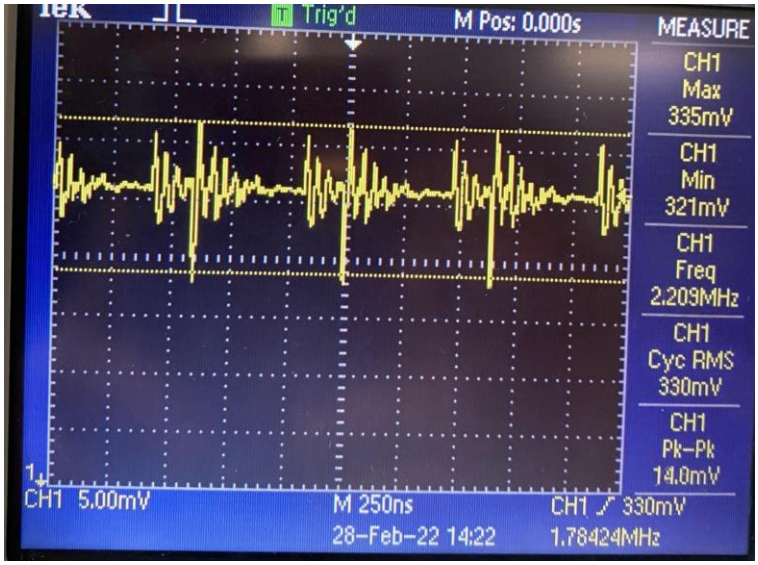

Figure 57: **TEC 2-0910 Ripple Voltage Measurement**

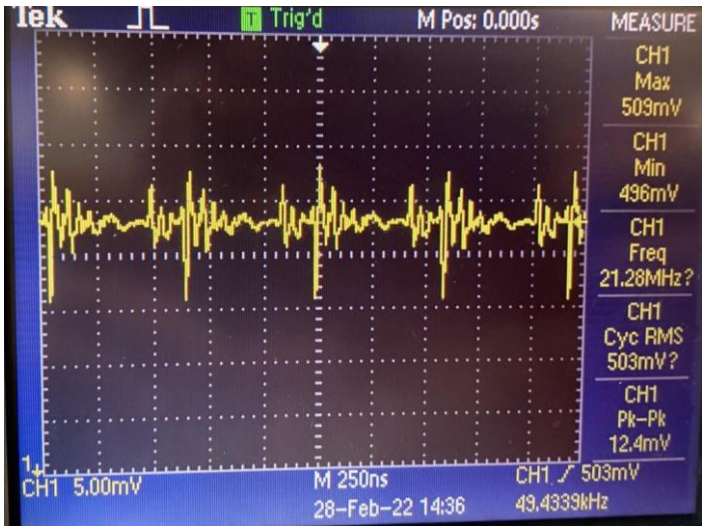

Figure 58: **TEC 2-0911 Buck Converter Ripple Voltage Measurement**

We were unable to connect the trim resistor to the boost converter because of its large dimensions. The initial measurements of output voltage for the Boost converter will be done as we get the right size resistor.

All DC-DC converters testing performed with a room temperature environment of 25C and an average Relative Humidity (RH) of 30%.

6.1.7.1 Current Status of Battery and DC to DC Power Converters

As described above, the DC-DC converters are functional, but not fully meeting the expected specifications. The boost converter failed to confirm that the converter operates within its specified limits. needed an external resistor, however, the two buck converters worked as expected.

Future work must include testing and analysis of the complete system. These tests will be intended to confirm the DC-DC converters would turn on with a maximum load on the output, the input voltage would be set to the minimum and toggled off and back on while measuring the output voltage and current. The output voltage and ripple and noise may also be measured to see if the lower input voltage setting has any effect on the output stability or ripple. This test ensures that the output voltage remains within specified regulation limits when the input voltage varies from minimum to maximum operating voltage, as defined in the DC-DC converter specification. During this test, the output load is usually set to nominal or maximum current as specified. Another test that can be run is testing output operating temperature and over-temperature protection (OTP). For this test, a thermal chamber can raise and lower the DC-DC converter temperature to simulate the operating temperature range. Additionally, testing output transient response deviation and time will determine how well the output voltage responds to a sudden change in output current. Finally, testing each DC-DC converter separately would show the internal power dissipated by the DC/DC converter and how efficiently input power transfers to the converter output.

6.2 Software Subsystems

The RED software consists of three main subsystems: data collection, data visualization, and server hosting. The software can collect temperature data from inside the RED and transform the data into a graph that is then uploaded to a website. The software operates in two separate steps. In the first step, the data collection subsystem is run, while the other two subsystems are run in the second step.

The goal of the software is to offer the fire department and the engineers a convenient way to analyze the performance of the RED after it has been used. With the current implementation the software can only collect temperature data. Firefighters can search the graphs for temperature spikes, allowing them to determine if the device is safe for another use. And engineers working on this project in the future can utilize the graphs while testing the device. There is also an avenue for future development of the software offering more tools for both the firefighters and engineers of the RED. For example, collecting the battery level of the device and the strength of incoming radio signals.

This section explains how the software operates, how it was tested, and why specific design choices were made.

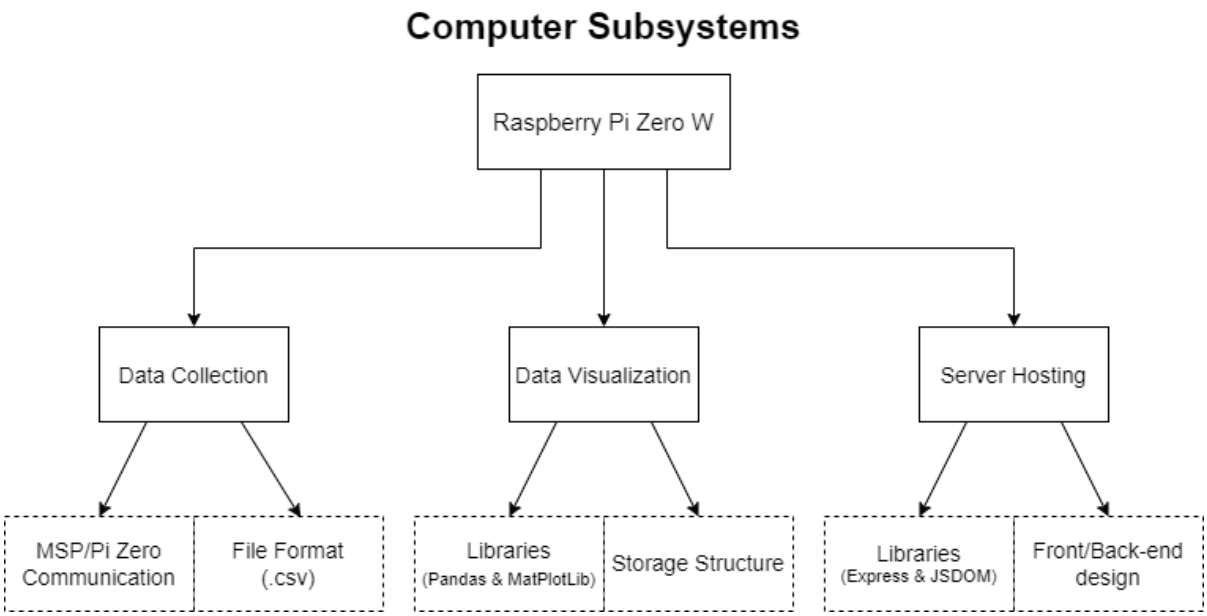

***Figure 59*: Computer Subsystems Diagram**

6.2.1 Raspberry Pi Zero W Microcomputer

6.2.1.1 Microcomputer Selection

Initially, the CS team chose to work with the ESP32 (ESP), a low-level microprocessor. The team attempted to design software utilizing the ESP but came to the realization that an external device would be necessary to achieve the CS team's goal for the software. After researching alternative options, the CS team chose the Raspberry Pi Zero W (PZW) for the software implementation in the RED. The PZW is small but powerful, the PZW supports multiple languages, unlike most low-level microcontrollers that only support versions of C. Having the flexibility of languages was important in abstracting the process of collecting data, visualizing data into graphs, and hosting graphs on a web server.

6.2.1.2 Pi Zero W Setup

The CS team had to set up the PZW according to their needs. The setup involved downloading the project code along with its necessary libraries and configuring the WiFi chip as an access point (AP). The CS team created documentation for this setup, which can

be seen in **Appendix M: Raspberry Pi Zero W Setup Documentation**, as a reference when setting up future PZWs.

6.2.2 Data Collection

6.2.2.1 Data Collection Design Concept

The goal for data collection was to collect the internal temperature of the RED while it is in use and store it in the PZW file system for review. To achieve this, the CS team had to figure out how to read the temperature of the RED internals, and how to store the temperature values. A temperature sensor allows the team to read the temperature of the RED internals. When a temperature sensor is connected to an Analog to Digital Converter (ADC), it allows the analog signal from the temperature sensor to be read as a digital value. The MSP has onboard ADCs, unlike the PZW. To collect data, the PZW and MSP will communicate with each other, the MSP will store the values from the temperature sensor, and the PZW will request them to be sent over via General-Purpose Input/Output (GPIO). This digital value is then stored on a .csv (comma separated-values) file, which is used in the data visualization process to feed the data into the visualization script.

6.2.2.2 Data Collection Testing

To test data collection, the CS team tested communication between the PZW and MSP430 (MSP). The CS and ECE teams wrote code for the PZW and MSP to communicate with each other via GPIO pins. The PZW was set to receive data, and the MSP was set to transmit data. The test involved sending 32 bits of data from the MSP to the PZW. To verify that the test worked, the PZW displayed any data received via GPIO to the terminal screen, allowing the CS and ECE teams to verify that the data was sent and received correctly.

6.2.2.3 Current Status of Data Collection

The current working status of the data collection system can be seen in the figure below, the PZW can receive data and store it into a .csv file. To complete the system, the PZW must be able to request the MSP to read the temperature sensor connected to its onboard ADC.

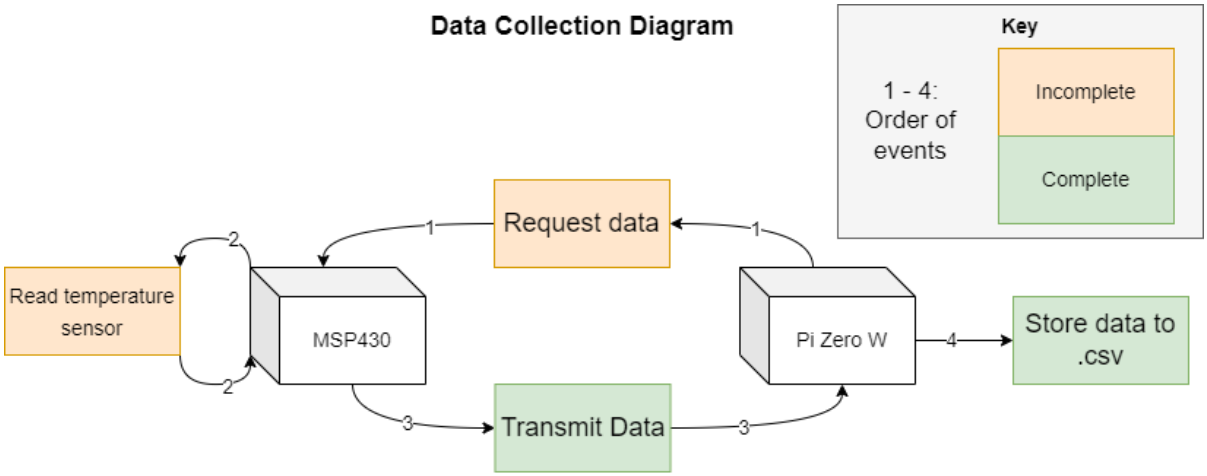

***Figure 60*: Data Collection System Diagram**

6.2.3 Data Visualization

6.2.3.1 Data Visualization Design Concept

To visualize the data collected in the previous section, the CS team utilized two Python libraries called Pandas and MatPlotLib. Pandas is a data analysis library, its purpose in data visualization is that it allows the user to parse .csv files into a table. MatPlotLib is a data visualization library that can take tables of data and generate graphs. The data visualization system utilizes the two libraries to store the data collected into a table that can be transformed into a graph. The graph is then stored as a .png (image) file where it can be accessed by the web server.

6.2.3.2 Data Visualization Testing

To test the data visualization system, the CS team created a .csv file with dummy temperature readings and ran the .csv file through the data visualization script. The CS team then compared the graph to the .csv file that was created and verified that the values from the .csv file matched up with the graph. After confirming the graph is accurate to the .csv file, the team checked if the graph was saved in the correct folder.

6.2.3.3 Current Status of Data Visualization

The current status of the data visualization can be seen in Figure 61 below. All components of the data visualization system are working and have been tested.

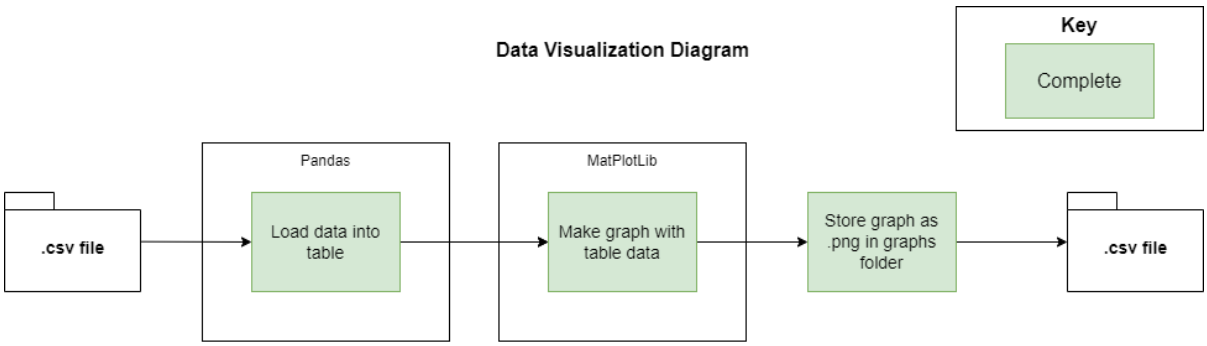

***Figure 61*: Data Visualization System Diagram**

6.2.4 Server Hosting and Website

6.2.4.1 Website Design Concept

The CS team had to determine an effective approach to display the visualized data. A website is ideal to view the data because there wouldn't be any need to export data from the PZW to another device. The PZW comes with an on-board WiFi card that can act as a wireless access point (AP) to the PZW. If the PZW were to host a web server, a user could connect to the AP and enter the address of the server in any web browser to view the website. The CS team then had to pick a way to host the web server. Initially, the team chose to use Apache, a popular web server software. After a couple weeks of experimentation and

development, the team realized that they needed to run javascript outside of the web browser to accomplish their goal with the website. Apache uses native JavaScript which does not allow this, a workaround was found through Node JS, a popular JavaScript runtime environment. Node JS has a library called Express JS which is a web application framework that can host web servers. With the combination of Node JS and Express JS, the CS team had their approach to display the data to the user.

Once the CS team had their approach to host the website, they had to determine an intuitive way to display data to the users. The approach settled on was having buttons that displayed graphs in a new window when clicked. The buttons are categorized by the date the RED was used. This offers a minimalist design which prevents confusion to new users to the website.

6.2.4.2 Server Hosting Testing

To test the server hosting capabilities of the PZW, the CS team wrote the code for the web server and configured the PZW to act as an AP using the documentation on the Raspberry Pi website. After completing the web server code and AP setup, the CS team started the server and attempted connecting to the website through multiple devices. The website was reachable from both computers and phones, and the functionality of the website worked for both platforms.

6.2.4.3 Current Status of the Website

The current working status of the web server and the website is fully functional. The website offers resizability for both desktop and mobile platforms, and the button functionality works on both platforms as well. Figure 62 displays an overview of the web server / website system.

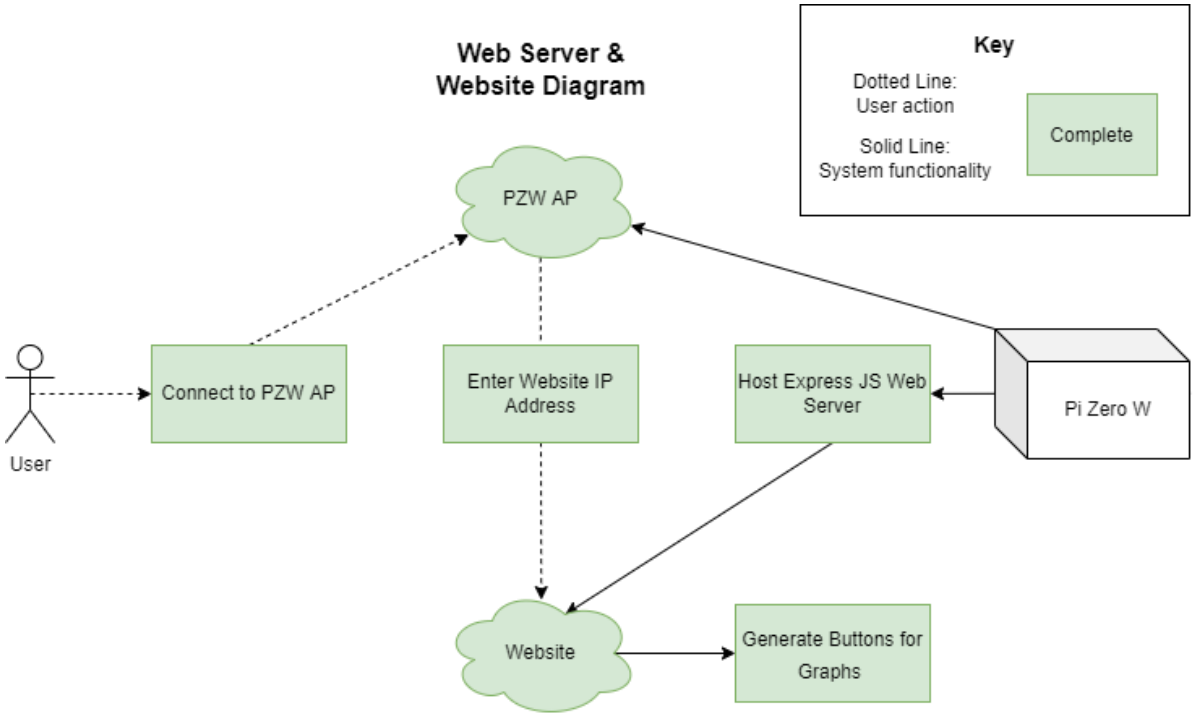

Figure 62: **Web Server / Website System Diagram**

6.3 Hardware Interface

The ECE and CS team tested the MSP430 and Raspberry Pi Zero (RZW) code. We started with the MSP430 transmitting and the RZW receiving. Initially it did not work. This was unexpected because the ECE team had tested the transmit function earlier, and it worked as expected. The code for RZW was minimal, and there was only a small chance of error.

It was then discovered that because one of the ECE team was powering the MSP430 with a laptop, and the RZW was powered by the wall, it created a difference in ground causing enough interference to corrupt the transmission. The resolution was simple: wiring the two boards such that they shared a common ground. That solved the problem. With a bit more testing, the boards were able to transmit data between them.

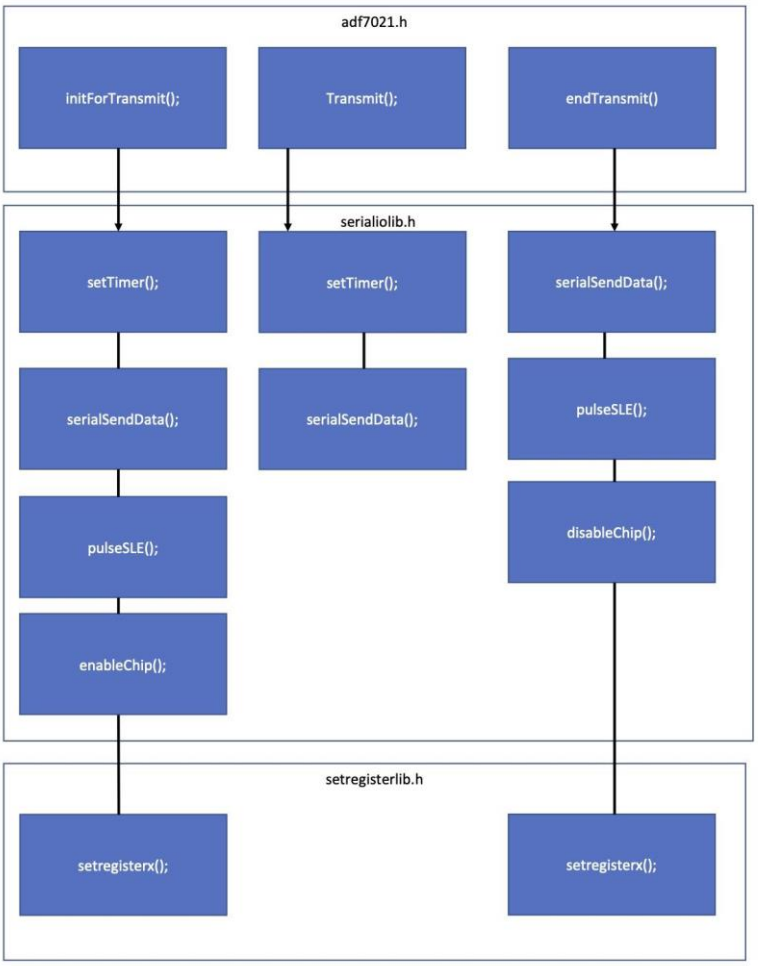

Figure 63: **Function Diagram of the Hardware Interface Code**

Figure 63 is a diagram of the interface code. Each large rectangle represents a library and the smaller blue rectangles it contains are the function inside that library. The arrows show what functions make up the macro functions. The solid lines link functions that make up the macro functions. As shown, there are three libraries. The macro library adf7021.h contains functions for communicating with the ADF chip. The macro functions consist of the two libraries registersetlib.h and serialiolib.h. These contain functions for the basics of serial communications. The diagram is only for the transmit side; it does not show the functions for reception even though it has been implemented. This is because there is no macro-library for reception. There are also many helper functions that assist in the implementation of the

functions shown. These are not in the diagram because they are in service of the most important functions which are shown in the diagram.

6.3.1 Current Status of the Hardware Interface

The hardware interface is functional. We tested it, and it is fully capable of transmitting and receiving data between peripherals. The main problem is not its ability to communicate but our ability to communicate the correct information to it when setting the ADF7021's registers. The fix would be to debug the register settings with the aid of the data sheet.

6.4 Mechanical Subsystems

This section describes the purpose of each mechanical component developed for the RED. The mechanical team was primarily responsible for designing an enclosure for the electrical components that would protect them from the harsh environments faced during the RED's operation on the fireground. The mechanical subsystems consist of a fully assembled enclosure and phase-change material heat sinks. The design process taken to create the enclosure is described from sections 6.4.1 to 6.4.4, while the design process for the phase-change material heat sinks is described in section 6.4.5.

6.4.1 Material Selection

To begin material selection, the mechanical team chose to purchase small batches of a few different materials that could be thermally stress tested to help determine which material would be best for constructing the enclosure. These batches consisted of high temperature nylon sheet, high temperature silicone sheet, and high temperature molded silicone. The materials were chosen based on extensive research and comparisons as well as preliminary SolidWorks thermal simulations.

The enclosure consists of a layering of 3D printed nylon-glass fiber composite and high temperature silicone. The inner components, end cap, and handle were all printed using a modified Ender 3 3D printer. The outermost layer was molded to the shape of the printed enclosure and shields the internal components from the hot environment it will be exposed to. These materials were selected after thermally testing multiple material samples and choosing the most effective materials within the team's manufacturing constraints. Carbon fiber filament was initially considered but then ruled out due to its property of blocking RF signals and being slightly more brittle.

6.4.2 RED Enclosure

When first looking to find a high temperature nylon filament for 3D printing the enclosure, the mechanical team chose FibreX PA6+GF30 glass fiber reinforced nylon filament. However, the team had to quickly pivot to a MatterHackers NylonG filament after finding that the FibreX filament had a melting point too high for the 3D printers available to the team. NylonG is also a glass fiber reinforced nylon filament which allows for fairly easy printing. This filament was used to construct the five main structural sections of the RED. To create this enclosure, CAD models were drafted based on the electrical team's size estimates. These CAD files were then exported and sliced in 3D printing software to create gcode. This gcode was then given to a modified Ender3 3D printer. The design process for the enclosure involved extensive brainstorming and prototyping of different assemblies that could achieve the desired outcome. The enclosure needs to not only survive the harsh environments of the fireground for the time it is in use, but it needs to be reusable with minimal components needing to be replaced.

The first structural section is the inner shell of the RED. This piece is designed to be an inner barrier to thermally insulate and physically shield the electrical systems. This section is 0.125” in thickness.

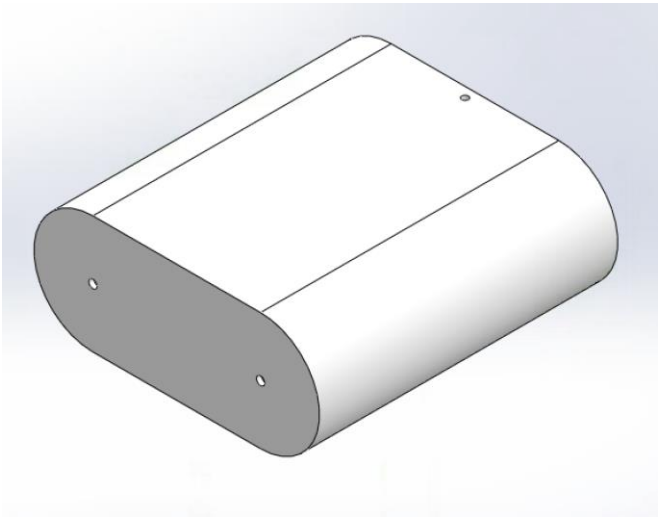

***Figure 64*: NylonG 3D Printed Shell**

The second structural section is the bumper section of the RED. This piece is designed to allow the device to fall onto either of its largest faces, which will allow for optimal transmission and reception of radio signals given the position of the monopole antenna. All of the edges of the RED are rounded to achieve these two optimal positions and keep the RED from standing on its edges. The bumper is optimized for this section of the RED which would likely be subject to repeated impacts.

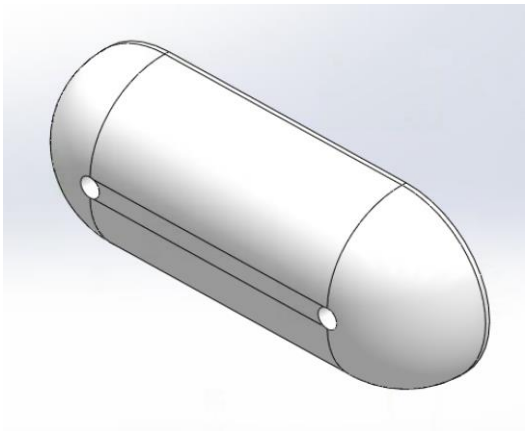

***Figure 65*: NylonG 3D Printed Bumper End Cap**

The third structural section is the end cap of the RED. This section is designed to seal the inner sheath which will insulate the electrical systems and add ingress protection. The end cap houses two separate O-rings which keep out water and debris from the inner chambers. The enclosure is connected to the end cap via two screws.

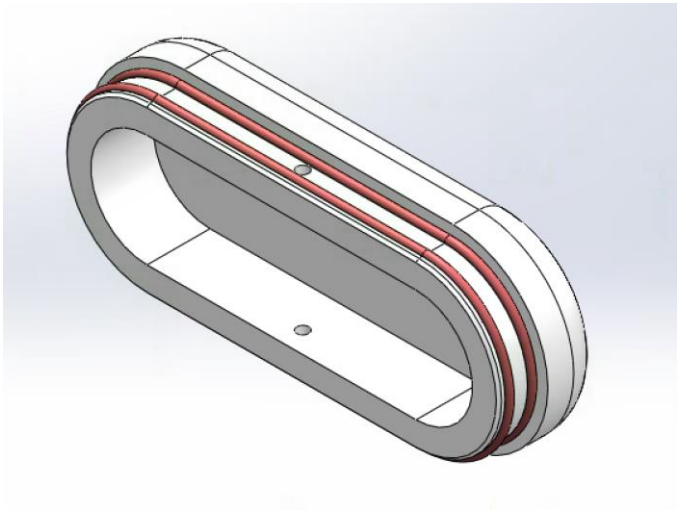

***Figure 66*: NylonG 3D Printed Handle End Cap**

The fourth section is the handle of the RED. This section is designed to connect with the end cap section and allow the RED to be carried around the fireground. This section is printed separately from the end cap to ensure structural integrity during the 3D printing process. The handle has threaded holes on its ends that allow it to be bolted to the end cap. The handle was made to accommodate a hand wearing a large, insulated firefighting glove.

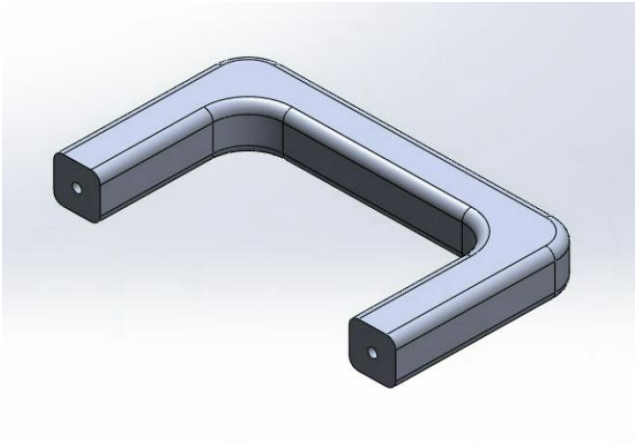

***Figure 67*: NylonG 3D Printed Handle**

The fifth section is the set of internal inserts in the RED which hold all of the electrical components inside of the enclosure shell. There are two identical inserts that slide right into the RED and provide structural support to the inner shell after being inserted. The inserts also act as standoffs for an additional layer of separation from the hot walls of the enclosure. The electrical components are housed on the inner faces of the inserts. Future work includes screwing the electrical components and heat sinks to these inserts.

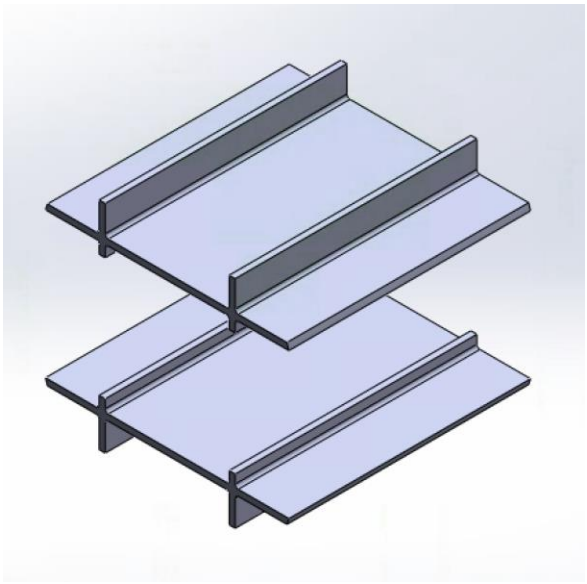

Figure 68: **NylonG 3D Printed Structural Inserts**

The figures below show exploded views of the full mechanical assembly.

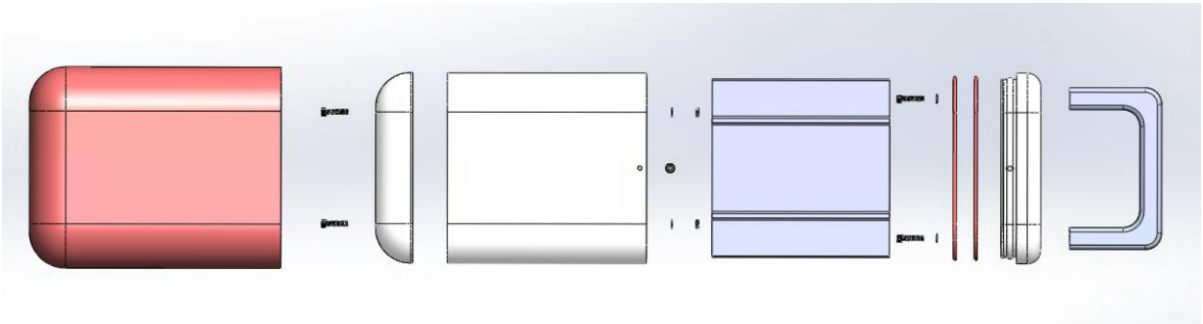

Figure 69**: Top view of Exploded RED Mechanical Assembly**

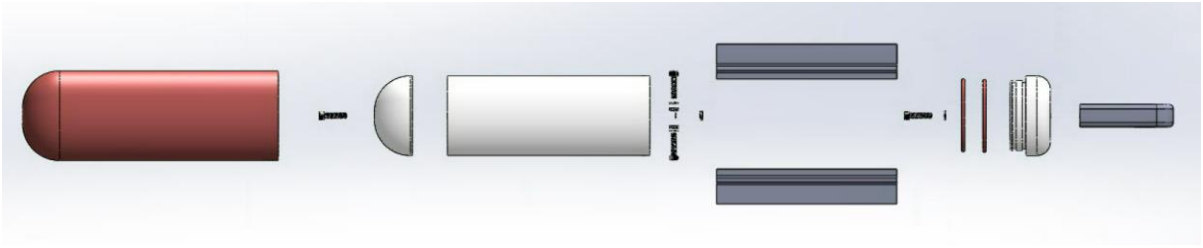

***Figure 70*: Side view of Exploded RED Mechanical Assembly**

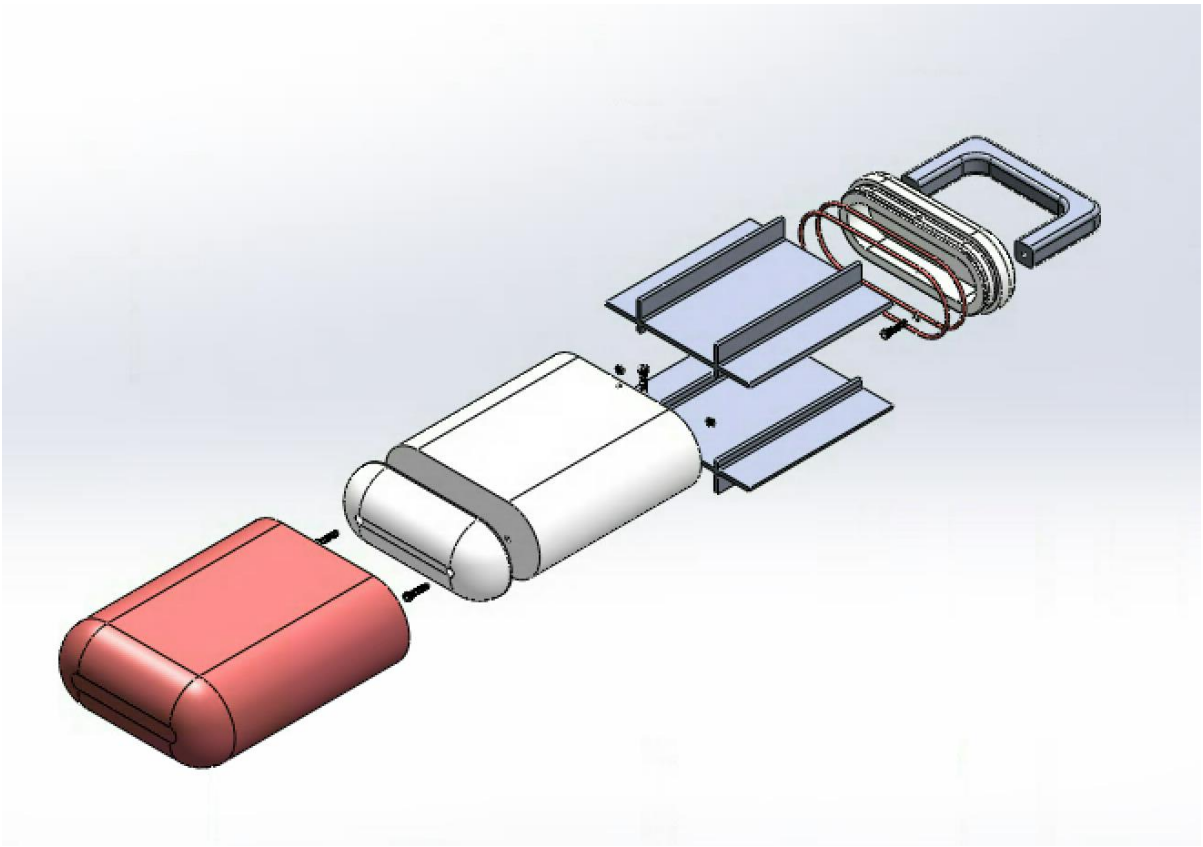

***Figure 71:* Isometric View of Exploded RED Mechanical Assembly**

6.4.3 Initial Enclosure Testing

To test the heat resistance of the composite enclosure, the parts were placed in an oven at 350 degrees Fahrenheit for fifteen minutes and then inspected afterward. This procedure was taken from the NFPA 1802 testing standards. Some minor melting and warping were noted in the composite, however, this may have been due to direct contact with the oven heating elements. These results suggested that a high temperature silicone sheath would help to reduce heat exposure for the enclosure.

6.4.4 Silicone Sheath

To minimize stresses caused by impacts to the RED and to add an extra layer of thermal insulation to protect the interior electrical components, a sheath made of high-temperature silicone was constructed to fit around the body of the RED and act as the outermost insulating layer for the device. This sheath was constructed by first 3D printing a mold to match the thickness and size the team wanted the sheath to be. The two-part Mold Max 60 was then mixed and degassed in a vacuum chamber to remove all air bubbles that were created while mixing. This strengthens the silicone sheath that would otherwise tear easily due to the air bubbles acting as stress concentrations in the structure. Cured samples of the silicone that were degassed were observed by the group to have fewer gaps and bubbles under a microscope than silicone that was cured without degassing. After degassing, the silicone was poured into a 3D printed mold consisting of two outer trays and an insert which was placed inside the trays with the poured silicone in between. This setup was then left to cure for 24 hours. Once the silicone had cured, the sheath was removed from the mold and fitted onto the device. To ensure the sheath maintained a tight fit, a silicone adhesive was applied between the inside of the silicone sheath and the 3D printed body of the enclosure. Now that the enclosure

6.4.5 Phase-Change Material Heat Sinks

The RED faces a unique situation when it comes to cooling systems, due to the fact that ambient temperature in the RED's operating environment will often be hotter than the components in the device that need to be cooled. This means that heat cannot flow out of the device, and there is a potential for heat to flow into the device from the outside and damage the electronics. The solution to this problem was to:

1. Minimize the heat entering the RED by increasing the thermal insulation around it via the silicone and 3D printed enclosure.

2. Store as much heat as possible from the electrical components to keep the internal temperature low.

In order to store heat, a material with a high thermal capacity was needed. Paraffin wax was a great candidate for this, as it is able to store high amounts of energy without vaporizing and causing significant pressure changes. These heat sinks are known as “phase change material (PCM) heat sinks”. The ME team decided to construct PCM heat sinks using 6061 aluminum tubing and paraffin wax. Aluminum was chosen because it is low cost, easy to cut and transfers heat away from the boards very quickly. The paraffin wax has a specific heat capacity roughly 3.25 times higher than aluminum and is therefore able to store far more energy before rising in temperature. Additionally, the paraffin wax is able to store high amounts of energy without vaporizing and causing significant pressure changes.

These heat sinks were constructed by 3D printing silicone molds to form end caps and cutting the aluminum into 4” sections. These sections were then capped on one side and melted paraffin was poured into the aluminum tube. To ensure low risk of overflowing paraffin wax, each PCM was filled with roughly 80% wax and 20% air. After capping the other side, the capped ends were re-dipped in Mold Max 60 to ensure the paraffin wax would not drip out once the PCMs were heated.

6.5 Thermal Testing

After developing the RED enclosure and PCMs, the mechanical sub-team began thermal stress testing of the enclosure and ECE subsystems within the enclosure. These tests were verified using the results of a SolidWorks thermal simulation. Additionally, the PCMs were thermally tested to ensure the quality of the silicone seals.

6.5.1 Enclosure Thermal Testing

Each of the teams required different levels of testing for their components before being implemented into the RED device. Each component must go through baseline testing to ensure they will be able to perform the necessary functions for their task.

For the ME team, the initial thermal testing of the enclosure is conducted in the WPI Fire Science Lab, where the team would put the different components of the enclosure into a test oven heated to 350^0F for 15 minutes and observe the results. Mainly, the team looked for any signs of mechanical failure as a result of the heat in the oven. This could come in the form of burn marks and melting of the materials being tested, examples of which are shown in the figures below. In doing so, the mechanical team can ensure that the materials meet NFPA temperature requirements and will be able to be safely used in a fireground. The mechanical team focused their tests on the two main components of the enclosure, those being NylonG filament, and our thermally resistant silicone.

***Figure 72*: NylonG Stress Testing Before**

Figure 73: **NylonG Stress Testing After**

After conducting tests of the NylonG components without the silicone sheath, the team saw significant melting of the components. This test affirmed the need for a protective outer layer of high temperature silicone. After the enclosure was assembled and the casting of the silicone mold was complete, the mechanical team moved to begin full thermal testing of the enclosure.

The mechanical team incorporated all aspects of the enclosure for final thermal testing in the foundry lab of Washburn Laboratories using an Omegalux LMF - 3550 oven. The goal of these tests was to ensure that the enclosure as an entire unit could withstand fireground temperatures with minor deformities, while also keeping the internal temperature of the device cool enough to house the electrical components. The testing in the Foundry was done in multiple stages, starting with just the enclosure and no electrical components, then adding components in subsequent trials. The internal temperature was measured using a thermocouple inserted through the bottom of the device where a retention screw would normally be found. In the first two cases, the RED enclosure was tested without electrical components, where one of the tests had the thermocouple in the center of the RED, and the

other was in the corner outside the 3D printed inserts. Below are the results of the temperature testing for the central and corner sections of the RED enclosure.

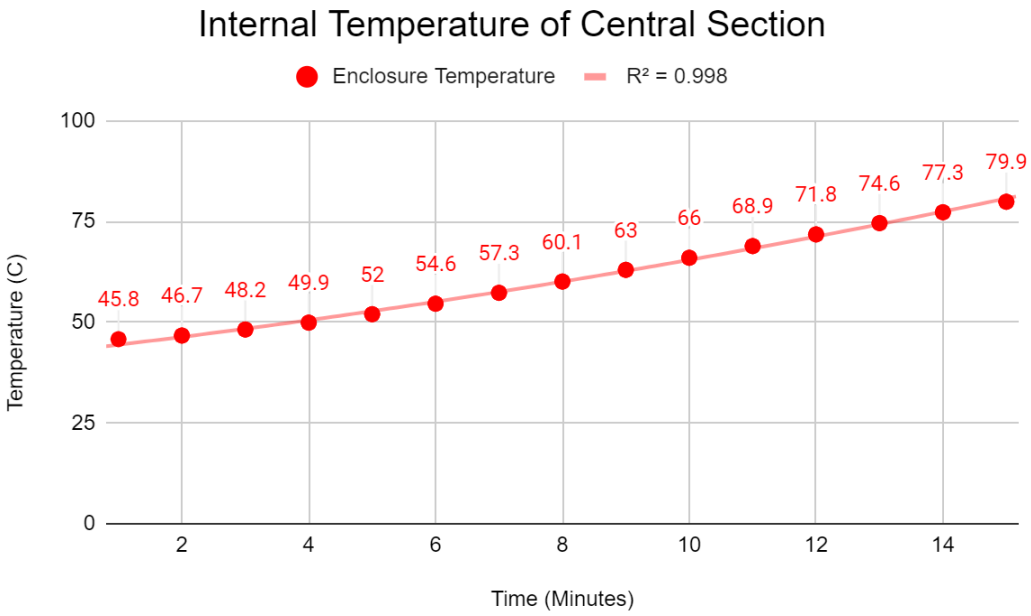

Figure 74: **Thermal penetration of the innermost chamber**

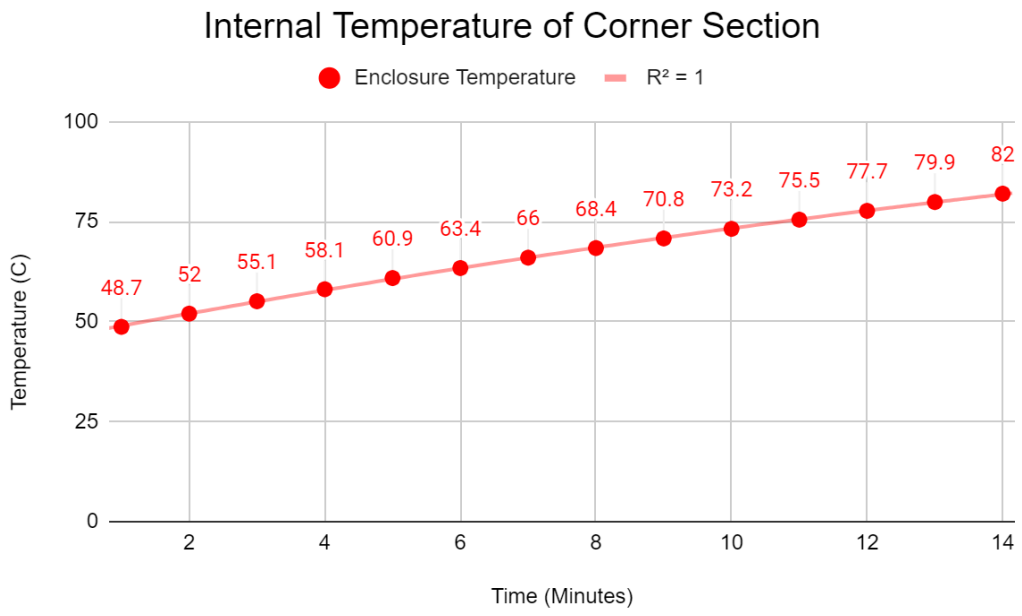

Figure 75**: Thermal penetration of the outer corner section**

With these initial trials, the mechanical team aimed to prove that certain areas of the inside of the enclosure experienced higher heat transfer from the outside, indicating ideal

locations for the electrical components. In these tests, the mechanical team found that the internal temperature did not rise above 40℃ over a 15-minute timeframe with the oven at 175℃ (350℉). We also saw that the rise in temperature for the thermocouple in the corner of the assembly was higher than that in the innermost chamber, affirming the results found in the SolidWorks thermal testing.

6.5.2 SolidWorks Thermal Simulation

While conducting thermal stress tests on the enclosure, the ME team also conducted a thermal simulation of the enclosure model in SolidWorks. The results of this simulation can be seen below.

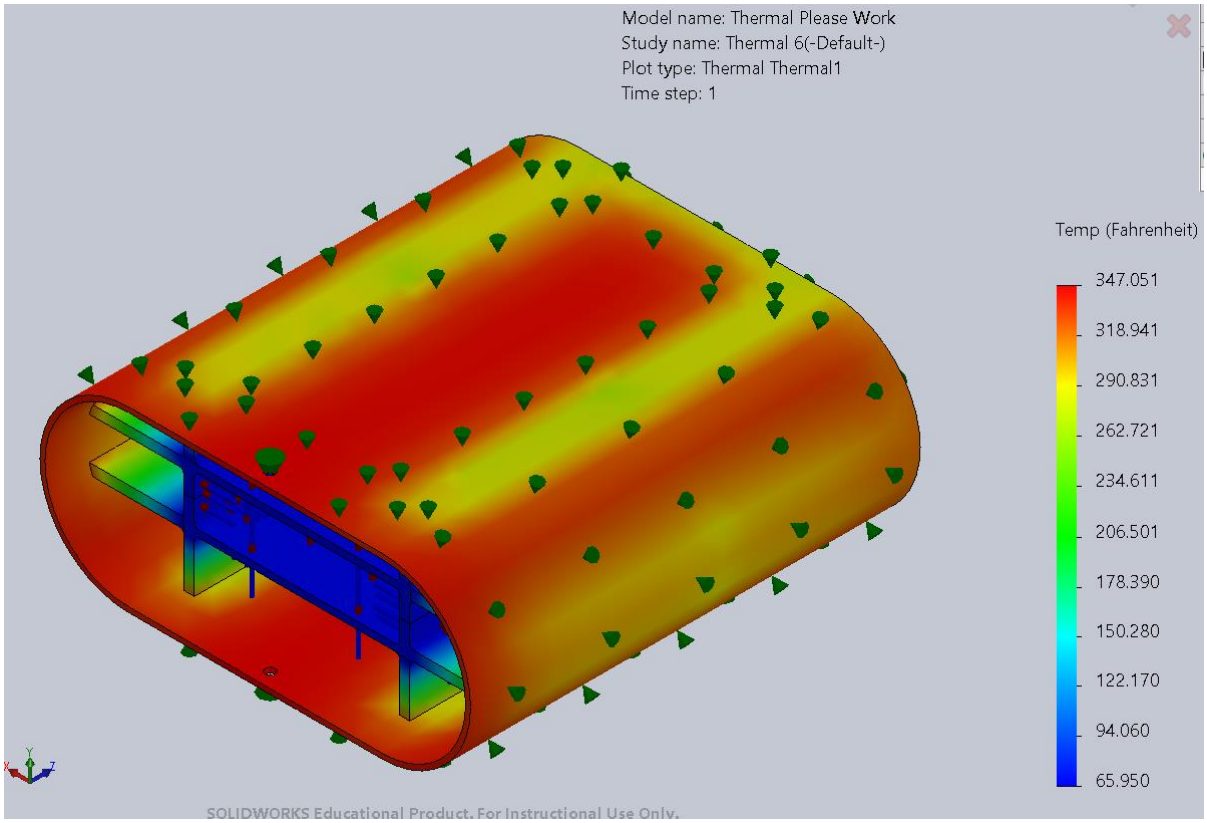

***Figure 76*: SolidWorks Thermal Simulation**

This simulation was conducted using steady state convection at 165℃, which is likely to be the same thermal stress it would be exposed to in a burning structure. The simulation shows that in the central chamber, the enclosure is able to maintain an ambient temperature

of 65.95℃. This is slightly lower than our thermal stress tests, which showed the internal temperature to be between 71-80℃. However, some variation between the model and tests are expected, as the real-world parts are 3D printed and may have slightly different properties than the parts in the model. The simulation also verifies the thermal stress testing in that the central chamber is better able to protect the ECE subsystems by having a lower ambient temperature than the corner sections. This led to the decision to mount the electrical systems to this inner chamber.

6.5.3 Electrical Component Thermal Testing

After fully assembling the RED enclosure, thermal testing of the available electrical components could be done. This testing was conducting using the same parameters as the enclosure thermal stress testing in accordance with NFPA 1802 testing procedures.

The first of the electrical components to be thermally tested within the RED was the LNA. This component was placed in the central chamber of the enclosure and heated to 175℃ for 15 minutes. Following this test, the only change in the LNA was damage to a single threaded connector that did not allow a proper connection. Due to this issue only occurring on one connector out of the four, it is difficult to say that the thermal testing definitely caused the issue. This could have also occurred from improper handling of the board or manufacturing issues. After replacing this connection however, the LNA worked as expected, showing the enclosure was able to protect it from the thermal stress test.

The other component tested was the bandpass filter which was placed in the top central chamber of the enclosure. This component could not be placed in the central chamber due to its larger size. These test parameters were identical to the LNA thermal test and the chamber reached a maximum temperature of 110.2℃. This is much higher than the previous test, however this could be due to the thermocouple being in contact with the roof of the enclosure rather than floating freely. This could cause the temperature reading to be higher

than the air temperature inside the enclosure. The ambient air temperature is likely a more relevant metric, as the electrical components would be mounted on standoffs, reducing conductive heat transfer. The bandpass filter proved to operate the same as before the thermal stress test, which shows the enclosure was able to protect the component from the thermal stress.

6.5.4 Current Status of RED Enclosure

Following the repeated rounds of thermal testing, the enclosure experienced minimal damage to its exterior. The end cap of the enclosure did experience some browning around the edges due to it being directly exposed to the high temperatures. However, all internal components and sections covered by the high temperature silicone are intact.

6.5.5 Phase Change Material Heat Sink Testing

Following the manufacturing of the PCM heat sinks, each unit was tested by being placed in an OmegaluxLMF - 3550 oven and heated at 95℃ for 10 minutes. These temperatures were determined due to the melting point of paraffin wax being ~55℃, and the extended time allows the heat to penetrate the aluminum tubing and heat the wax. The goal of these tests was to make sure the high temperature silicone has sealed either end of the aluminum tubing, so the paraffin wax could not leak from the tubing. During the initial testing, one of the PCMs showed signs of slight leaking, while the others remained fully intact, indicating that one had an issue in its construction. After repairing the first PCM with high temperature silicone, the mechanical team continued testing with all components, all of which proved effective, remained unscathed and performed as expected.

6.5.6 Current Status of Phase Change Material Heat Sinks

The PCM heat sinks are currently adhered to the MW7 and AFT board to provide passive cooling during subsystem testing. They were adhered with Gennel G109 thermal glue which creates a strong physical and thermal connection between the board and the heat sink.

Chapter 7: Conclusions and Future Work

7.1 Conclusions

The team's work established a need for a reliable, portable, and low-cost signal relay device and used engineering knowledge across three of WPI's disciplines to conceptualize, design, and layout an engineering solution: the Radio-Network Extender Device (RED).

The mechanical team concluded that functionality of the enclosure to insulate electrical systems was proven, and that phase-change material heat sinks that cool which passively the electrical system could survive within the enclosure. Testing was conducted to show that the enclosure protected the low noise amplifier and bandpass filter against thermal stress. The PCM heat sink was placed onto the power amplifier boards and sufficiently cooled the boards during testing.

The electrical team concluded that functionality was proven for the antennas, low noise amplifiers, bandpass filters, embedded signal processing, power amplifiers, and power supply. The antennas and bandpass filters worked best, and the team was also able to explain the limitations of each of the component parts in need of improvement. Most improvements identified involved manufacturing processes, such as soldering components to PCBs.

The computer science team concluded that functionality of the software components was proven. Testing was performed on each of the components to demonstrate that the separate components work as intended. The dummy test data was correctly transformed into graphs and displayed on the website. Visual improvements can be made on the website without impacting the functionality of the software.

Our team was able to show significant progress in the development of a RED and are hopeful to continue advising the project as a future MQP.

7.2 Component Testing

While much of our component-level work was successful, further design, testing, and integration would be required to achieve a full working prototype. This section outlines the work that a future team could carry out.

7.2.1 Internal Inserts

Future work includes integrating the mechanical and electrical subsystems together in a way that allows them to fit inside the enclosure. The current enclosure design includes two inserts which were designed to act as a structure that the electrical systems could screw into. The exact location of these screw holes and the locations of the pcb boards and antennae on the inserts still needs to be determined. Additionally, the geometry and size of these inserts should be optimized for the electrical and cooling system layouts. This would involve designing a support bracket or mounting hardware to keep the heat sinks attached to the boards (in addition to the thermal adhesive).

7.2.2 PCM Heat Sinks

The PCM heat sinks that were produced, are a proof of concept and are not necessarily optimized for the boards that they adhere to. To save time and money, the PCM heat sinks prototypes were cut from stock aluminum tubing. Ideally, these aluminum parts could be custom machined to a shape that conforms more efficiently to the board geometry.

7.3 System Testing to Full Prototype

7.3.1 PCM Heat Sinks

More testing is also needed to quantify both the effectiveness of these heat sinks and their duty cycles when operating in a room temperature environment and elevated temperature environment. This testing needs to be carried out when the heat sinks are integrated into the full RED system. The size of the heat sinks can be altered to increase or decrease their duty cycles.

7.3.2 Enclosure

Testing needs to be completed to further analyze the enclosure's compliance with NFPA 1802 testing standards. This includes vibration, corrosion, tumbling, mechanical stress and impact tests. The enclosure may need to undergo several additional re-designs to pass these standards.

7.3.3 Full Prototype Testing

Once the full RED prototype is put together, testing will need to be done to verify that all electrical, software and mechanical systems work together simultaneously.

7.4 System Stress Testing Based on NFPA 1802

Throughout this project, the RED team based the majority of their stress testing on the standards set by NFPA 1802, as this standard is specified for firefighter radios and is the closest to our device. In the testing done for the duration of this project, the project team focused testing on the thermal specification of the enclosure, as this is the most important

aspect of durability in a foreground. As the RED project moves forward, the device will be tested under more of these specifications laid out by NFPA 1802. It is in the opinion of the current RED team, that the future tests should include and focus on: water leakage, impact acceleration, power source performance, display surface abrasion resistance, corrosion resistance, tumble vibration, and electronic temperature stress as these are most relevant to the current iteration of the RED device, and will prove the RED's effectiveness in the fireground. Some examples of the specifications that must be met would be remaining operable in the tumble chamber for 3 hours and still remaining operational, submerging the device in water for 15 minutes after being in the oven at 350^0F for 15 minutes to test for leakage, and more. Should the RED pass these tests in the future, the likelihood of use in firegrounds shall rise with the effectiveness and durability proven.

7.5 Baseline Testing

Future work would involve conducting another baseline test with Meriden Fire Department with the complete prototype built for a better understanding of what aspect of the project would work well, and which not. The RED along with MD firefighters The two teams would split between the interior and the exterior of the shopping mall, hospital, and school to transfer the radio signal with the complete repeater prototype and collect the data again to compare it with the previous baseline test. This test would measure signal strength improvements and compare the results to those found in **Appendix F: Baseline Testing**. Also, we recommend including testing how the repeater design size and weight are comfortable to be carried by firefighters.

7.6 Improvements and Recommendations

ECE

The RED electrical system can be improved with higher quality manufacturing, which can be accessed with a larger budget. While we planned for manufacturing our design

to be the most significant challenge of the project as we had no prior RF manufacturing experience, we also believed that we had access to adequate facilities. However, we quickly learned that WPI did not have the necessary printed circuit board manufacturing capabilities and surface-mount soldering equipment. We attempted to work around this issue by ordering circuit boards from professional manufacturers, purchasing our own soldering equipment, and working with charitable professionals at NewEdge Signal Solutions. Unfortunately, these attempts were inadequate and introduced shipping delays. Electrical system block functionality may have been proven in spite of these challenges, but to achieve higher performance, quality, and development speed, more resources are required.

CS

The software capabilities of the RED can always be refined and expanded. For example, to improve functionality, physical switches could be added to switch the software back and forth from data visualization mode and data collection mode. The CS team was careful to design software that can be improved depending on a fire department's specific desires.

ME

The ME team would improve the RED by finding either a better material for shielding the outside of the enclosure or a better way to mold the high temperature silicone used. The process used to mold caused many delays which stopped the team from running more thermal tests on the enclosure and the electrical subsystems.

7.7 Firefighter Feedback

Revisiting baseline tests in Meriden will provide the opportunity to gather direct feedback from firefighters. This would involve recommendations and changes for further development to best reflect Meriden's standard operating procedures, ergonomic needs, and environmental stress concerns.

References

AFA. (n.d.). *Bi-Directional Amplifier (BDA) Solutions*. AFA Protective Systems. https://www.afap.com/communication/bda/#:~:text=The%20Bi-Directional%20Amplifier%20(BDA,coverage%20for%20public%20safety%20radios.

Amendolare, V., Cyganski, D., Duckworth, R., Makarov, S., Coyne, J., Daempfling, H., & Woodacre, B. (2008). WPI precision personnel locator system: Inertial navigation supplementation. 2008 IEEE/ION Position, Location and Navigation Symposium, 350–357. https://doi.org/10.1109/PLANS.2008.4570055

Arduino Zero. Arduino Zero | Arduino Official Store. (n.d.). https://store.arduino.cc/usa/arduino-zero.

Averill, J. , Moore-Merrell, L. , Barowy, A. , Santos, R. , Peacock, R. , Notarianni, K. and Wissoker, D. (2010), Report on Residential Fireground Field Experiments, Technical Note (NIST TN), National Institute of Standards and Technology, Gaithersburg, MD, [online], https://tsapps.nist.gov/publication/get_pdf.cfm?pub_id=904607 (Accessed March 24, 2022)

FLIR K1. (n.d.). Retrieved May 04, 2021, from https://www.flir.com/products/k1/

Microsemi. (n.d.). microsemi-mps2r10-606-switch-datasheet.

Mini-Circuits. (n.d.). BPF-C495_2b-1700236. Brooklyn.

Motorola Solutions. (2021, March). NFPA 1802 Executive Summary Guide. Chicago.

Motorola Solutions. (2019, November). APX8000XE_DataSheet. Schaumburg.

Mouser Electronics. (n.d.). *OPA2333SHKQ Texas Instruments: Mouser*. Mouser Electronics. https://www.mouser.com/ProductDetail/Texas-Instruments/OPA2333SHKQ?qs=Z9twEOuL%252B%2FK1aW889QyMng%3D%3D.

National commission on terrorist attacks upon the United States. (n.d.). Retrieved April 27, 2021, from https://govinfo.library.unt.edu/911/report/911Report_Ch9.htm

National Fire Protection Association. (2021). *NFPA 1801: Standard on Thermal Imagers for the Fire Service, 2021 Edition*. National Fire Codes . https://codesonline-nfpa-org.ezpxy-web-p-u01.wpi.edu/code/ef0d82eb-8a0a-4c26-8581-104c71dd6357/.

National Fire Protection Association. (2021, January). *NFPA 1802: Standard on Two-Way, Portable RF Voice Communications Devices for Use by Emergency Services Personnel in the Hazard Zone, 2021 Edition*. National Fire Codes. https://codesonline-nfpa-org.ezpxy-web-p-u01.wpi.edu/code/c9b6fffd-a13e-4182-b460-f21fdf4e7e84/.

National Fire Protection Association . (2021, May 11). NFPA 1221 Standard for the Installation, Maintenance, and Use of Emergency Services Communications Systems.

peppe8o. (2020, January 12). *Raspberry PI Zero WH datasheet*. peppe8o. https://peppe8o.com/raspberry-pi-zero-wh-datasheet/.

Pololu Robotics & Electronics. (n.d.). *Pololu Adjustable 9-30V Step-Up Voltage Regulator U3V50AHV*. Pololu Robotics & Electronics. https://www.pololu.com/product/2571.

RF-LAMBDA. (2019, December 16). RLNA50M05G43.

SignalBooster.com. *Bi-Directional Amplifiers BDA vs DAS Distributed Antenna Systems*. SignalBooster.com. (2021). https://www.signalbooster.com/blogs/news/bi-directional-amplifiers-bda-vs-das-distributed-antenna-systems#:~:text=BDA%20solutions%20are%20typically%20under,of%20installing%20a%20BDA%20system.

Swenson. (2020, December 21). *Landmark residential fire study shows how crew sizes and arrival times influence saving lives and property*. NIST. Retrieved March 22, 2022, from https://www.nist.gov/news-events/news/2010/04/landmark-residential-fire-study-shows-how-crew-sizes-and-arrival-times

Sysmax Industry Trading Co., Ltd.. (2016, October 25). NL1834 Datasheet. https://www.manualshelf.com/manual/nitecore/nl189/datasheet-english/page-4.html

Where there's smoke, there's a signal. (2021, February 12). Retrieved April 27, 2021, from https://www.dhs.gov/where-theres-smoke-theres-signal

WISPER. (2021, March 25). Retrieved April 27, 2021, from https://www.oceanit.com/products/wisper/

Appendices

Appendix A: Survey Responses

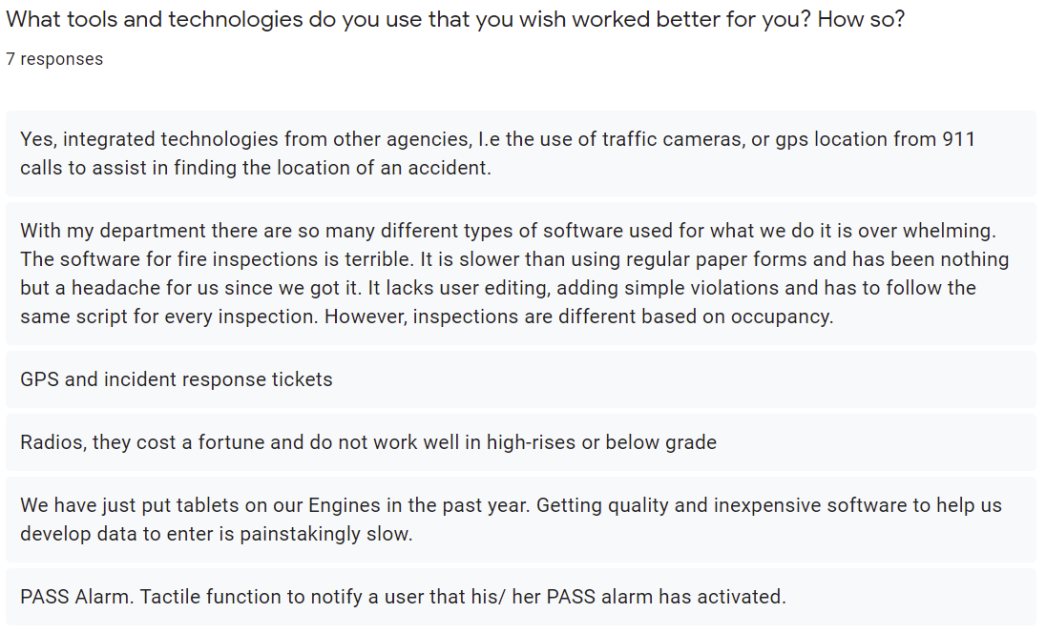

***Figure A*: Firefighter Survey Responses One**

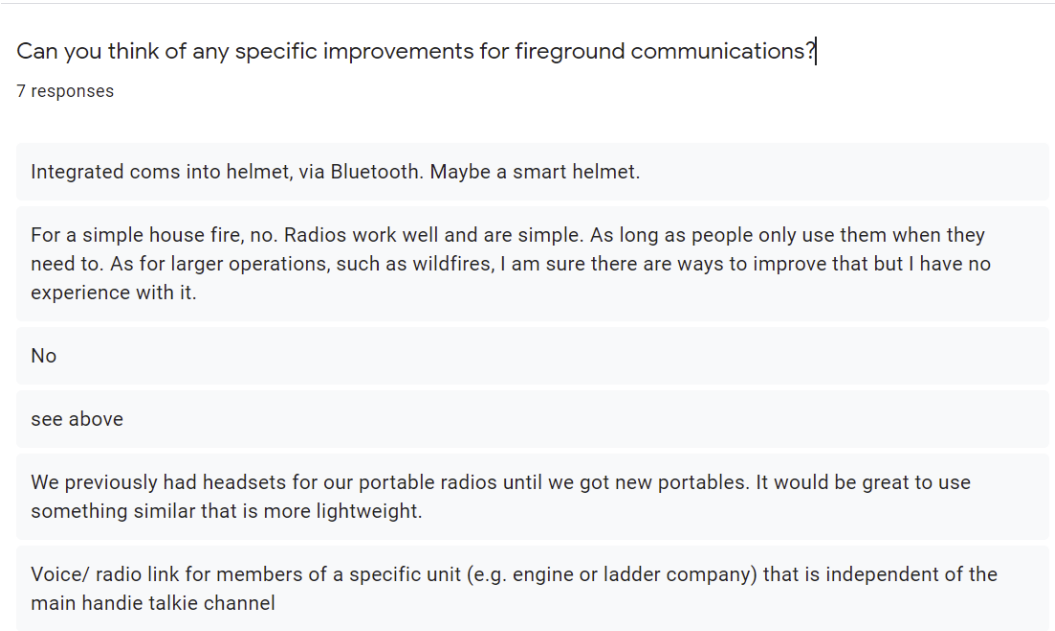

***Figure B*: Firefighter Survey Responses Two**

Appendix B: Team Organization

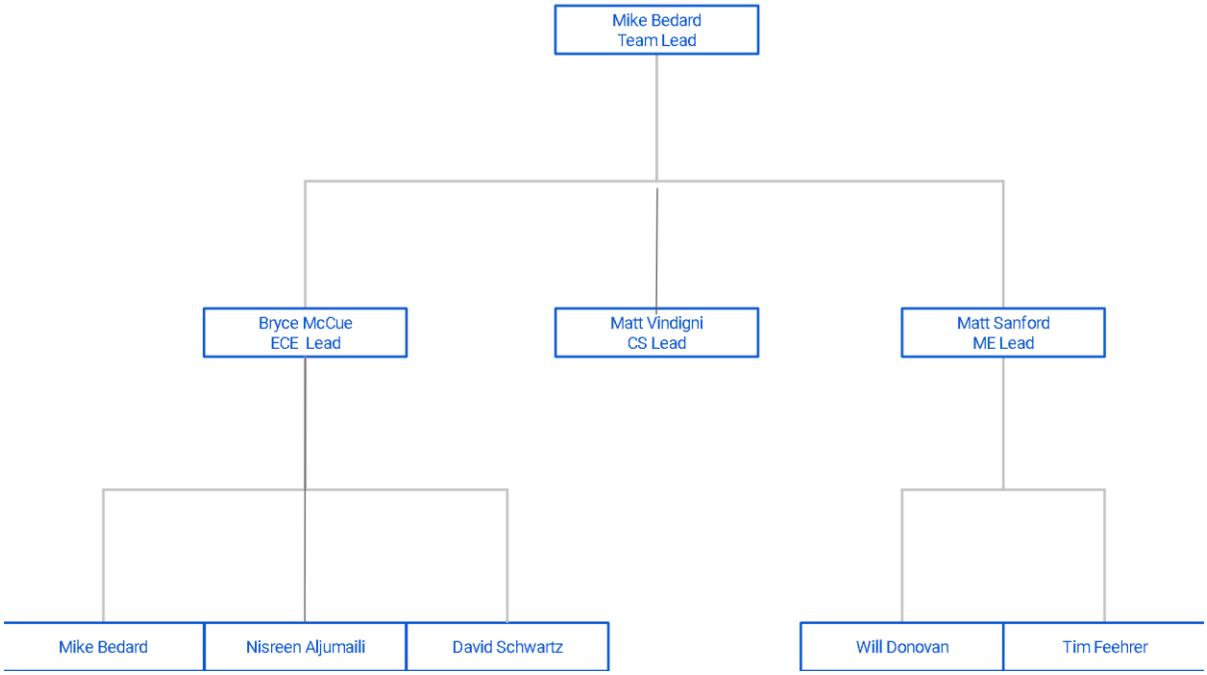

***Figure C*: Team Organization Chart**

Appendix C: Team Responsibilities

ECE Team Responsibilities:

Antenna:

Tasks:

- Design: David
- PCB Layout: David
- Selection: David, Nisreen
- Fabrication and Soldering: David
- Testing: David

T/R Switch:

Tasks:

- Simulation: David
- Selection: David

Low Noise Amplifier:

Tasks:

- Selection: Mike
- PCB Layout: Mike
- Soldering: Bryce
- Testing: Mike

Bandpass Filters:

Tasks:

- Design: Mike
- PCB Layout: Mike
- Selection: Mike
- Soldering: Bryce, Nisreen, David
- Testing: Mike, David

ADF:

Tasks:

- Selection: Bryce and David
- Programming: Bryce

- Soldering: Mike
- Testing/Debugging: Bryce, David, Matt V

Embedded Computing:

- Selection: Bryce, David, Matt V
- Coding: Bryce (ADF to MSP430 interface), David (MSP430 CLK/GPIO), Matt V (Raspberry Pi)
- Soldering: Nisreen
- Testing/Debugging: Bryce, David

Power Amplifiers:

Tasks:

- Selection: Mike
- PCB Layout: Mike
- Soldering: David (MW7), Nisreen (AFT), Mike (MW7)
- Testing: Mike

Battery:

- Selection: Nisreen, David

Buck Converters:

- Selection: Nisreen, David
- Testing: Nisreen, David

Boost Converters:

- Simulation: Nisreen
- Selection: Nisreen, David
- Testing: Nisreen, David

ECE Logistics:

Logistics:

- Equipment and lab setup: Nisreen
- Paper oversight: Nisreen

- ECE Team meeting slides: Bryce and David
- Day-to-day direction: Bryce
- NewEdge lab/components: Mike
- BOMs: Whole team
- Component inventory and budget: David
- Industry outreach: Nisreen
- Baseline testing oversight: Mike
- Baseline testing documentation: Nisreen
- WPI Electric Reflow Oven education: Galahad

ME Team Responsibilities:

Preliminary Research: Whole Team

- WISPER
- NFPA
- PPL
- GLANSER
- Pass Devices
- Manufacturing techniques/options
- Cooling systems and heat sinks

Interviews: Whole Team

- NFPA
- Worcester Fire
- Meridian Fire
- FDNY
- WPI Professors:
    - Cyganski
    - Wyglinski
    - Makarov
    - Duckworth

Material Research and Testing

Tasks:

- Selection of sample materials: Whole team
- Testing of sample materials: Whole team
- Ordering new materials for manufacturing: Matt

Phase Change Material Heat Sink
Tasks:

- Research: Whole team
- Design: Tim
- Manufacturing: Matt
- Thermal Testing: Matt and Will

RED Enclosure
Tasks:

- Design: Whole team
- CAD: Tim
- 3D Printing: Matt
- Thermal Testing: Whole team
- Vacuum Chamber: Will
- Silicone sheath construction: Whole team

Insulation of ECE Systems:

- SolidWorks Thermal Simulation: Will
- Thermal Stress Testing: Whole Team

CS Team Responsibilities:

Matt V completed all tasks unless othwerwise specified

Data Collection
Tasks:

- Research: Matt V and Bryce
- Design: Matt V and Bryce
- Implementation and coding: Matt V, Bryce, and David
- Testing: Matt V, Bryce, and David

Data Visualization
Tasks:

- Research
- Design
- Implementation and coding
- Testing

Server Hosting and Website
Tasks:

- Research
- Design
- Implementation and coding
- Testing

Appendix D: NFPA 1802 Testing Specifications

(TABLE 1) NFPA 1802 TEST SUMMARY View Full Published Standard	
MECHANICAL TESTING	**DESCRIPTION**
Audio Speech Quality	A Perceptual Objective Listening Quality Analysis (POLQA) test is performed.
Heat and Immersion Leakage Resistance	Devices placed in a high-temperature test chamber, heated to 350°F (177°C) for 15 minutes then immersed into 4.9ft (1.5m) of water at 72°F (22°C) for 15 minutes. Repeated 6 times then tested for speech quality, basic radio operation in hazard zone mode, and data logging.
Vibration Resistance	Devices placed in package tester compartments and vibrated for 3hours then tested for speech quality and data logging.
Impact Acceleration	Three devices (one exposed to 72°F (22°C), one exposed to -4°F (-20°C), one exposed to 160°F (71°C)), are dropped from 9.8ft (3m) 8 times onto concrete to impact each face, one corner, one edge then tested for speech quality and data logging.
Corrosion	Salt spray the devices for 48 hours. Then store the devices in 50% humidity for 48 hours then tested for speech quality.
Display Surface Abrasion	Abrasive pad to be rubbed on display with 2.2lb (1kg) load, for 200 cycles.
High Temperature Functionality	Devices placed in a chamber heated to 500°F (260°C) for 5 min then tested for speech quality and data logging.
Heat and Flame	Devices placed in a chamber and exposed to direct flame for 10 sec. Exterior of device/RSM (Housings, knobs, buttons, cables, display, etc) and data logging are evaluated.
Product Label Durability	Device product labels are examined after heat and immersion test, corrosion test, high temperature test.
Cable Pullout	A force of 35lbf (156N) applied in an axial direction to device wiring.
Case Integrity	442lb (200kg) applied to the right, left, front, back sides of the device housing then tested for speech quality and data logging.
Water Drainage	Water is introduced into all openings, indentations, and grills until water overflows. Speech and data logging is tested.
Tumble	Devices are placed in a specified tumbling apparatus rotating at 15rpm for 3 hours. (2,700 tumbles)
TIA Transmit Power	Devices tested for carrier output and RF power output.
TIA Carrier Frequency Stability	Devices tested for frequency stability and operating frequency accuracy.
TIA Receiver Sensitivity	Devices tested for analog and digital reference sensitivity.
Power Source Performance	Devices continuously operated for at least 8 hours on standard duty cycle 10-10-80 at max rated transmit power.
Electronic Temperature Stress	Devices are operated after temperature exposure of -20°C for 4-hours, and +71°C for 4-hours.
Antenna VSWR Swept Frequency	Antenna performance must be maintained after Drop/Impact, Tumble and Corrosion tests.
SOFTWARE SAFETY FEATURES	
Hazard Zone Mode	Device default powers up in hazard zone mode, minimum volume is 24dB and capable of two actions to power off. Channel, talkgroup, talk path and other programmed voice announcements when in hazard zone mode and transitioning out of hazard zone mode are at a minimum of 82dBa.
Self-checks	Device self-checks on initial power up, periodic self-checks and self-diagnostics every 5 minutes. Device checks RSM connectivity, antenna connection, temperature exposure, battery level of at least 50%.
Data Logging	Device logs the 2000 most recent device actions/events and is downloadable by the emergency services organization.
Audible and Visual Alerts	Alerts during RSM connection failure, battery levels, emergency, self-check failure, over temperature, power cycle, connecting new bluetooth or wired accessory, out-of-range and loss of connection to a system.
Visual Indicators	LEDs and display backlights illuminate during emergency, connected RSM failure, internal over-temperature, out-of-range, transmit and receive, bluetooth activity, self-check failure.

***Figure D*: NFPA 1802 Testing Specifications**

Appendix E: Firefighter Interviews

First, Mike Bedard and Matt Sanford traveled to Meriden, CT to meet with Deputy Chief Dunn and discuss the need for a radio signal extender within Meriden Fire Department. During the discussion, Chief Dunn expressed his concern for the loss of radio signal his firefighters experienced while on calls. Currently, the firefighters often use their cell phones to communicate after losing signal during less emergent (for example, fire alarms) or sensitive situations (for example, deaths or serious injuries). Additionally, the firefighters may post a person in the location that they lost signal to relay their communications back to the command unit. Chief Dunn and the team agreed that this was a danger to the fire crew by undermanning an interior team during an incident. Chief Dunn confirmed that the department would like to work with the team to develop a RED, and a timetable was set for initial baseline testing during the summer.

Next, the team conducted baseline testing at Meriden Mall and at MidState Medical Center. These tests are described in detail in **5.1 Results of Baseline Testing in Meriden** and **Appendix F: Baseline Testing**. Over the course of these tests, the team spoke with fire crews about their understanding of the signal loss issue as well as what kind of ergonomic features the firefighters would prefer. All firefighters confirmed Chief Dunn's request that REDs be larger than cell-phone size in order to prevent the devices being lost during fireground operations. Chief Dunn also explained that a RED would likely be carried by a designated Safety Officer, or in some cases, a Lieutenant or Chief. This means that the REDs would not likely have to operate near the seat of the fire, but rather in a more moderate environment. And finally, Meriden firefighters requested that REDs have a large carrying handle so that the large protective gloves worn during interior operations would not interfere with RED operation and placement.

Appendix F: Baseline Testing

We first split up team members and firefighters between the interior and exterior of the building. The interior team will activate their portable to transmit the phrase “signal test” every 30 seconds until signal is lost, while both teams track location and time of loss. Location was tracked using publicly available floor plans, fire department pre-plans, or simple fire escape maps. Time was tracked with stopwatches for test duration, and wristwatches for the time of day signal is lost. When signal was lost, the teams noted the location and time. The interior team traveled to the last known location of transmission and repeated the test phrase every ten seconds until signal was lost. This allowed for more precise characterization of signal loss.

Then, we moved the exterior team into the building. The fixed location that they moved to was determined by building construction. For example, when testing in the mall, the exterior team moved to the interior hallway arch on the floor that the interior team was on. The test continued before, with the interior team moving deeper into the building, and the “exterior” team remaining in place.

Finally, we evaluated the effect of cross-floor attenuation. One team remained in a fixed, central position on one floor. The other team walked on a floor below, and signal losses were tracked. In the cases tested, no additional floors were added across the test iterations. However, if no loss had occurred, an additional floor between teams would have been added until signal loss occurred.

In these tests, signal strength was not measured numerically with sophisticated equipment. Rather, we tracked instances of signal loss and distortion that are obvious to the user.

This process is subject to change depending on feedback because MFD may have more specific or demanding scenarios they want us to test as designs continue. Regardless,

by identifying specific limitations of the system we tried to improve, we were able to revise our specifications and set clear goals.

Appendix G: Power Amplifier PCBs

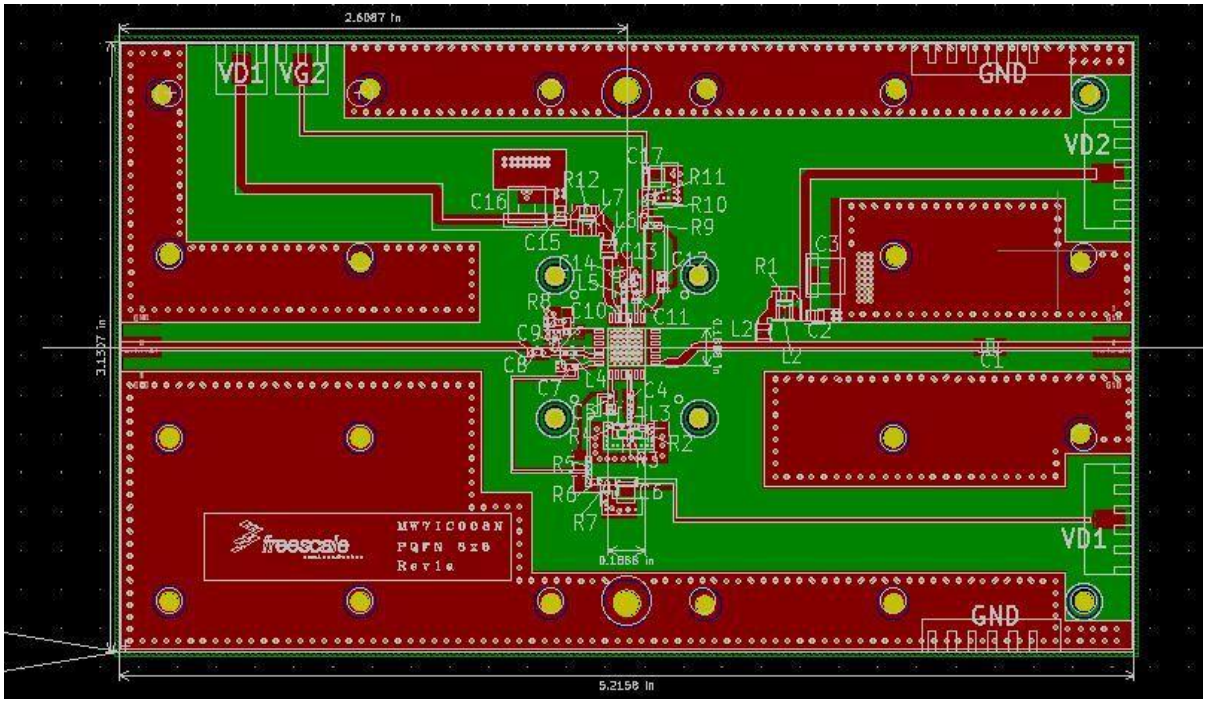

MW7IC008NT1

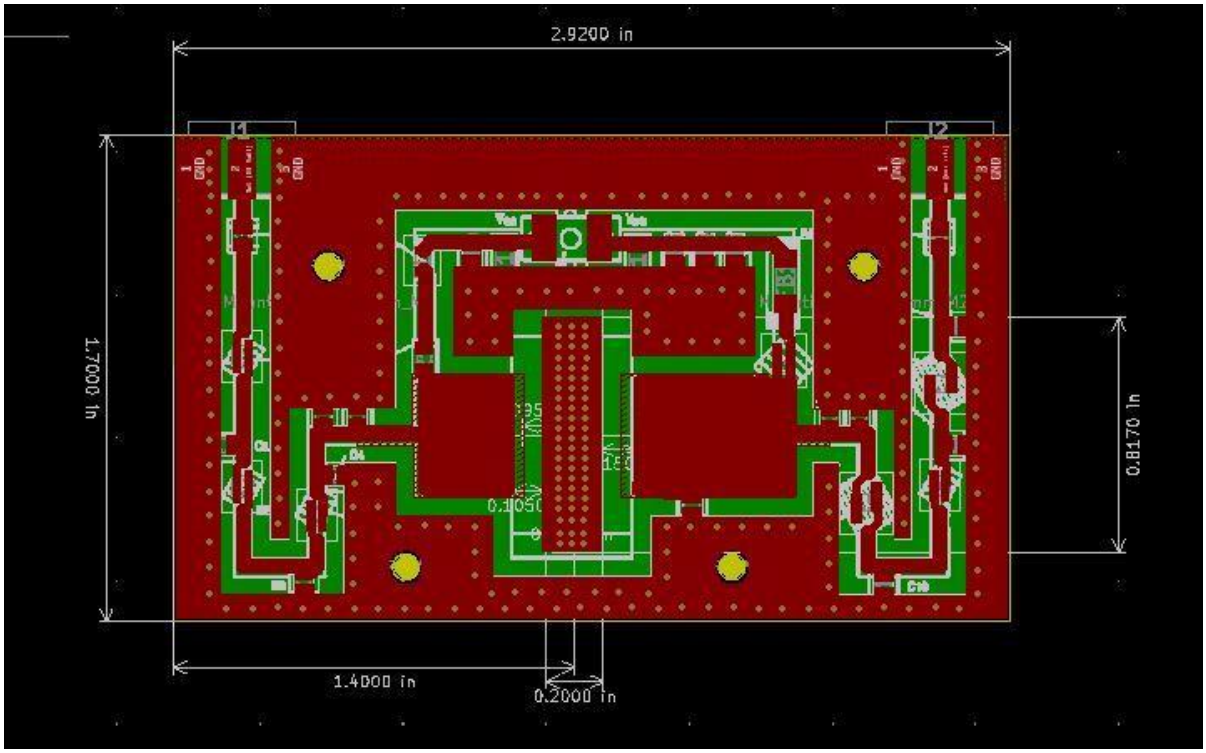

AFT05MS031NR1

Appendix H: Electrical Test Procedures

Procedural testing and verification of the electrical system were first performed on a per-module basis, while testing of system integration has yet to be achieved. The requirements of each electric module are derived from their position as "functional blocks" in the greater system. This lends to the demonstration of "proof-of-concept" because it establishes that the individual blocks of the electrical system are able to receive their specified inputs and provide specified outputs. For instance, a power amplifier requirement may list an input power range from 0-10dB and a nominal gain of 20dB. such performance specifications would be tested according to the procedures described in this section. Future work will involve implementing a testing procedure for proper feedback and control between the different system blocks, once such control systems are finalized and implemented.

Measurements with RF Analyzer

For one or two-port networks such as the filters, amplifiers, matching networks, and antenna systems, the standard practice adopted by the ECE division was to use the in-lab Keysight Fieldfox RF Analyzer to measure the scattering parameters of the network. Each scattering or "S" parameter corresponds to one of the three phenomena EM waves exhibit upon incidence with a macroscopic medium or network. These are reflection, transmission, and absorption. For instance, for a passive bandpass filter meant to pass FM signals centered at 460 MHz, the primary requirements of the network would be a low reflection (S11 ideally 0) and higher transmission (S21 ideally 1) at 460 MHz, while higher reflection (S11 ideally 1) and lower transmission (S21 ideally 0) at frequencies other than 460 MHz. Figure E shows an example frequency sweep of S11 and S21 of a bandpass filter on the Fieldfox. Note this is on a decibel scale, so 0dB corresponds to 1 and -infinity dB corresponds to 0.

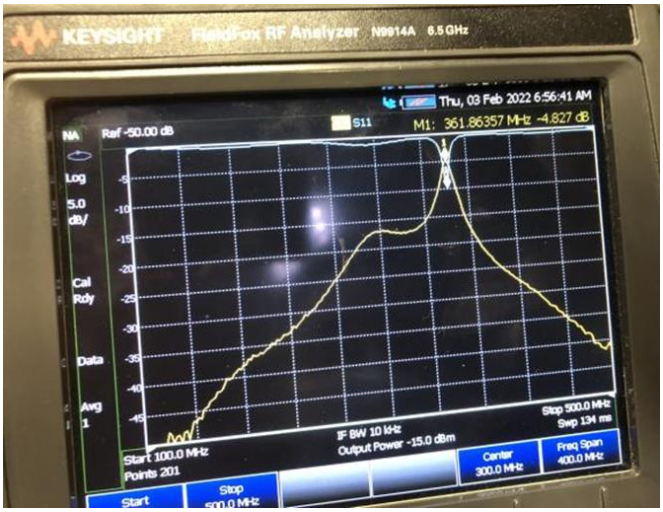

Figure E: Frequency Sweep of S11 and S21 of a Bandpass Filter on the Fieldfox.

Faraday Cage

When testing radio systems, it is important to keep in mind FCC regulations and channel allocations in the city or region one is broadcasting. Towards eliminating the potential for interference between our transceiver and local emergency communication services, the team was generously given access to the Faraday cage at the WPI Wireless Innovation Laboratory directed by Professor Alexander Wyglinski. The Faraday cage provides a chamber enclosed by conductive metal that forms a high-reflection barrier between the interior and exterior of the cage.

Anechoic Chamber

Individual analysis of an antenna views the transducer as a one-port network, meaning only the S11 reflection coefficient is measurable on the Fieldfox. This information provides a good indicator for how the antenna will act as a transducing *load* when it terminates a transmitting system, as well as a transducing *generator* when it initiates a receiving system. However, antenna pairs in operation form two-port networks—a transmitter and receiver pair. Towards measuring an individual antenna's performance as part

of the pair of communicating antennas, the team was generously given access to the WPI anechoic chamber in the Wireless Innovation Laboratory directed by Professor Alexander Wyglinski. The anechoic chamber enables more accurate measurement of radiation patterns by eliminating reflections of transmitted waves from echoing and forming standing wave patterns in the measurement area. A horn antenna will be used to measure the 3-dimensional radiation pattern and intensity of the antennae operating as transmitters. The polarization may also be determined by rotating the aperture of the horn relative to the transmitter. To measure the antennae operating as receivers, the horn antenna may be used as the transmitter, excited by a signal generator at a designated frequency.

Digital Data Lines

The operations of the MSP430 microcontroller unit go through three stages of testing and development. The first is successfully compiling the code in the IDE. Then the program is loaded onto the embedded processor and executed. Lastly, outputs of the state machine in the form of digital data lines such as a serial peripheral interface were validated using an oscilloscope.

Testing System Integration

Connecting ECE Blocks

With all the electrical blocks completed, the next stage of the project would involve connecting each block to form the fully functioning prototype (see electrical block diagram for more detail). The electrical system would then be mounted to the inner sides of the internal inserts via screws and slid into the enclosure.

Field Testing of New Device

Integration of Electric Modules

System-level testing of electrical hardware involved connecting the separate modules together via coaxial transmission lines. While a finalized product will integrate the entire system on a PCB and use microstrip lines for transmission, the modular approach is beneficial for the prototyping stage of development because it allows for individual stages to be tested, adjusted, and changed without requiring an entire re-make of the board. System-level testing will be performed in steps for each pair of modules, after which pairs of modules will be combined to subsystems or "legs" of the entire system. For the first leg, the antenna, T/R switch, LNA, and bandpass filter will form an RF front-end whose S-parameters can be measured with the RF analyzer. For the digital signal processing stage, the ADF7021 transceiver IC will be connected to the analog RF transmission from the output of the bandpass filter, and its digital will output will be recorded by the MSP430 to verify that it is properly decoding the FM signals sent through the RF front end. Then, for the transmit end, the power amplifier, bandpass filter, T/R switch, and antenna modules will be connected and tested through coax lines alike to the RF front-end. This procedure determines whether the individual modules, which on their own meet input-output specifications, will meet the system-level specifications when cascaded together.

Appendix I: RF Cables

During testing, the ECE team used the RF cables with SMA connectors that were provided in the Fieldfox setup kit. These cables terminated on both ends as SMA straight plugs. These cables were for test purposes only given their minimal protective coating. These cables are characterized below:

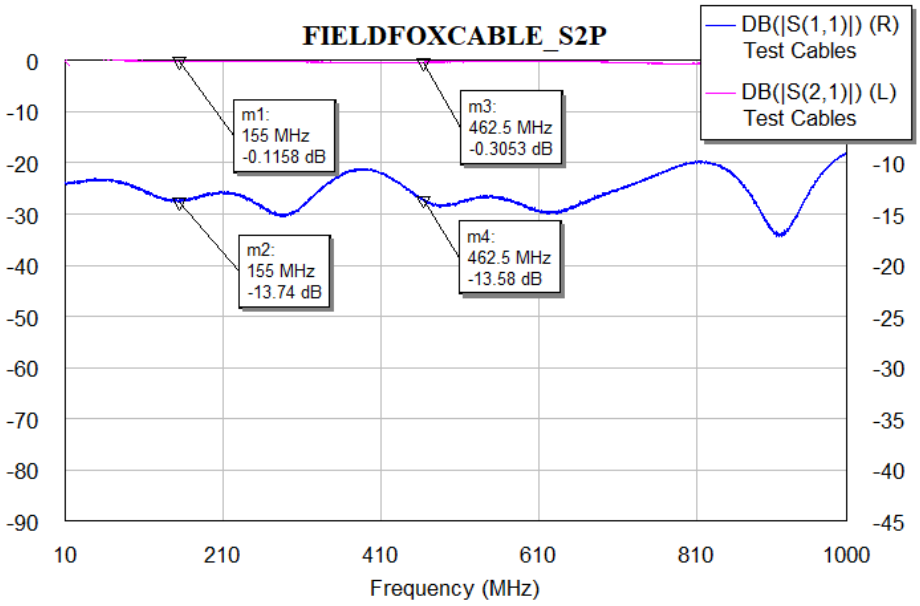

Figure F: Fieldfox RF Cables

As shown in Figure F, the RF test cables used during this project exhibit between about -0.1 dB and -0.3 dB insertion loss at the RED frequencies of interest. Because the team was more concerned with improving much higher magnitudes of loss in system blocks (such as initial filter and LNA losses described in previous sections), the RF test cable losses of no more than -0.4 dB were deemed acceptable for testing purposes.

To evaluate options for future system integration, the team purchased Johnson RG316 cable assemblies. Like the Fieldfox RF cables, the Johnson RG316 uses SMA straight plug to

SMA straight plug in order to reduce potential losses caused by 90-degree turns at SMA ports. These cables are characterized below:

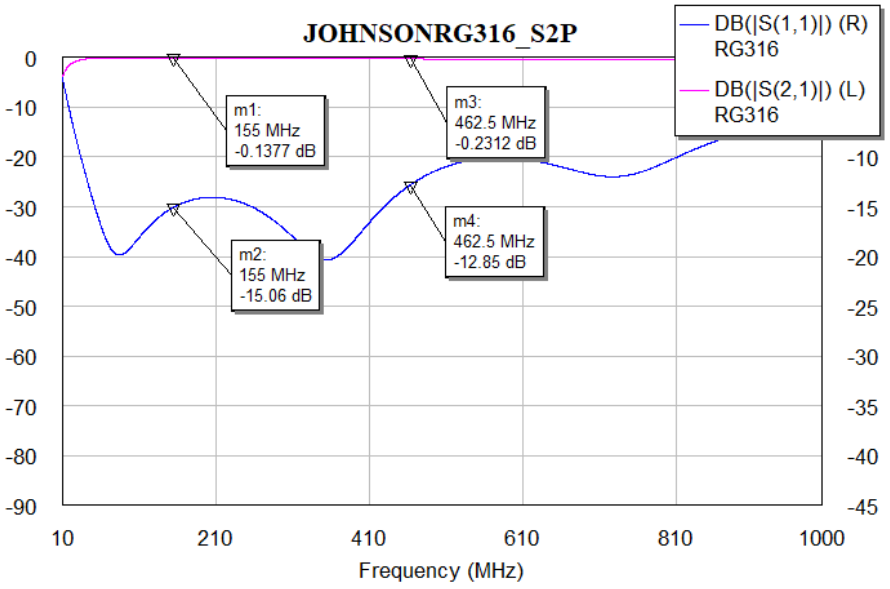

Figure G: RG316 RF Cables

Figure G shows that the cables did not exhibit a significant loss improvement over the RF test cables. However, the RG316's were more rugged, so the team determined that these would be an acceptable choice for a system integration.

Appendix J: Raspberry Pi Zero W Setup Documentation

Raspbian Setup

Download and run the Raspbian Imager

- Open the following webpage: https://www.raspberrypi.com/software/ and install the raspbian installer that corresponds with your operating system
- Put a microSD card into the computer you installed the imager on
- Run the imager and select the microSD card you inserted by clicking on the storage section

- Format the microSD card by selecting “Erase” in the Operating System section

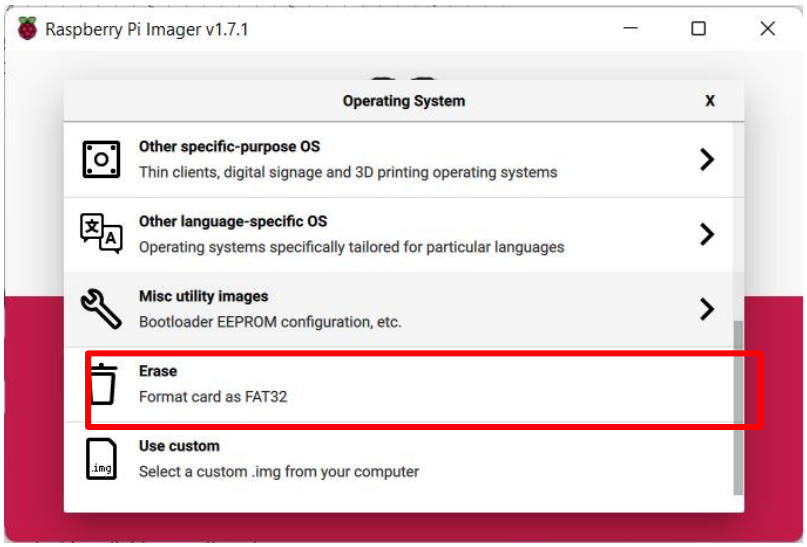

- After formatting the microSD card, select the Raspberry Pi OS (32-bit) in the Operating System section

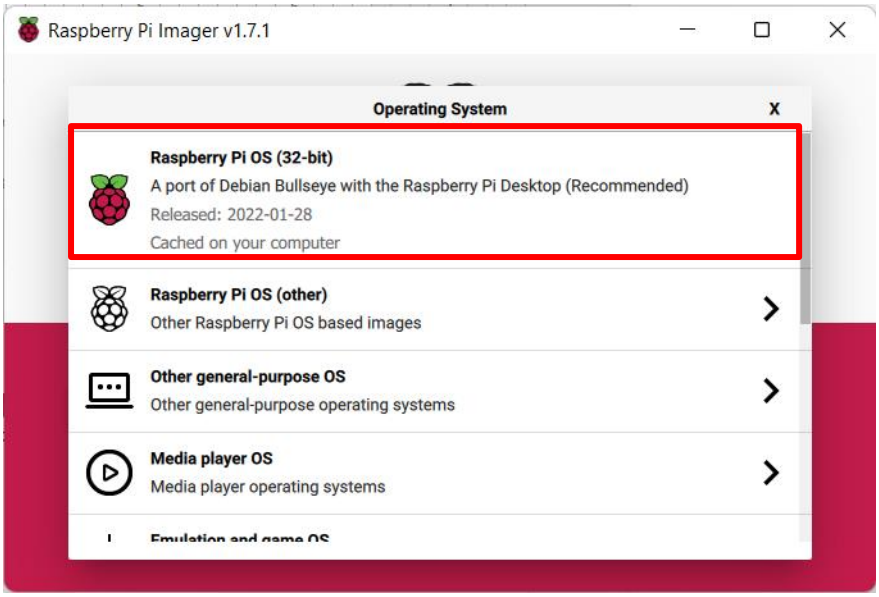

- Once done installing, you can remove your microSD card, and close out of the Imager program.

Set Raspbian Settings

- Insert your microSD card into your Raspberry Pi Zero W and connect necessary peripherals
    - Keyboard + Mouse
    - HDMI monitor
    - MicroUSB power cord
- Turn on your Pi Zero W and fill out the prompted information
    - Location, timezone and language
- Connect your Pi Zero W to a Wi-Fi network
    - This is necessary to perform the steps in the Software Setup section

Software Setup

Clone Github Repository

- cd to desired working directory in terminal and run the following commands:
    - sudo apt install git
    - git clone https://github.com/mvindigni/RED.git

Additional Dependencies

- open terminal and enter the following command
    - sudo-apt-get install libatlas-base-dev

Setup Virtual Environment

- cd to working directory in terminal and run the following commands:
    - python3 -m venv red.venv
    - source ./red.venv/bin/activate
    - python3 -m pip install -r requirements.txt

Setup AP

- Consult the Raspberry Pi configuration documentation
- Follow section “Setting up a Routed Wireless Access Point”
    - You can ignore Enable Routing and IP Masquerading section
- https://www.raspberrypi.com/documentation/computers/configuration.html